

**Michael Edler**

# Preparation and Characterization of Nanostructured Solar Energy Materials and Nanocomposite Solar Cells

---

zur Erlangung des akademischen Grades eines Doktors der  
technischen Wissenschaften

erreicht an der

**Technischen Universität Graz**

Betreuer:

Assoc.Prof. DI Dr. Gregor Trimmel

Institut für Chemische Technologie von Materialien

Christian Doppler Labor für Nanokomposit-Solarzellen

Technische Universität Graz

Deutsche Fassung:

Beschluss der Curricula-Kommission für Bachelor-, Master- und Diplomstudien vom 10.11.2008

Genehmigung des Senates am 1.12.2008

### **EIDESSTATTLICHE ERKLÄRUNG**

Ich erkläre an Eides statt, dass ich die vorliegende Arbeit selbstständig verfasst, andere als die angegebenen Quellen/Hilfsmittel nicht benutzt, und die den benutzten Quellen wörtlich und inhaltlich entnommene Stellen als solche kenntlich gemacht habe.

Graz, am .....

.....

(Unterschrift)

Englische Fassung:

### **STATUTORY DECLARATION**

I declare that I have authored this thesis independently, that I have not used other than the declared sources / resources, and that I have explicitly marked all material which has been quoted either literally or by content from the used sources.

.....

date

.....

(signature)

*To Elena and Elisa*

## Acknowledgement

I would like to thank my supervisor Assoc.Prof. Dipl.-Ing. Dr.techn. Gregor Trimmel for his perpetual support and engagement, which has been very helpful during all the time. In addition, I am very grateful for the friendly working atmosphere at our institute (Institute for Chemistry and Technology of Materials) and especially within our working group. I really appreciated the fruitful discussions. In this context, I would like to point out the support, advice and ideas of DI Achim Fischereeder, DI Wernfried Haas, Stefan Moscher, DI Alexander Schenk and especially Dr. Thomas Rath. Furthermore, I would like to thank Sarah Meyer and Manuel Wieser, who carried out small experimental projects.

Many important parts of this thesis could only be realized due to successful collaborations. Therefore, I owe my gratitude to Birgit Kunert and Prof. Roland Resel for their support concerning XRD-Analysis, DI Wernfried Haas and Prof. Ferdinand Hofer for electron microscopic investigations and Dr. Heinz Amenitsch for the support concerning GIWAXS analysis. For XPS measurements I would like to thank DI Matthias Edler and Prof. Wolfgang Kern and for the support concerning DLS-analysis I am grateful to Mag. Angela Chemelli and Prof. Otto Glatter.

Financial support by the Christian Doppler Research Association and the Austrian Federal Ministry of Economy, Family and Youth, FFG, and ISOVOLTAIC AG is gratefully acknowledged.

My deepest gratitude is dedicated to my family and especially to Angela, who supported and motivated me all over the time. This thesis would not have been possible without you!

## Abstract

Nanocomposite solar cells consist of a mixture of organic and inorganic semiconductors and hence combine the benefits of two classes of materials such as the simple solution based processing of polymers and the tuning of the electronic and optical properties of nanoparticles by changing their size and shape. In recent years our working group has developed in-situ preparation techniques for inorganic nanoparticles within polymer matrices using soluble, thermally convertible precursors with the intent to obtain pure inorganic phases.

The first part of this work is focused on the investigation of poly(p-phenylene vinylene)/copper indium sulfide (PPV/CIS) solar cells which were prepared via the thermal conversion of precursor materials for the donor as well as the acceptor material. The emphasis was set on temperature resolved investigations of the formation of CIS within the PPV matrix using GIWAXS analysis with synchrotron radiation. In addition a series of PPV/CIS solar cells was prepared to prove the reproducibility of this type of nanocomposite solar cells.

In the second part new poly(2,7-silafluorene-4,7-di(2'-thienyl))-2,1,3-benzothiadiazole (PSiFDBT)/CIS solar cells are prepared and the investigation and evaluation of various processing parameters resulting in power conversion efficiencies up to 2.8 % is shown. CIS was formed via thermal decomposition of respective metal xanthates, which are known to release only volatile byproducts and therefore result in very pure inorganic nanoparticles. For the preparation of this type of solar cells blends of PSiFDBT and xanthates, dissolved in an appropriate solvent, were coated onto glass/ITO/PEDOT:PSS substrates, followed by a mild thermal conversion step (200 °C) and were completed via deposition of the back electrodes.

The emphasis of the third part is placed on the synthesis of metal salts of dialkyldithiocarbamates in order to obtain alternative precursors to the xanthates, concerning the formation of CIS. Although these precursor materials were not suitable for nanocomposite solar cells, due to their high decomposition temperatures up to 350 °C, they were used for the formation of inorganic semiconducting metal sulfides (CIS and CZTS), which could be applied in thin film solar cells. The formation of the nanostructured semiconducting materials was

investigated using XRD-analysis. In addition, the CZTS layers were studied via TEM, TEM-EDX, XPS, Raman and UV-vis analyses.

## Kurzfassung

Nanokomposit-Solarzellen bestehen aus einer Mischung von organischen und anorganischen Halbleitermaterialien und verbinden somit die Vorteile von zwei Materialklassen. Einerseits können diese Zellen durch die verwendeten Polymere auf einfache Weise mittels Lösungen hergestellt werden, andererseits können die elektronischen und optischen Eigenschaften der anorganischen Nanopartikel variiert werden, indem ihre Größe und Form verändert wird. In letzter Zeit hat sich unsere Arbeitsgruppe mit der In-situ-Herstellung von anorganischen Nanopartikeln in einer Polymermatrix beschäftigt und dabei lösliche und thermisch umwandelbare Ausgangsstoffe verwendet.

Der erste Teil dieser Arbeit behandelt die Untersuchung von Poly(p-phenylen-vinylen)/Kupfer-Indium-Sulfid PPV/CIS Solarzellen, die durch thermische Umwandlung von Ausgangsstoffen sowohl für das Donor- als auch das Akzeptormaterial hergestellt wurden. Der Schwerpunkt liegt auf einer temperaturlösten Untersuchung der CIS-Bildung innerhalb einer PPV-Matrix. Hierfür wurden GIWAXS-Analysen mittels Synchrotronstrahlung durchgeführt. Überdies wurde eine Serie von PPV/CIS Solarzellen hergestellt, um die Reproduzierbarkeit dieses Solarzellentyps zu bewerten.

Der zweite Teil dieser Arbeit befasst sich mit neuen Poly(2,7-silafluoren-4,7-di(2'-thienyl)-2,1,3-benzothiadiazol (PSiFDBT)/CIS Solarzellen und zeigt die Untersuchungen und Optimierungen von unterschiedlichen Prozessparametern, welche zu Zelleffizienzen von 2,8 % führen konnten. CIS wurde hierbei mittels thermischer Umsetzung von Xanthaten hergestellt, welche dafür bekannt sind, dass nur flüchtige Nebenprodukte bei ihrer Zersetzung entstehen und somit sehr reine anorganische Nanopartikel gebildet werden können. Diese Art von Solarzellen wird aus Lösungen von PSiFDBT und den jeweiligen Xanthaten hergestellt. Diese werden auf Glas/ITO/PEDOT:PSS-Substrate aufgebracht und thermisch bei 200 °C umgewandelt. Abschließend werden noch Rückelektroden aufgedampft, um die Solarzellen zu vollenden.

Der dritte Teil hat seinen Schwerpunkt auf der Synthese von Metall-Dialkyldithiocarbamaten, um zusätzlich zu den Xanthaten alternative Ausgangsstoffe für die CIS-Bildung zu erhalten. Obwohl es sich herausstellte, dass diese Ausgangsstoffe aufgrund ihrer hohen

Zersetzungstemperatur (bis zu 350 °C) nicht in Nanokomposit-Solarzellen verwendet werden können, wurden sie zur Herstellung von anorganischen Metallsulfiden benützt (Halbleitermaterialien: CIS und CZTS), die in Dünnschicht-Solarzellen ihre Anwendung finden könnten. Die Bildung der nanostrukturierten Halbleitermaterialien wurde mittels XRD-Analyse untersucht. Zusätzlich wurden die CZTS-Schichten noch mittels TEM, TEM-EDX, XPS, Raman- und UV-vis Spektroskopie analysiert.



## Index:

1	Preface.....	1
1.1	World's energy demand .....	1
1.2	Photovoltaics .....	2
1.3	Aims of this thesis.....	3
2	Basics .....	4
2.1	Nanocomposite solar cells.....	4
2.2	State of the art of nanocomposite solar cells.....	4
2.3	Direct formation of nanoparticles within the polymer matrix.....	6
2.4	Device architecture and operational mechanisms.....	7
2.4.1	General mechanism for nanocomposite solar cells.....	7
2.4.2	Single layer assembly .....	8
2.4.3	Bilayer assembly .....	9
2.4.4	Bulk heterojunction assembly.....	10
2.5	Characteristic solar cell parameters .....	12
2.6	Solar cell materials.....	14
2.6.1	Requirements for beneficial solar cell materials .....	14
2.6.2	Conjugated polymers .....	14
2.6.3	Copper indium sulfide .....	16
2.6.4	Copper zinc tin sulfide (CZTS).....	17
3	Results and discussions .....	18
3.1	Polymer/CIS nanocomposite solar cells .....	18
3.2	PPV/CIS nanocomposite solar cells .....	19
3.2.1	Introduction.....	19
3.2.2	Results and discussion.....	20
3.2.3	Conclusion .....	26
3.3	PSiFDBT/CIS nanocomposite solar cells using new metal xanthates .....	27
3.3.1	Precursor materials .....	27
3.3.2	Precursor route to nanocomposite solar cells .....	28

3.3.3	Aim .....	29
3.3.4	Results and discussions .....	30
3.3.5	Conclusion .....	69
3.4	Preparation of inorganic semiconductor materials using metal salts of dialkyldithiocarbamates .....	70
3.4.1	Dialkyldithiocarbamates.....	70
3.4.2	Formation of copper indium sulfide.....	73
3.4.3	Formation of copper zinc tin sulfide thin layers .....	78
4	Experimental part.....	90
4.1	Chemicals and materials.....	90
4.2	PPV/CIS – nanocomposite solar cells .....	91
4.2.1	Preparation of PPV/CIS solar cells.....	91
4.2.2	Preparation of the samples for Grazing Incidence Wide Angle X-ray Scattering (GIWAXS) analysis.....	91
4.3	PSiFDBT/CIS – nanocomposite solar cells.....	92
4.3.1	General preparation of nanocomposite solar cells.....	92
4.3.2	Pretreatment of the ITO substrates .....	93
4.3.3	Preparation of the samples for Grazing Incidence Wide Angle X-ray Scattering (GIWAXS) analysis.....	94
4.3.4	Iterative improvement of the efficiency of polymer/CIS solar cells .....	95
4.3.5	Iterative improvement of the efficiency of PSiFDBT/CIS solar cells .....	98
4.3.6	Sample preparation for TEM EDX analysis .....	104
4.4	Synthesis of metal-dialkyldithiocarbamates .....	106
4.4.1	Sodium diallyldithiocarbamate .....	106
4.4.2	Sodium dihexyldithiocarbamate .....	107
4.4.3	Sodium dibenzylthiocarbamate .....	108
4.4.4	Syntheses of metal dialkyldithiocarbamates .....	109
4.5	Preparation of CIS layers via metal-dialkyldithiocarbamates .....	114
4.6	Preparation of CZTS layers.....	115
4.7	Characterization techniques.....	117
4.7.1	X-ray powder diffraction analysis.....	117

4.7.2	Scanning electron microscopy (SEM) .....	117
4.7.3	Transmission electron microscopy (TEM) .....	117
4.7.4	Raman spectroscopy .....	118
4.7.5	Reflectance and transmission measurements .....	119
4.7.6	Surface profiler .....	119
4.7.7	X-Ray photoelectron spectroscopy .....	119
4.7.8	Elemental analysis .....	119
4.7.9	Fourier transform infrared spectroscopy (FTIR) .....	119
4.7.10	Nuclear magnetic resonance spectroscopy (NMR).....	120
4.7.11	Dynamic light scattering analysis (DLS).....	120
4.7.12	I-V characterization .....	120
4.7.13	IPCE measurements.....	120
4.7.14	Contact angle analysis .....	121
4.7.15	Grazing Incidence Wide Angle X-ray Scattering (GIWAXS) analysis.....	121
5	Summary and outlook .....	122
6	Bibliography.....	126
7	List of figures .....	134
8	List of tables .....	138
9	List of publications .....	140
10	Curriculum vitae .....	142

# 1 Preface

## 1.1 World's energy demand

Development of civilization is accompanied by constantly increasing demand for energy. Although energy consumption decreased in 2009 (-1.1 %) for the first time in thirty years due to financial crisis, an energy consumption growth of 5 % was reached in 2010. Today, world's energy consumption exceeds 400 EJ and more than 80 % of this energy is still generated via the combustion of fossil fuels, [1][2] (see Figure 1) which increases the formation of greenhouse gas and consequently contributes to the global warming.

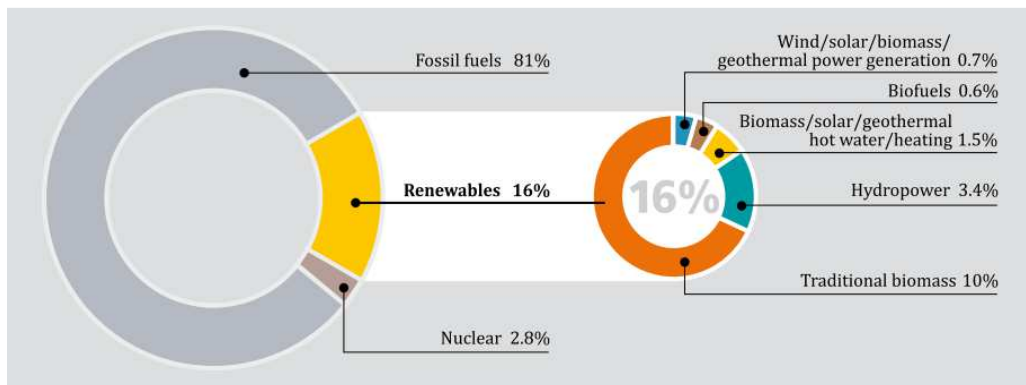


Figure 1: Energy share of global energy consumption[2]

However, decreasing resources of fossil fuels and increasing environmental consciousness regarding the greenhouse gas effect caused by CO<sub>2</sub> have opened the market for alternative energy suppliers such as traditional biomass, hydropower, wind, geothermal and solar power. Today, more people than ever before derive energy from renewables and as capacity continues to grow, prices continue to fall and consequently shares of global energy from renewable energies can increase. [2]

## 1.2 Photovoltaics

Supply of energy from the sun to the earth is about  $3 \cdot 10^{24}$  joules, which exceeds world's current energy consumption 10,000 times. [3] Thus, a very small fraction (less than 0.02%) of solar power available on earth could supply energy for the entire demand. However, photovoltaic technology is still too expensive to be competitive to other primary energy sources. [4] This is why a lot of work has to be done to reduce production costs and to enhance the performance of solar cell devices.

The first generation of solar cells stands for single junction devices mostly consisting of single crystal- or multi crystalline silicon. Power conversion efficiencies up to 25 % could be reached, [5] which is quite close to the theoretical limit for single junction devices of about 30 %. [6] Production costs of this type of solar cells still exceed a competitive level. The second generation of solar cells tries to fight high prices of the first generation. In this context thin film solar cells are produced using materials such as  $\text{CuInGaSe}_2$ ,  $\text{CuInS}_2$ ,  $\text{CdS}$ ,  $\text{CdTe}$  and amorphous silicon deposited on cheap substrates. Good absorption behavior of these binary and ternary metal sulfides as well as a high number of usable production techniques compatible to large scale fabrication have attracted considerable interest. Although the preparation of thin film solar cells can decrease the production costs, prices are still too high to be competitive to primary energy suppliers. Organic solar cells belong to the third generation of photovoltaic devices and use low cost materials such as conjugated polymers or small molecules. These materials enable the fabrication of solution processable solar cells compatible to large scale production techniques. However, these solar cells show only moderate cell performances compared to the first and second generation of solar cells. Solarmer Energy, Inc., for instance, pointed out a power conversion efficiency of 8.13 % [7] and Heliatek as well as Konarka of 8.3 % [8][9][10], whereas the best results for polymer solar cells, published in literature, range between 6 and 7.4 %. [11][12][13][14] (Dye sensitized solar cells are not considered in this work.) These polymer solar cells were prepared with blends of low band gap polymers and soluble fullerene derivatives. Although most of scientific interest is dedicated to this type of organic photovoltaic, the introduction of inorganic semiconductor nanoparticles instead of fullerenes shows some very interesting benefits. It combines the advantages of two classes of

materials such as the simple solution based processing of the conjugated polymers and the possibility of tuning the electrical and optical properties of the inorganic nanoparticles by their size and shape. Although power conversion efficiencies of these hybrid nanocomposite solar cells are still quite low compared to polymer fullerene devices, they have started to reach promising results [15][16][17], and consequently could become an alternative to the leader of the organic photovoltaic.

### **1.3 Aims of this thesis**

Subject of this work was the preparation and characterization of polymer nanocomposite solar cells and inorganic semiconductor materials. In this thesis polymer nanocomposite solar cells stand for hybrid solar cells consisting of a polymer as donor material and chalcopyrite nanoparticles as acceptor material.

The scientific work, summarized in this thesis, is divided into three main topics:

- A detailed in-situ GIWAXS analysis on the formation of PPV/CIS (Poly(p-phenylenevinylene)/copper indium sulfide) solar cells, which have already been the topic of previous theses at our institute, was performed.[18][19][20] The active layers of the solar cells were prepared via thermal conversion of a polymer precursor, respective metal salts and thioacetamide.
- Preparation and characterization of PSiFDBT/CIS (poly(2,7-silafluorene-4,7-di(2'-thienyl)-2,1,3-benzothiadiazole)/copper indium sulfide) solar cells is described in the subsequent chapter. CIS nanoparticles within the polymer matrix are prepared via the thermal conversion of copper and indium salts of O-2,2-dimethylpentan-3-yl dithiocarbonate (Cu- and, In-xanthate(heptyl)).
- Investigation of metal dialkyldithiocarbamates as alternative precursors for nanocomposite solar cells. In this context, the synthesis, thermal decomposition and preparation of CIS and CZTS layers, using the respective metal dialkyldithiocarbamates, were studied.

## **2 Basics**

### **2.1 Nanocomposite solar cells**

Nanocomposite solar cells, also called hybrid solar cells, belong to a new class of solar cell devices and contain conducting polymers as donor materials and inorganic nanoparticles as acceptor materials, which are sandwiched between two electrodes such as indium tin oxide (ITO) and aluminum.

### **2.2 State of the art of nanocomposite solar cells**

The founding stone for solar cells was laid in 1839, when Alexandre Edmond Becquerel and his father Antoine Cesar Becquerel discovered the photovoltaic effect while experimenting with electrodes and electrolyte solutions. They could observe the development of voltage depending on incident light. [21][22]

A key point of the field of organic electronics was in 1977, when Heeger, MacDiarmid, and Shirakawa discovered that the conductivity of polyacetylene, which is a conjugated polymer, could be increased tremendously due to oxidation with iodine.[23] Further milestones for the development of organic photovoltaic were the introduction of a bilayer heterojunction assembly by Tang et al., who obtained solar cells having power conversion efficiencies of about 1 % (in 1986) [24] and the first publication of rectifying heterojunctions of polymers and so-called buckminsterfullerenes in 1993.[25] From that time onwards the power conversion efficiencies of polymer fullerene solar cells could be considerably improved reaching values for devices on the laboratory scale of more than 8 %. [9][8][7] In comparison to polymer fullerene solar cells nanocomposite solar cells show nearly the same working principle (see page 7). However, instead of fullerene derivatives inorganic nanoparticles are used as acceptor materials. Thus, advantages of two classes of materials could be combined such as the simple solution based processing of the conjugated polymers and the possibility of tuning the inorganic nanoparticles in size and shape. Based on the quantum size effect,[26][27] the band gap of nanoparticles and consequently their energy levels can be varied by tuning the diameter of the nanoparticles. This is a powerful tool for the design of efficient solar cell devices. Series of

inorganic semiconducting materials have been applied in nanocomposite solar cells. Binary materials such as zinc oxide, [28][29][30][31][32][33] titanium oxide,[34][35][36][37][38] lead sulfide, [39][40][17] zinc sulfide [41], ferrous sulfide [42] and cadmium sulfides/selenides/telurides [43][44][45][46][47][48][15][49][50][16] were commonly used for preparation. In addition, copper indium sulfides/selenides, which belong to ternary semiconductor materials, were used as well.[51][52][53] The best efficiencies, published, were achieved using a blend of poly[2,6-(4,4-bis-(2-ethylhexyl)-4H-cyclopenta[2,1-b;3,4-b']dithiophene)-alt-4,7-(2,1,3-benzothiadiazole)] (PCPDTBT) and cadmium selenide tetrapods, which are branched particles of the inorganic semiconductor. These devices could achieve power conversion efficiencies up to 3.13 %.[15] The assembly of the record devices as well as its certification is depicted in Figure 2.

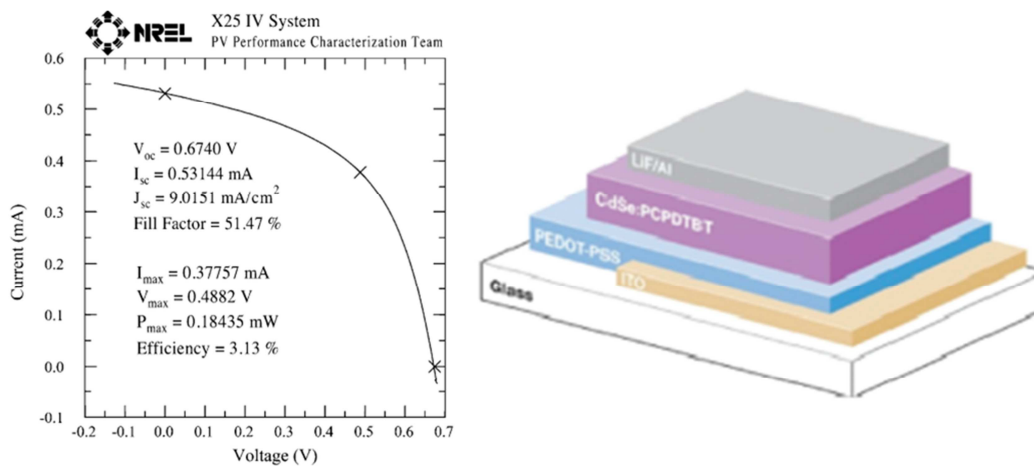


**Figure 2: Efficiency certification from National Renewable Energy Laboratory (left); device assembly [15] of the nanocomposite record device (right)**



## 2.3 Direct formation of nanoparticles within the polymer matrix

Good film forming properties, which are essential for the preparation of efficient solar cells are dependent on the solubility of the nanoparticles. In the classical route capping ligands such as oleic acid and trioctylphosphine oxide (TOPO) are used to keep the nanoparticles in solution. These ligands, however, disturb the electrical connection between the polymer and the nanoparticles and between the nanoparticles itself and consequently reduce solar cell performances.[54] Strategies to increase conductivity are to exchange the capping agents with short-chain ligands (mostly pyridine) and to remove the excessive capping agents. (hexanoic acid treatment)[16][55][56] Further strategies are the use of thermo-cleavable ligands or the synthesis of nanoparticles in polymer solutions without any capping ligands. Prasad et al., for instance, used tert.-butyl N-(2-mercaptoethyl)carbamates surrounding the surface of cadmium selenide nanocrystals. Thermal treatment of the samples led to the decomposition of the carbamate ligands and consequently to a decrease of the ligand sphere. [57] Watt and coworkers showed the direct formation of lead sulfide nanoparticles in poly(2-methoxy-5-(2'-ethyl-hexyloxy)-p-phenylene vinylene) (MEH-PPV). Similar approaches were conducted for other binary nanoparticles [58][49][52]. In addition, the synthesis of copper indium disulfide (CIS) could be realized via a mild thermal conversion step of blends of a conjugated polymer, copper acetate, indium chloride and thiourea. Thermally generated sulfur species react with the  $\text{Cu}^+$  and  $\text{In}^{3+}$  ions of the respective metal salts and lead to the formation of copper indium disulfide within the polymer matrix. [51] This process, however, is accompanied by the formation of non-volatile byproducts and therefore only solar cells showing poor cell performances could be prepared. In order to prevent non-volatile and hence contaminating byproducts Haque and coworkers presented the formation of cadmium sulfide nanoparticles using metal xanthates as precursor materials. [50][59] Metal xanthates are known to decompose at moderate temperatures and to release only volatile byproducts. (carbon oxide sulfide and alkenylic residues) Thus, they are ideal candidates for the formation of highly pure metal sulfide nanoparticles within a polymer matrix. It has to be noted, that our working group has developed a similar xanthate route towards polymer/CIS solar cells, which is topic of the chapter 3.1.

## 2.4 Device architecture and operational mechanisms

Photovoltaic devices absorb and transform light into direct current. The main difference in the working principle of organic photovoltaics and inorganic solar cells is the formation of electron hole pairs, so-called excitons, within the active layer of the organic solar cells, whereas free charge carriers are built within the classical inorganic solar cells. An exciton is a neutral bound state of an excited electron and a positive charge carrier (hole).[60]

### 2.4.1 General mechanism for nanocomposite solar cells

Conversion of light into electric power starts with the absorption of incident photons. As consequence excitons are generated, which diffuse within the active layer. If the excitons arrive at a donor acceptor interface before they can recombine, charge separation leads to the formation of free charge carriers. (For exciton dissociation a driving force is needed, which provides a potential that exceeds the binding energy of the excitons.) Subsequently, electrons are transported via the acceptor material towards the cathode and the holes use the donor material to get to the anode.

In detail this process can be summarized by the following steps. [61][62]

Photon absorption and formation of excitons: Absorption is dependent on the absorption coefficient as well as the layer thickness of the photoactive layer. Many conjugated polymers show band gaps in the range of 2-3 eV. Thus, light of larger wavelengths (> 620 nm) cannot be absorbed. For that reason low band gap materials such as CIS (1.5 eV = 826 nm) are introduced as acceptor materials in nanocomposite solar cells to improve the yield of absorption. The incident light generates electron hole pairs because electrons transit from  $\pi$ -HOMO to  $\pi^*$ -LUMO bands. These electron hole pairs have binding energies up to 0.4 eV [63] and show only limited life times.

Exciton diffusion: These quasi particles diffuse within the active layers as long as no recombination processes, photoluminescence or thermal quenching take place or they do not hit the donor acceptor interface. Since excitons have limited lifetimes and therefore show limited diffusion lengths ( $\approx 10$  nm) ideal designed photovoltaic solar cells should consist of a

large donor/acceptor interface, which enables as many excitons as possible to reach the dissociation site. Thus, interpenetrating comblike structures of the active materials only allowing a maximum diffusion length of 10 nm is thought to be an optimum inner structure for nanocomposite solar cells.[64]

Charge carrier separation: If excitons arrive at the interface of the donor and the acceptor material, they will be separated due to an internal electric field. This means that the offset (the energy difference of the LUMOs of the donor and the acceptor material) has to be bigger than the binding energy of the excitons.

Charge transport: In conjugated polymers typical hopping processes are responsible for charge transport. Localized energy minima (traps), however, reduce the charge mobility. These minima could be a result of impurities or structural defects within the active layer.

Collecting of the charges: The transfer of the charges from the active layer to the respective electrode materials is dependent on the Fermi levels of the electrodes and on the energy levels of the donor's HOMO and the acceptor's LUMO.

### **2.4.2 Single layer assembly**

The first organic photovoltaic devices were based on a single layer junction, in which charge separation occurs at the interface of the light harvesting material and the electrodes. However, only poor power conversion efficiencies could be obtained due to inefficient charge separation at the interfaces. [4][65] The rectifying behavior of single layer devices can be explained by the formation of a Schottky barrier between the p-type organic layer and the metal with the lower work function. At the Schottky junction band bending occurs within the depletion region. This corresponds to an electric field, which is the driving force for dissociation of the excitons. (see Figure 3) [66]

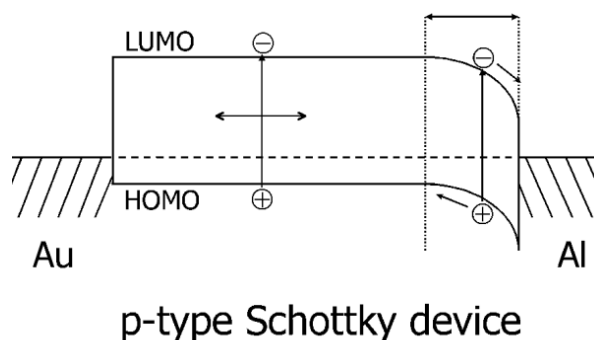


Figure 3: Single layer device with Schottky contact[66]

### 2.4.3 Bilayer assembly

The introduction of a bilayer structure led to considerable improvement of the cell performance, which is the result of the formation of a heterojunction of a donor and an acceptor material similar to the pn-junction in inorganic solar cells. [24] The idea behind the heterojunction is to use two materials having different ionization potentials and electron affinities. Thus, strong potentials arise at the heterojunction. If the offset of the LUMO levels is larger than the binding energy of the excitons, the electrons will be attracted by the material with larger electron affinity, whereas the holes will be accepted to the material with lower ionization potential.(see Figure 4)[67] A big advantage of the bilayer assembly is the monomolecular charge transport. After separation of the excitons, electrons are transported within the n-type material, whereas holes travel within the p-type semiconducting material. Consequently recombination processes are significantly reduced. Bilayer assemblies were produced either by sequential deposition techniques or by a combination of casting and thermal deposition.

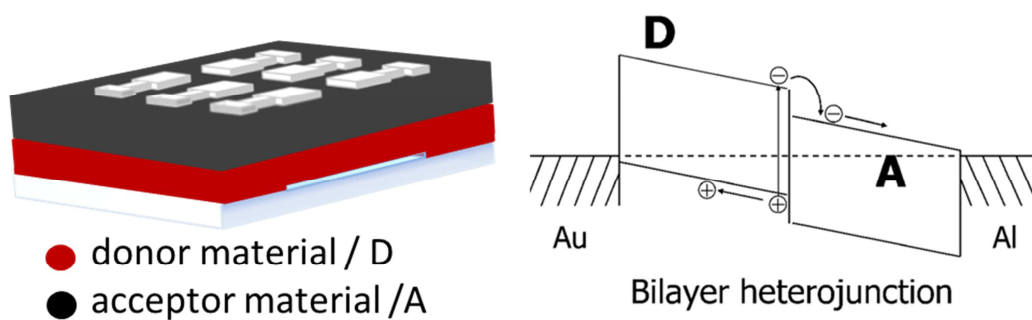


Figure 4: Bilayer heterojunction device (left) working principle for charge separation of a bilayer photovoltaic solar cell (right)[66]

#### 2.4.4 Bulk heterojunction assembly

Since excitons (electron hole pairs) have a limited lifetime and consequently a limited diffusion length (10 nm) only a small fraction of excitons, which are built within the active layer (layer thickness  $\approx$  100 nm) reaches the donor-acceptor-interface and can be separated into free charge carriers using a bilayer assembly. The rest of the electron hole pairs are lost through recombination processes and for that reason photocurrent of this solar cell assembly is quite low. In order to circumvent this limitation donor and acceptor materials were mixed in bulk. Thus, interpenetrating networks of the donor and the acceptor material were built during the formation of the active layer. So the interface could be extended [68][69] and led to more efficient charge separation.

There are also a few drawbacks. Current can only be generated if the separated charges are transported towards the respective electrodes. This means that percolating paths, of the donor material towards the anode and of the acceptor material towards the cathode are needed. Normally, these paths are built due to phase separation of the active materials, which is hard to control in size and shape. Moreover, the dense network of donor and acceptor material increases the possibility for recombination.

However, bulk heterojunction solar cells could achieve high power conversion efficiencies and hence have become accepted to be the most commonly used device assembly for polymer based photovoltaic.

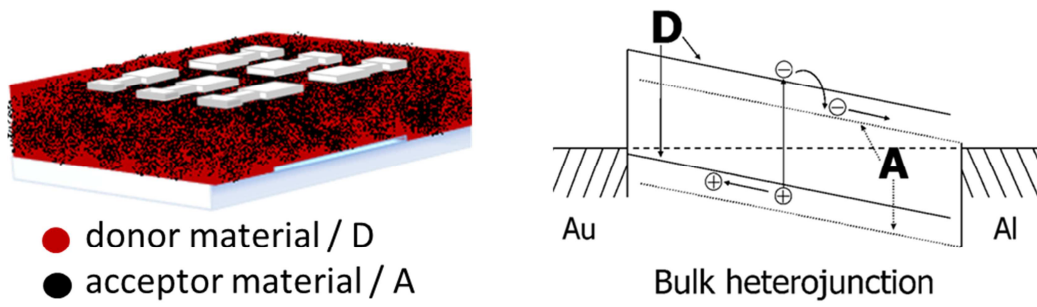


Figure 5: Bulk heterojunction device (left) working principle for charge separation of a bulk heterojunction photovoltaic solar cell (right)[66]

## 2.5 Characteristic solar cell parameters

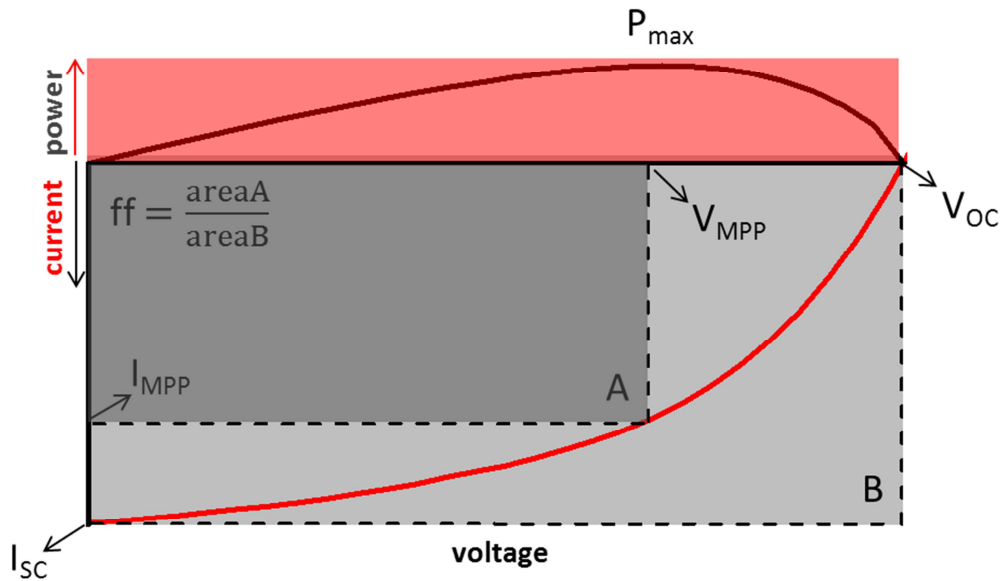


Figure 6: Characteristic solar cell parameters

The electric performance of solar cells can be described by its I-V curves under dark and illuminated conditions. For this purpose current is recorded, while the voltage across the device is varied in a controlled manner using an applied load resistance. Characteristic parameters such as the open circuit voltage ( $V_{OC}$ ), short circuit current ( $I_{SC}$ ), voltage at maximum power point ( $V_{MPP}$ ), current at maximum power point ( $I_{MPP}$ ), fill factor and the power conversion efficiency can be derived from I-V plots under illumination. (see Figure 6)

$V_{OC}$  is measured at zero current output, which is given under flat band conditions. It is mainly determined by the energy difference of the HOMO level of the donor material and the LUMO level of the acceptor material.[70] In addition,  $V_{OC}$  can also be influenced by the work function of the electrode materials.

$I_{SC}$  is recorded at zero applied voltage. This value is mainly influenced by the absorption properties of the active materials, the exciton dissociation and the charge transport.

Photovoltaic solar cells have an operating point where the product of the current ( $I_{MPP}$ ) and the voltage ( $V_{MPP}$ ) results in the maximum power output. This is known as the maximum power point.

The fill factor (ff) is a value, which describes the quality of the diode characteristic. It is defined as the ratio of the maximum obtainable power ( $I_{MPP} * V_{MPP}$ ) to the theoretical obtainable power ( $I_{SC} * V_{OC}$ ).

$$ff = \frac{I_{MPP} * V_{MPP}}{I_{SC} * V_{OC}}$$

The power conversion efficiency (PCE/ $\eta$ ) is defined to be the ratio of the maximum obtainable power to the power of the incident light ( $P_{in}$ ).

$$\eta = \frac{I_{SC} * V_{OC} * ff}{P_{in}} * 100 \% = \frac{I_{MPP} * V_{MPP}}{P_{in}} * 100 \%$$

The incident photon to current efficiency (IPCE), also called external quantum efficiency (EQE), is the percentage of electrons collected per incident photon.[71]  $\lambda$  stands for the respective wavelengths.

$$IPCE = \frac{1240 * I_{SC}}{\lambda * P_{in}}$$

In comparison to the incident photon to current efficiency the internal quantum efficiency describes the ratio of the electron conversion to absorbed photons.



## 2.6 Solar cell materials

### 2.6.1 Requirements for beneficial solar cell materials

A semiconductor can only convert photons with the energy of its band gap in an efficient way. Photons of lower energy cannot be absorbed and photons of higher energy are reduced to band gap energy and lose their excessive energy in thermal processes. Thus, the curve of efficiency versus band gap shows a maximum dependent on the solar radiation spectrum. This is why ideal semiconducting materials should show a direct band gap between 1.1 and 1.7 eV.[72] In addition, they should be composed of cheap, abundant and nontoxic elements and should be compatible to large scale processing techniques.

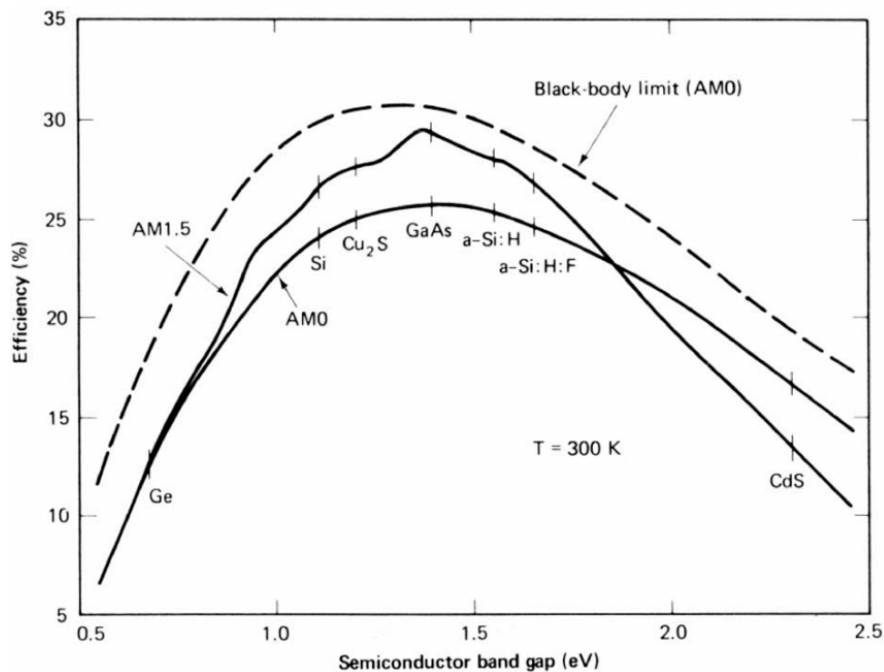


Figure 7: Dependency of the power conversion efficiency versus the band gap[72]

### 2.6.2 Conjugated polymers

The properties of conjugated polymers are based on an extended  $\pi$ -electron system. The overlapping  $p_z$  orbitals, resulting from  $sp^2$  hybridization, form a bonding and an antibonding orbital. The bonding orbital of low energy forms the so-called valence band and the antibonding orbital of high energy forms the conduction band. The band gap is defined to be the difference

in energy between those two orbitals. If light is absorbed by the semiconducting polymer, electrons are lifted from the valence to the conduction band and hence become mobile.

Shirakawa and coworkers were the first to discover this behavior in polyacetylene [23] and hence smoothed the way for a successful development of the conjugated polymers in the field of optoelectronics. They were awarded the Nobel Prize for their scientific work in 2000.

Important conjugated polymers for photovoltaic applications can be categorized into the p-phenylenevinylene-based, the carbazole-based, the thiophene-based, the fluorene-based and the miscellaneous conjugated polymers. At the beginning of the investigation of polymer fullerene solar cells p-phenylenevinylene-based conjugated polymers were mainly used because of the knowledge which had existed due to successful applications in light emitting devices.[73] In recent years, however, more and more low band gap polymers were designed to be able to improve the power conversion efficiencies of organic solar cells.[12][13] For accurate design of conjugated polymers many important parameters have to be considered. Conjugated polymers, which are used in organic photovoltaics, have to possess strong absorption ability, high hole mobility, suitable HOMO-LUMO energy levels, high stability, and good film forming properties.[74]

The optical properties of a conjugated polymer are determined by the energy positions of the HOMO and LUMO energy levels. On the one hand a small band gap ensures a higher yield of absorption but on the other hand the open circuit voltage of organic solar cells is linearly dependent on the built in voltage, which is defined as energy difference between the HOMO energy level of the p-type donor material and LUMO energy level of the n-type acceptor material. In addition, an offset of at least 0.4 eV has to be assured in order to guarantee charge separation at the donor-acceptor interface. This is why the position of the energy levels of the acceptor material has to be kept in mind for accurate designing of low band gap polymers. Since the HOMO/LUMO energy levels of PCBM are quite similar to those of nanocrystalline copper indium disulfide, low band gap polymers, which were designed for polymer fullerene solar cells, should also be compatible to polymer CIS nanocomposite solar cells.

### 2.6.3 Copper indium sulfide

Chalcopyrite structured semiconductor materials are promising candidates for pure inorganic photovoltaic applications. CuInGaS<sub>2</sub> thin film solar cells, for instance, showed promising power conversion efficiencies up to 20 %.[9]

Copper indium disulfide (CIS) belongs to the group of I-III-VI compounds and crystallizes in a tetragonal chalcopyrite structure, which can be derived from the diamond structure and therefore belongs to the adamantane compound family. [75]

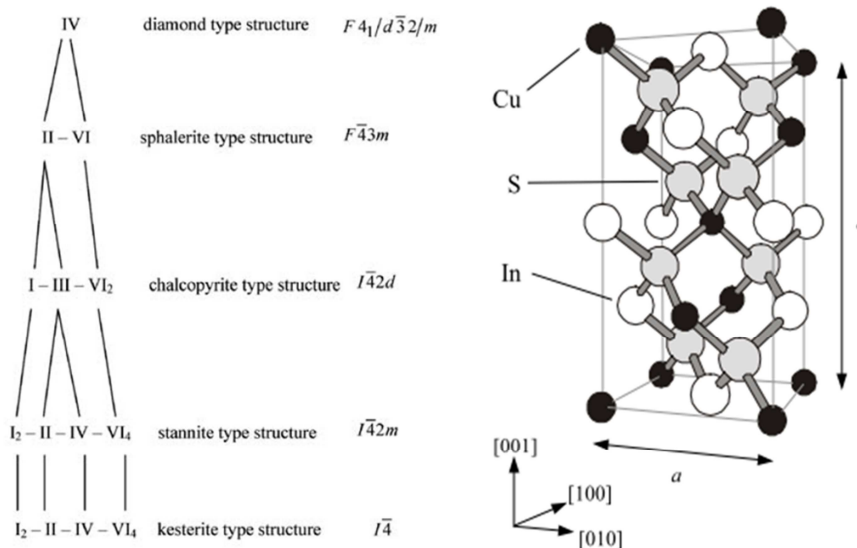


Figure 8: Adamantine compound family (left)[75] chalcopyrite crystal structure of CIS (right)[76]

CIS, which was first synthesized by Hahn et al.,[77] shows a strong absorption ability (absorption coefficient of  $10^5 \text{ cm}^{-1}$ ), an optimum band gap for photovoltaic applications of about 1.5 eV (direct band gap) as well as the ability to show either n-type or p-type semi-conductivity depending on the copper to indium ratio. An excess of indium leads to the formation of a n-type semiconductor, whereas an excess of copper leads to the formation of a p-type semiconductor.[78] There are three polymorphic forms of CIS at different temperatures. Generally CIS crystallizes as chalcopyrite structure up to temperatures of 980 °C, at higher

temperatures phase transitions to zinc blende (980 – 1050 °C) and wurtzite (>1050 °C up to the melting point) are observed. Although most of scientific work is dedicated to the chalcopyrite and zinc blende structure, wurtzite structured CIS could provide interesting benefits for photovoltaic applications. The band gap, for instance, of wurtzite phase of CIS could be tuned over a wide range of energy due to more flexible occupancy of the copper and the indium atoms in the lattice sites. [79]

CIS is mainly used in pure inorganic thin film solar cells, but its optical and electrical properties are also suitable for nanocomposite photovoltaics.

#### **2.6.4 Copper zinc tin sulfide (CZTS)**

Indium is a scarce element on earth's crust and therefore very expensive. To overcome these limitations indium can be replaced by zinc and tin, which are cheap and abundant elements resulting in the formation of CZTS. CZTS is a p-type semiconductor, which also belongs to the adamantine compound family. It has a direct band gap of 1.5 eV, and shows comparable absorption behavior to CIS. [80][81][82] In recent years very promising power conversion efficiencies could be realized. Todorov et al., for instance, demonstrated a hybrid solution particle CZTS approach, which has enabled fabrication of photovoltaic devices with power conversion efficiencies up to 9.7 %. For these devices he used Cu- and Sn-chalcogenides dissolved in hydrazine as well as particle based Zn-chalcogenide precursors obtained by the addition of elemental Zn powder to the tin solution.[83]

## 3 Results and discussions

### 3.1 Polymer/CIS nanocomposite solar cells

In recent years hybrid nanocomposite solar cells have attracted increasing attention and have been studied extensively, which resulted in promising power conversion efficiencies.[15][16][17] This type of solar cells effectively combines the advantages of two classes of materials: a) solution based processing techniques, low consumption of materials and flexibility due to the polymer matrix may allow a fast and inexpensive production of photovoltaic modules on large scale[84]; b) high optical absorbance due to contribution of the conjugated polymer as well as the inorganic nanoparticles[85]; c) the properties, such as band gap, of inorganic nanoparticle semiconductor materials can be varied due to the unique possibilities of tuning them in size and shape.(spherical nanoparticles, tetrapods...)[49][15] Moreover, this approach allows an enormous number of combinations of inorganic and organic semiconductors as active materials for solar cell devices. Examples for blends of conjugated polymers and inorganic semiconductors like CdSe, CdS, CuInS<sub>2</sub>, PbS and ZnS have already been published.[86][87][85][15][16][17][51][52] However, there are also a few drawbacks concerning the solubility of inorganic compounds and the need for stabilizing cappers, which cause a loss of the cell performance, due to contamination of the active materials.

In the last few years, our working group has focused on the development of in-situ preparation methods of inorganic metal sulfides directly within the organic polymer matrix and managed to work out a production procedure to overcome the problems mentioned above. An in-situ formation method of CIS, zinc sulfide and cadmium sulfide nanoparticles within a poly(3-(ethyl-4-butanoate)thiophene) (P3EBT) matrix could be published in literature.[51][52] In these works the binary and ternary metal sulfides were formed by the reaction of the respective metal salts with thiourea or thioacetamide using a mild thermal conversion step (<200 °C). In addition, a precursor route for PPV/CIS solar cells could be developed using precursor materials for both the polymer and the CIS nanoparticles.[19][20]

## 3.2 PPV/CIS nanocomposite solar cells

### 3.2.1 Introduction

The preparation of poly(p-phenylenevinylene) (PPV)/CIS solar cells via thermal conversion of a PPV-precursor material, respective metal salts and thioacetamide is described in this chapter. PPV was the first polymer, which was implicated in organic light emitting diode (OLED) applications [73] and PPV and its derivatives still belong to the most popular conjugated polymers for OLEDs. The HOMO and LUMO levels are reported to be -5.1 and -2.7 eV having a band gap of about 2.4 eV.[88] PPV was first polymerized in the sixties by McDonald and Campbell using a Wittig reaction to obtain the requested product. However, their attempt to convert p-xylylene-bis-(triphenylphosphonium chloride) (Pre-PPV) with therephthalaldehyde to PPV resulted in insoluble products only having very low molecular weights. Wessling et al.[89] introduced a soluble precursor based synthesis route starting the reaction with 1,4-bis(chloromethyl)benzene and tetrahydrothiophene. The Wessling route is depicted in Figure 9.

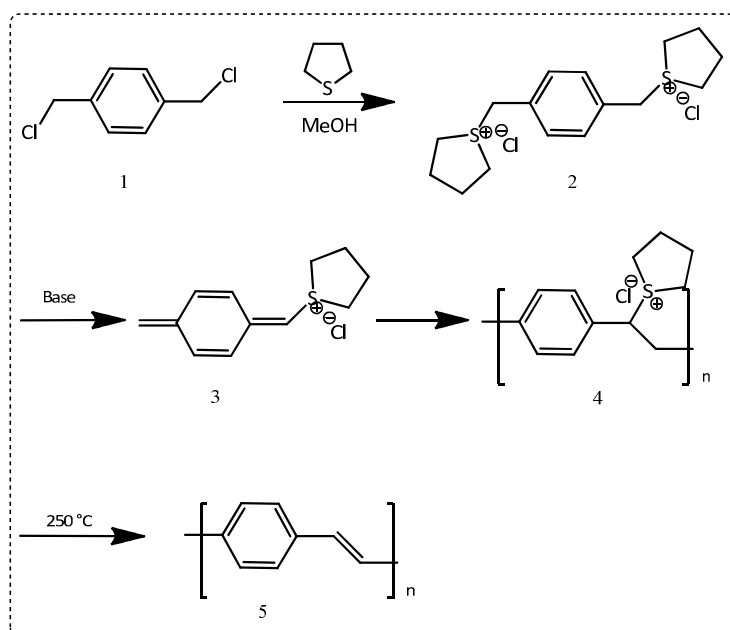


Figure 9: Synthesis of PPV via the Wessling route[74]

The intermediate, the already polymerized Pre-PPV (4), is water soluble, processable and a commercially available precursor material, which can be thermally (250 °C) converted into conjugated PPV. [74] In the meantime, a few more synthesis routes - mostly modified Wessling procedures, using alternative sulfur compounds to tetrahydrothiophene, have been developed to be able to obtain PPV as well as PPV-derivatives. [90][91][92]

Thermo-cleavable precursor polymers such as Pre-PPV, poly-(3-(2-methylhexan-2-yl)-oxy-carbonyldithiophene (P3MHOCT) and a copolymer of a diphenylthienopyrazine and terthiophene (P3TMDCTTP), which can be thermally converted into insoluble and conjugated PPV, polythiophene (PT) and poly(thiophene-2,5-diyl-alt-thieno[3,4-b]pyrazine) (PTTP), result in quite rigid active layers disclosing better crystallinity and structural order compared to conjugated polymers, having solubilizing side chains.[93][94] Using P3HT, for instance, the content of the alkyl side chains, which cannot harvest any photons and consequently do not contribute to the improvement of power conversion efficiencies, can amount to 30-50 % of the polymer material weight. Moreover, the attached alkyl side chains lead to softer active layers and therefore to less stable devices due to morphological effects. Soft layers, for instance, promote materials' diffusion such as diffusion of aluminum, which is a common used electrode material. The opportunity, to consecutively stack several layers without any risk to wipe off a subjacent coating, is an additional benefit of the converted insoluble PPV.

In the last few years, our working group has focused on the development of direct and simple preparation methods for inorganic metal sulfides with intention to be able to obtain pure semiconductor phases such as copper indium sulfide (CIS), copper zinc tin sulfide (CZTS), zinc sulfide and various other metal sulfide semiconductor materials.[95][52][51][96] Making use of this knowledge and the already mentioned properties of Pre-PPV a simple procedure for the preparation of nanocomposite solar cells had been developed at the institute.

### **3.2.2 Results and discussion**

The active layer of these solar cells consists of PPV as donor material and CIS nanoparticles as acceptor material. Figure 10 depicts a device assembly consisting of a transparent indium tin oxide anode, coated onto a glass substrate, a PPV hole transport layer, a bulk heterojunction

active layer and an aluminum cathode. The in-situ formation of PPV as well as CIS nanoparticles within the polymer matrix provides an easy handling and therefore a very effective route to the active material. For the conversion to CIS a blend of copper iodide, indium chloride and thioacetamide (TAA) as sulfur source were used. In this context, TAA thermally decomposes to respective sulfide species and reacts with the metal salts to form CIS. Mechanisms are proposed in the diploma thesis of Santis and the doctoral thesis of Maier.[20][18] In my work complementary experiments were performed to investigate temperature resolved CIS formation using GIWAXS with synchrotron radiation. In addition, reproducibility of the solar cell devices was studied.

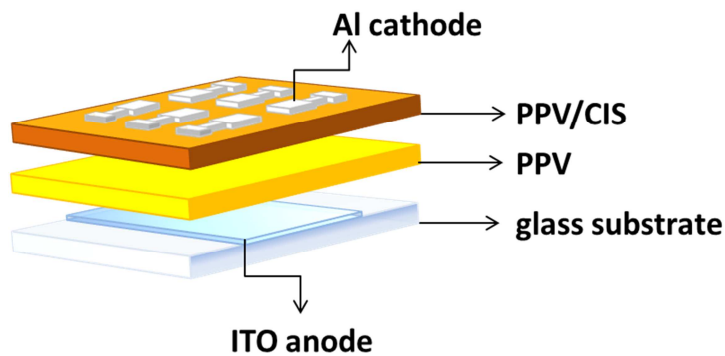


Figure 10: Device assembly of a PPV/CIS nanocomposite solar cell

### 3.2.2.1 Temperature resolved investigation of CIS formation within the polymer matrix

The formation of CIS nanoparticles was investigated using in-situ GIWAXS analysis. In order to be able to simulate the original annealing process during X-ray measurements a special Teflon heating chamber, which allowed the thermal conversion of the precursor layers under inert- and vacuum conditions, was constructed by Dr. Thomas Rath and Hans Schlegl. (see Figure 11)





Figure 11: Special measurement chamber integrated into the GIWAXS measurement set up

Obtained GIWAXS patterns are illustrated in Figure 12. It clearly shows a few sharp peaks at the beginning of the experiment. Although these reflexes cannot be assigned to special compounds, they probably stem from complexes of the metal salts with pyridine or thioacetamide.

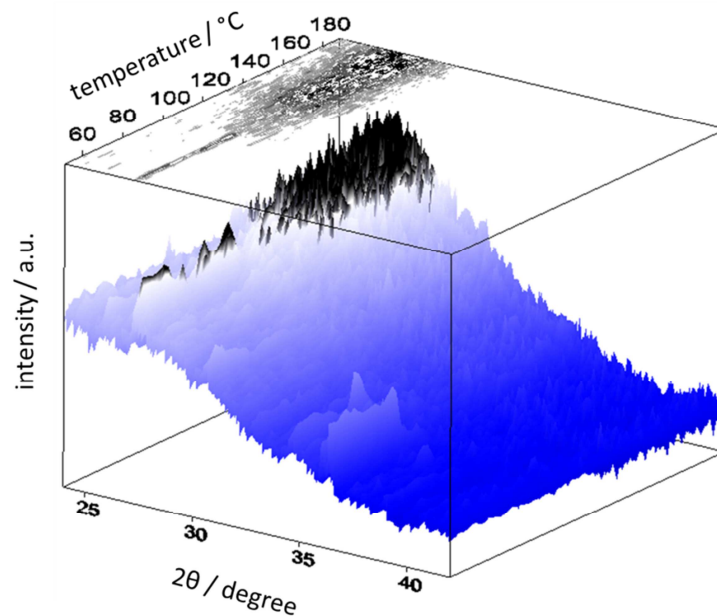
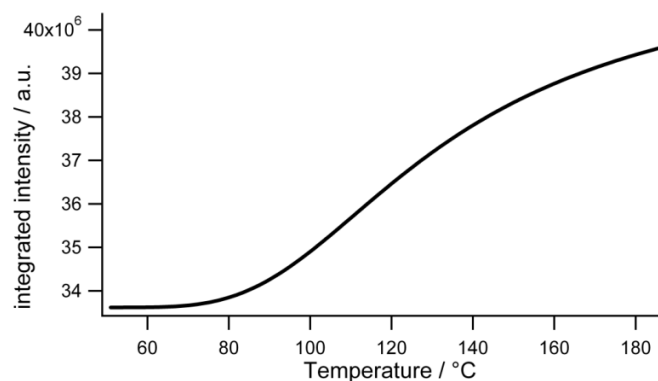


Figure 12: GIWAXS patterns of a PPV/CIS active layer

At temperatures of 90 - 100 °C these peaks start to disappear at once. At the same temperature a very broad peak starts to evolve at 28°, which is conform to the (112) reflex of the CIS chalcopyrite structure. The very broad signal could be attributed to the formation of a quite amorphous phase of CIS nanoparticles.

Lorentz corrected integrated intensity calculated from GIWAXS patterns are plotted versus temperature in the following graph. (see Figure 13)



**Figure 13: Lorentz corrected integrated intensity from 25-32° 2θ versus temperature**

This illustration clearly shows an increase of the integrated intensity, which is having its onset between 80 - 100 °C. Thus, at these temperatures an augmentation of the X-ray scattering takes place, which is attributed to the formation and growth of CIS nanoparticles. The in-situ development of the nanoparticles could be observed and it showed that the conversion of the inorganic precursor materials starts at temperatures of 100 °C. Thus, complete conversion of the inorganic precursor materials can be supposed at temperatures of 250 °C, which are needed to convert Pre-PPV.

### **3.2.2.2 Reproducibility tests**

The active layer of the PPV/CIS solar cells arises from precursor materials of the donor as well as the acceptor material. Therefore a thermal conversion of Pre-PPV, copper iodide, indium chloride and TAA is necessary. Additionally due to thermal decomposition many volatile byproducts are generated such as tetrahydrothiophene, hydrochloric acid, acetic acid and ammonia. Thus, their evaporation is combined with an enormous change of the inner structure

of the coated layers.[18] In order to obtain working solar cells all of these byproducts should be removed from the active layer as they do not contribute to current generation at all. Moreover, these leftovers could cause structural defects as well as energy traps resulting in considerable reduction of the cell performance. Furthermore, an interpenetrating network of CIS nanoparticles within the PPV matrix should be formed developing a preferably large donor acceptor interface to gain high power conversion efficiencies. Neither formation of nanostructured, interpenetrating networks nor total elimination of arising byproducts is easy to handle. There are a few parameters that can be varied in order to preventively influence the formation of the active layer during the thermal conversion step. For instance, alteration of the concentration of the precursor solution, variation of the final ratio of PPV/CIS, addition of surfactants, use of various solvents and regulation of the heating program can be tuned. In this context, the use of different solvents is limited because of Pre-PPV, which is dissolved in water, and the solubility of the metal salts. The remaining parameters have already been optimized and showed best results being produced as described in the experimental part. However, using optimized conditions did not result in constant cell performances. This is why a series of solar cells was prepared to check reproducibility of the PPV/CIS system.

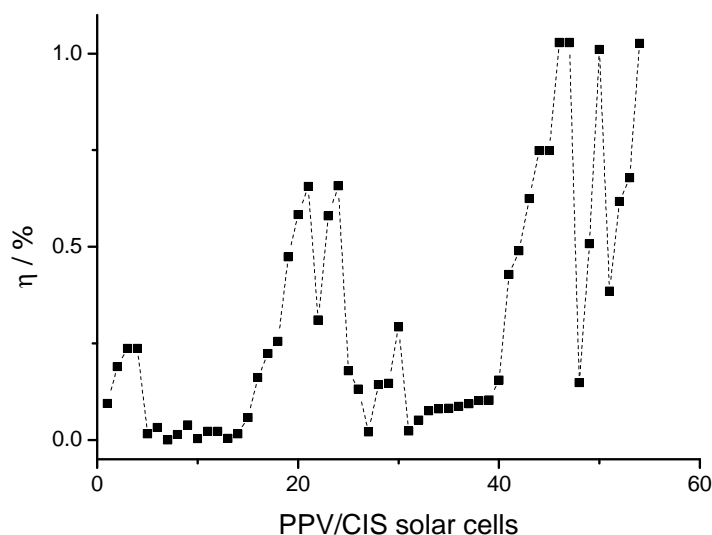


Figure 14: Efficiencies of PPV/CIS solar cells

Figure 14 depicts the efficiencies of more than fifty solar cells. It definitely shows a tremendous variation of the obtained performances of the solar cells, which were all prepared in the same way. Efficiencies up to 1 % could be obtained. A series of parameters, such as temperature and humidity during the coating step strongly influenced the drying of the precursor layer and consequently the formation of the nanostructured network during the thermal conversion step. Thus, it was not possible to reproduce constant efficiencies for PPV/CIS solar cells without further investigations and experiments, which may help to control the drying of the precursor solution and the thermal conversion step. These experiments, however, are beyond the scope of this work.

Besides the finding of poor reproducibility of the devices, a couple of solar cells displayed quite good cell performances up to power conversion efficiencies of 1 %, which is a respectable result for nanocomposite solar cells. (see Figure 15)

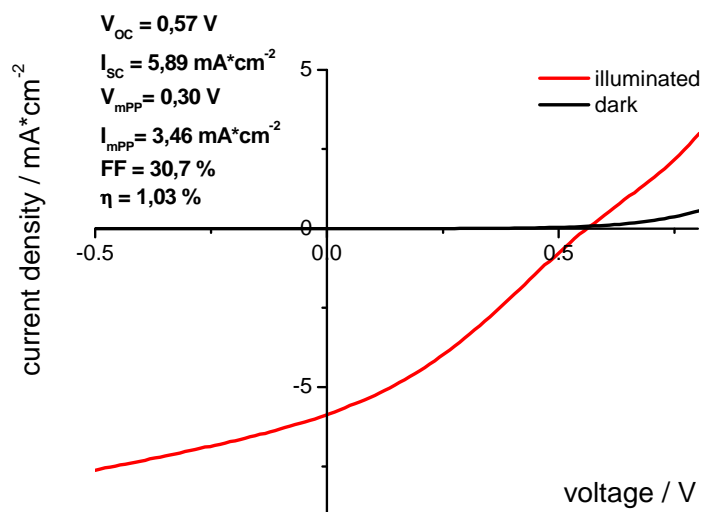


Figure 15: I-V curve of a PPV/CIS solar cell

These solar cell devices showed open circuit voltages ( $V_{oc}$ ) of 0.57 V, current densities ( $I_{sc}$ ) of nearly  $6 \text{ mA/cm}^2$  and a fill factor of about 30 %. The fill factor was quite low compared to other organic photovoltaic systems exhibiting fill factors of 50 – 70 %. (P3HT/PCBM)[97]

Additionally Incident Photon to Current Efficiency (IPCE) analysis was performed to display the ability of PPV/CIS solar cells to convert photons to current depending on the wavelength of the incident light. The results of the IPCE measurement and UV-vis spectra of pure PPV and a pure CIS phase are illustrated in Figure 16. The solar cell produces current at wavelengths lower than 850 nm, which is in accordance to the absorption onset of CIS. PPV starts to absorb light at wavelengths of 500 nm. Since the absorption spectrum was recorded from a thin film layer of PPV the small maximum at a wavelength of 570 nm has to be attributed to interference phenomena. Thus, it clearly shows an additional conversion of photons, which can be assigned to the light absorption of the inorganic nanoparticles.

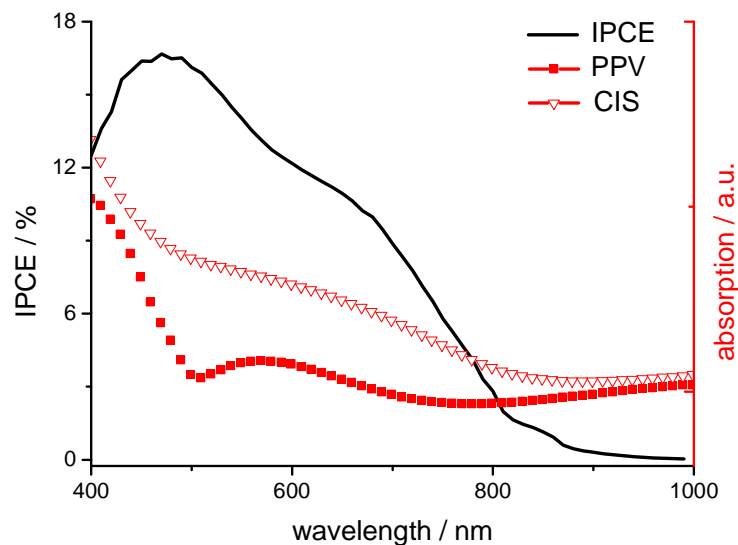


Figure 16: Comparison of the IPCE spectra of a PPV/CIS solar cell and the UV-vis spectra of a PPV and a CIS thin film.

### 3.2.3 Conclusion

Temperature resolved formation of CIS nanoparticles within the PPV matrix was investigated and proved for PPV/CIS solar cells using GIWAXS analysis at the Synchrotron in Trieste. In this

context, it was shown that the inorganic nanoparticles start to evolve at temperatures of 90 - 100 °C. Thus, a complete conversion of the precursor materials should be ensured at temperatures of 250 °C, which were used for the preparation of the PPV/CIS solar cells. Continuing the work of previous colleagues a series of PPV/CIS solar cells was produced in order to check the reproducibility of these devices. These experiments showed good power conversion efficiencies up to 1 %. However, in-situ formation of acceptor as well as donor material seems to be a very complex procedure, as it is described above, and consequently constant reproducibility of device efficiencies was not possible. We suppose that the mixture of three different solvents (water, ethanol and pyridine), which was necessary for the preparation of the precursor solution, as it is described in the experimental part, could be a very critical parameter. Slightest variations of the ingredients could lead to the formation of active layers showing totally different inner structures. For that reason no further investigations were performed and a new nanocomposite solar cell system was introduced.

### **3.3 PSiFDBT/CIS nanocomposite solar cells using new metal xanthates**

#### **3.3.1 Precursor materials**

Metal xanthates (metal dithiocarbonates) as precursor materials proved to be a powerful tool for the formation of pure CIS nanoparticles via the Chugaev rearrangement. [98] All developing side products (carbon oxide sulfide and alkenylic residues) are volatile and evaporate during the thermal conversion step. (see Figure 17)

In parallel to this work, Haque et al. introduced the formation of cadmium sulfide nanocomposite solar cells using a cadmium ethylxanthate pyridine complex. Due to advantages of the copper free direct formation of the inorganic nanoparticles power conversion efficiencies of 2.2 % could be presented. [50,59]

In order to assure solubility in common used non-polar organic solvents, which are compatible to conjugated polymers, a series of xanthates having different alkyl-chains was synthesized. [99] Best solubility in various solvents was obtained by the attachment of dimethylpentan-3-yl residues and consequently copper and indium salts of O-2,2-dimethylpentan-3-yl

dithiocarbonate were used as precursor materials for all the following solar cells. A detailed description of the syntheses of these dithiocarbonates as well as the formation of CIS and corresponding investigations are published in the diploma thesis of Dipl.- Ing. Alexander Schenk. [99]

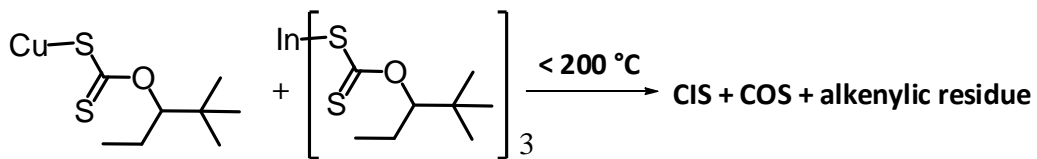


Figure 17: Formation of CIS using metal dithiocarbonates

### 3.3.2 Precursor route to nanocomposite solar cells

To obtain nanocomposite solar cells via the xanthate precursor route a conjugated polymer and the metal xanthates are dissolved in one solution. Afterwards the precursor solution is coated onto a cleaned ITO glass substrate via drop coating, spin coating or doctor blading followed by a mild thermal conversion step, which is necessary for the in-situ formation of pure CIS nanoparticles (acceptor material) within the polymer matrix (donor material). This procedure is depicted in Figure 18. Subsequently back electrodes have to be deposited onto the active layer to complete this type of bulk heterojunction solar cells.

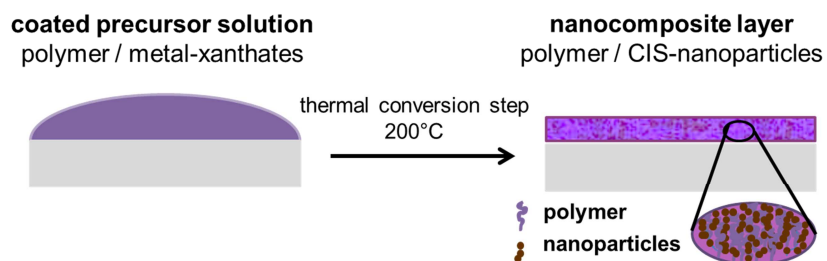


Figure 18: Precursor route to nanocomposite solar cells

### **3.3.3 Aim**

In this chapter various production parameters of polymer/CIS nanocomposite solar cells using the metal xanthate route are investigated. Different donor materials, modified assemblies, diverse compositions of the active materials and varied processing parameters were tested and analyzed to improve the power conversion efficiency of the devices.



### 3.3.4 Results and discussions

#### 3.3.4.1 Pretreatment of Indium tin oxide (ITO) substrates

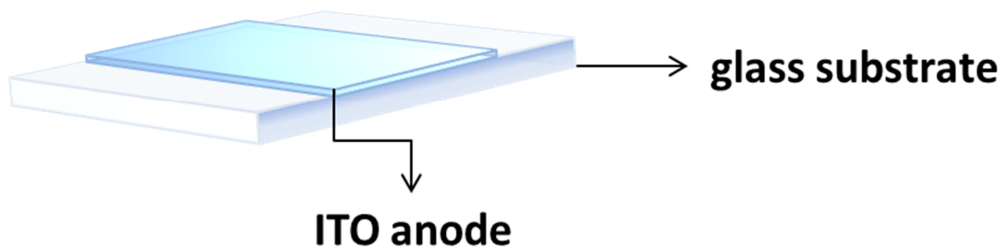


Figure 19: ITO coated glass substrate

ITO is still one of the most commonly used electrode materials for light emitting diodes and photovoltaic applications due to high conductivity [100] and a band gap of about 3.7 eV. [101] The high band gap makes ITO transparent up to near – infrared and of high reflectivity beyond that. [102] A series of experiments was performed to find an adequate pretreatment for ITO coated glass substrates (see Figure 19), which have permanently been used as translucent anode material for our photovoltaic applications. The focus of these experiments was the finding of constant conditions for the wetting of the substrates resulting in good cell performances. Therefore contact angles from ITO-substrates of three different producers using various pretreatments were measured. The results are illustrated in Table 1. Surprisingly, all of the substrates, which had been cleaned in a standardized way using deionized water and isopropyl alcohol ultrasonic baths, showed higher deviations for the contact angles than the original substrates. Moreover, the quite high deviation values indicate a noteworthy inhomogeneity of the commercial purchased ITO substrates and consequently the necessity to find proper pretreatments to guarantee homogeneous working conditions. For this purpose the substrates were treated with potassium hydroxide, hydrochloric acid, aqua regia, nitric acid and

oxygen plasma using modified literature protocols.[103][104][105][106] Short treatments with acids help to flatten the rough ITO surface and consequently influence the wetting behavior of the substrates.

**Table 1: Contact angle of differently pretreated ITO substrates**

<b>substrate / dimension</b>	<b>pretreatment</b>	<b>contact angle</b>	<b>deviation</b>
<b>/mm<sup>2</sup></b>		<b>degree</b>	<b>degree</b>
<b>KINTEC / 24*75</b>	no	57,9	± 0,82
	standard	67	± 6,61
<b>SNP / 24*75</b>	no	64,8	± 1,98
	standard	71,1	± 3,55
<b>DELTA / 24*75</b>	no	78	± 2,24
	standard	64,3	± 7,9
<b>DELTA / 15*15</b>	no	51,9	± 1,64
	KOH	48,3	± 0,68
	HCl 12%	46,4	± 1,2
	HCl/HNO <sub>3</sub> /H <sub>2</sub> O	48,8	± 1,04
	HNO <sub>3</sub> 2M	53	± 3
	plasma	21	± 0,35

All of the etching pretreatments resulted in a decrease of the contact angle of water droplets indicating a better wetting of water based solutions such as commercial available PEDOT:PSS solutions. Oxygen plasma etching showed the biggest change, reaching a contact angle of 21 °, with the smallest deviation. Thus, all further ITO substrates, used, were cleaned with deionized water and isopropyl alcohol followed by an additional oxygen plasma etching step.

### 3.3.4.2 Introduction of a PEDOT:PSS hole transport layer

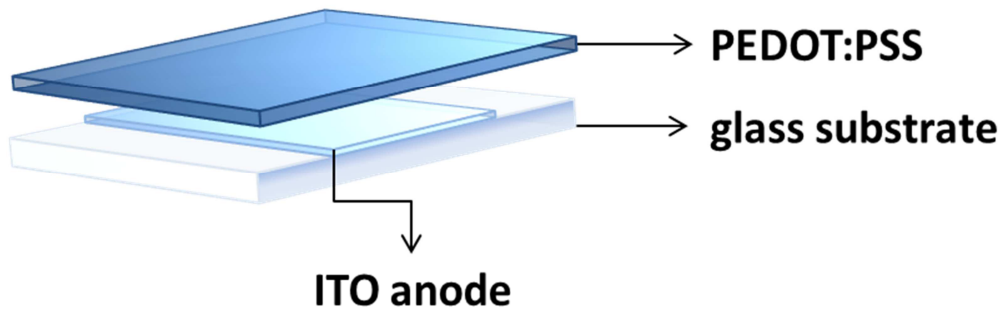


Figure 20: PEDOT:PSS hole transport layer

Poly(3,4-ethylenedioxythiophene)/poly(4-styrenesulfonate) (PEDOT:PSS) is widely used in the fabrication of organic photovoltaic applications. The polymer interlayer (see Figure 20), which is generally inserted between the translucent ITO electrode and the active layer, has two main functions. It prevents a direct contact between the anode and the active material in order to suppress degradation due to interactions of these two materials and it works as hole transport layer lowering the barrier height and thus, favoring the injection of holes. [107] In addition, PEDOT:PSS seems to have a beneficial influence for the wetting of overlying polymer layers. Solar cells made of PSiFDBT as donor material and CIS as acceptor material, for instance, only resulted in reasonable efficiencies with an additional PEDOT:PSS interlayer. (see Figure 21) Devices without PEDOT:PSS showed I-V curves, which are typical for shorted cell devices. As a consequence all of the following solar cells were made with an additional PEDOT:PSS hole transport layer.

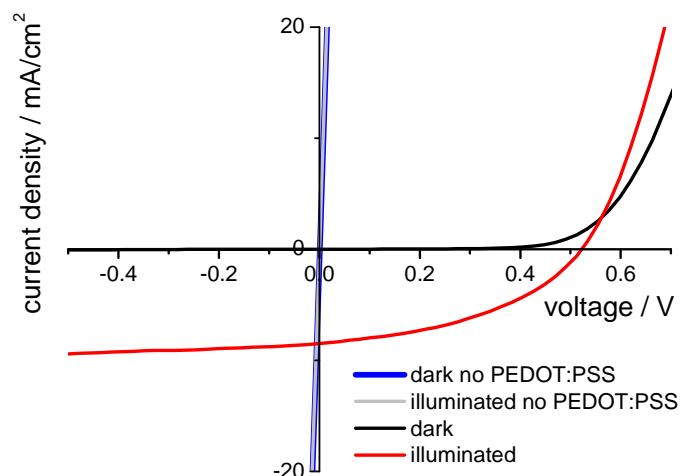


Figure 21: Comparison of I-V curves of solar cells with and without PEDOT:PSS interlayer

### 3.3.4.3 Dynamic light scattering analysis (DLS) of the precursor solutions

Since particles in precursor solutions cause inhomogeneous coatings the formation of agglomerates should be avoided. This is why the solubility of the ingredients and the aging of the solution has been investigated. The formation of agglomerates in precursor solutions, consisting of poly(2-methoxy-5-(3'-7'-dimethyloctyloxy)-1,4-phenylenevinylene) (MDMO-PPV) copper- and indium xanthates, was analyzed using dynamic light scattering. DLS is commonly used for determination of hydrodynamic radii of polymers and nanoparticles. Fluctuation of the intensity of the scattered light can be related to the velocity of the moving particles in the solution. Thus, the diffusion coefficient can be determined and hydrodynamic radii are estimated using the Stokes Einstein relation. For the DLS measurements a red laser (632.8 nm) was taken in order to diminish absorption effects. Absorption of the laser induces a warm up of the solution and consequently pretends the presence of smaller hydrodynamic radii.

Filters were used in order to reduce absorption as it is shown in Figure 22. The black curve (DLS measurement of a polymer/xanthate solution using a strong filter) showed less absorption activity than the red curve (weak filter). However, reduction of absorption owing to filters is

combined to a loss of signal intensity and this is why a little absorption had to be accepted to obtain usable results.

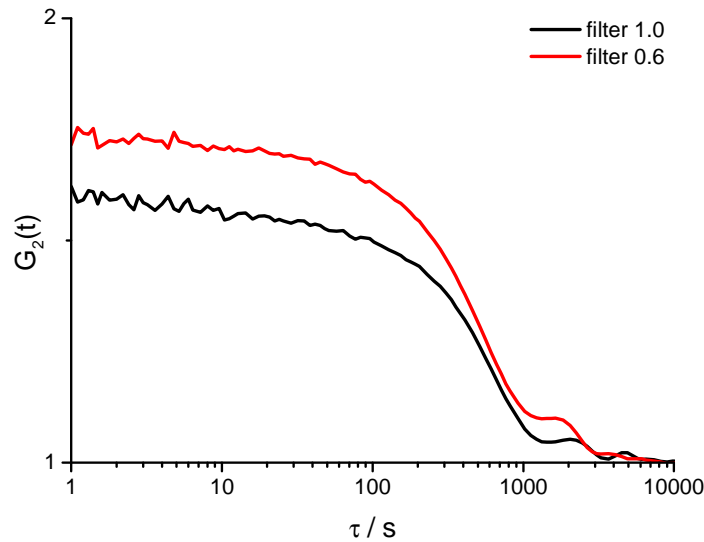


**Figure 22: Influence of absorption of the laser light on the DLS measurements**

Three types of precursor solutions were investigated. These solutions consisting of MDMO-PPV and copper-/indium O-2,2-dimethylpentan-3-yl dithiocarbonate (Cu-/In- xanthate(heptyl)) or copper-/indium O-3,3-dimethylbutan-2-yl dithiocarbonate (Cu-/In- xanthate(hexyl)) were dissolved either in chloroform or chlorobenzene. The results are depicted in the following Figure 23. It clearly shows that solutions of copper and indium xanthate(hexyl) form larger agglomerates than precursor solutions made of xanthate(heptyl). In addition, there is a considerable increase of the xanthate(hexyl) agglomerates, which were stirred for 22 hours, indicating aging of these solutions. Precursor solutions containing xanthate(heptyl) agglomerates showed only a slightly increasing trend of the growth of the hydrodynamic radii, which means that these solutions should be quite stable within 24 hours. In this context, the presence of MDMO-PPV as polymer matrix did not have any influence on the agglomeration of the precursor materials. Resulting from these investigations the use of Cu-/In-xanthate(heptyl)

as precursor materials and chlorobenzene as solvent was chosen for further experiments due to better stability of the precursor solutions.

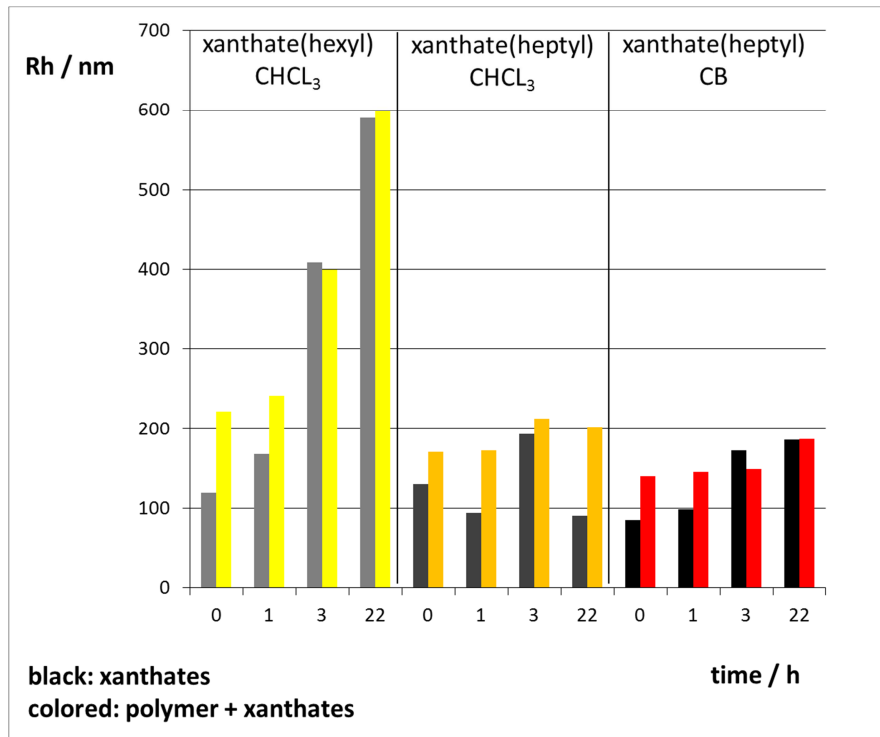


Figure 23: DLS results of the respective precursor solutions

### 3.3.4.4 Comparison of various conjugated polymers as donor materials

Five different, conjugated polymers were chosen to prepare solar cell devices using the metal xanthate route. An alternating copolymer of 2,7-silaflorene and 4,7-di(2'-thienyl)-2,1,3-benzothiadiazole (PSiFDBT); Poly[(4,4'-bis(2-ethylhexyl)-dithieno[3,2-b:2',3'-d]silole)-2,6-diyl-alt-(2,1,3-benzothiadiazole)4,7-diyl] PSBTBT; Poly[(9,9-dioctylfluorenyl-2,7-diyl)-co-bithiophene] (F8T2); Poly[(9,9-dioctylfluorenyl-2,7-diyl)-alt-(2,5dimethyl-1,4-phenylene)] (PFDMB); Poly[(9,9-N-dihexyl-2,7-flourene-alt-9-phenyl-3,6-carbazole) (FPC) were investigated and their application in nanocomposite solar cells was evaluated. The structures of the polymers are depicted in Figure 24.

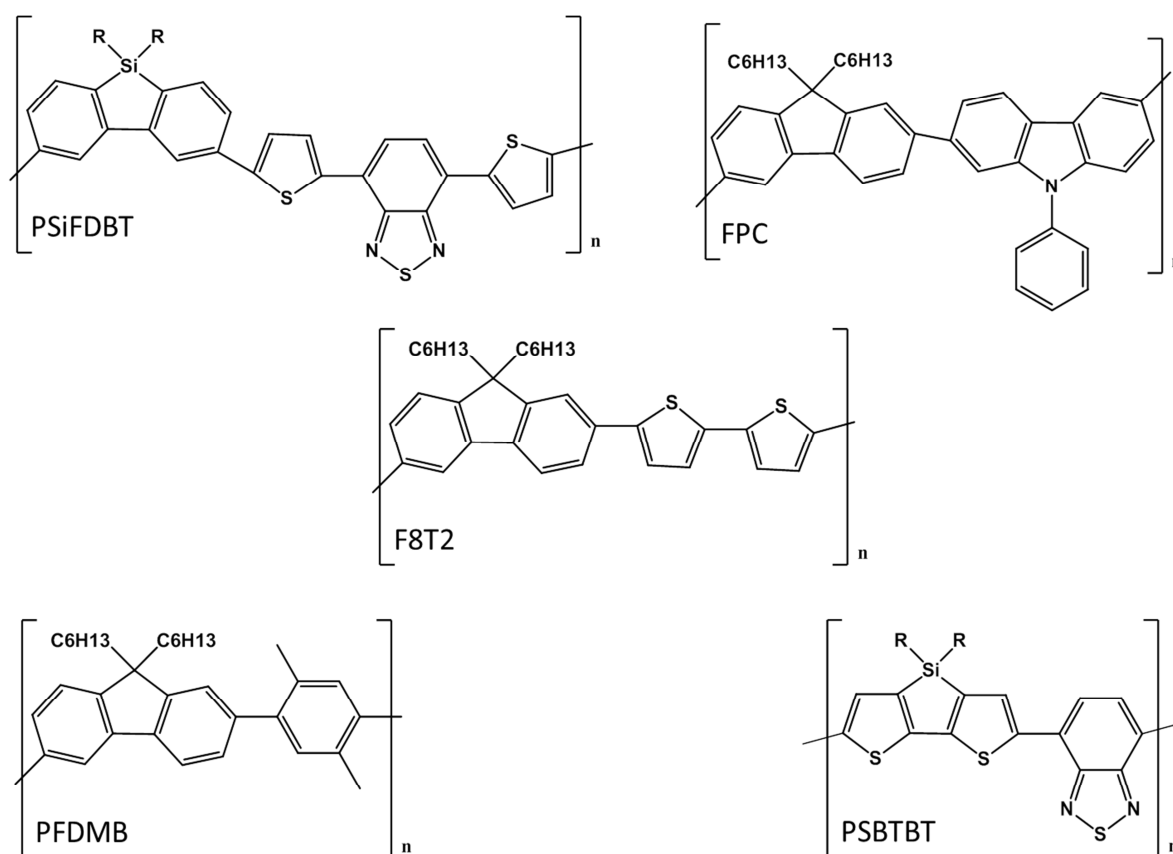


Figure 24: Chemical structures of conjugated polymers, which were tested in polymer/CIS nanocomposite solar cells.

F8T2 was chosen because of enhanced stability in the presence of moisture and oxygen.[108] FPC and PFDMB are polyfluorene derivatives, which are known to show high open circuit voltages in combination with proper acceptor materials.[109] PSiFDBT and PSBTBT are low band gap polymers, which could already achieve power conversion efficiencies of more than 5 % with PCBM derivatives as acceptor phase. [110][111][112] Thus, they are perfect candidates to check the potential of the direct precursor route for the preparation of nanocomposite solar cells. Data for optical properties as well as molar mass averages are listed in the following table. (Table 2) PSiFDBT and PSBTBT have very low band gaps and consequently they offer beneficial absorption properties in the visible range of light. PSBTBT and FPC attract attention because of their low number average molar mass ( $M_n$ ), which makes these polymers more soluble. In addition PSiFDBT and F8T2 show a bimodal distribution of the molecular weights indicating the presence of short as well as long conjugated polymers chains.

**Table 2: Properties of conjugated polymers** [113][110][114][111][115][74][116]

<b>polymer</b>	<b><math>M_n</math> (PDI)</b>	<b>HOMO</b>	<b>LUMO</b>	<b><math>E_g</math></b>	<b><math>\lambda_{max}</math></b>
	g/mol (-)	eV	eV	eV	nm
<b>PSiFDBT</b>	2540 (1.6) / 60910 (2.6)	-5.39	-3.57	1.82	535
<b>PFDMB</b>	27659 (2.7)	-5.4	-2.6	2.8	330
<b>PSBTBT</b>	8500 (2.9)	-5.05	-3.27	1.53 - 1.78	655
<b>F8T2</b>	12400 (1.4) / 90844 (1.33)	-5.41	-2.52	2.89	447
<b>FPC</b>	4778 (1.9)	-5.1	-1.8	3.3	333

The HOMO and LUMO levels of each polymer and of nano- as well as microcrystalline CIS are illustrated in Figure 25. In combination with the energy levels of CIS all polymers show the obligatory offset, which is the driving force for charge separation at the interface of the donor and the acceptor material. Thus, all of the polymers should be compatible to CIS in order to prepare working nanocomposite solar cells. In addition, the formation of interface defects and traps within the CIS phase during the thermal conversion step may influence the energy levels of CIS as well.



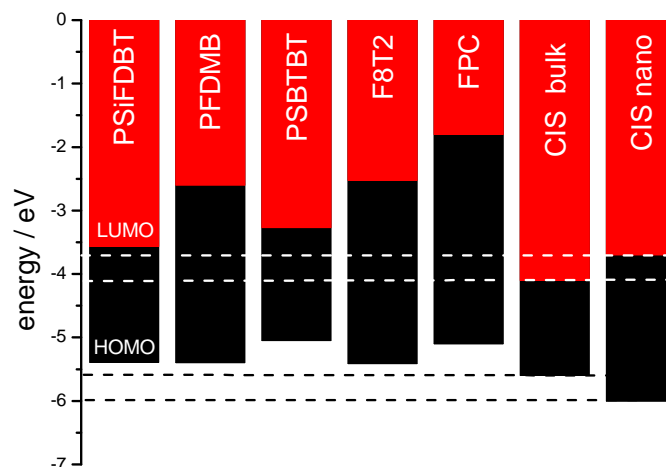


Figure 25: HOMO and LUMO levels of the active materials

It is difficult to compare solar cells having different donor materials, because each of the polymers has unique properties. That is why lots of parameters, such as solubility and viscosity of the coating solution, concentration, ratio of donor to acceptor material, wetting, behavior during the thermal conversion step, thickness of the active layer, etc., have to be considered and adopted to the respective conjugated polymer and the assembling of the photovoltaic device. Consequently, a simple comparison of solar cells, which were exactly made the same way, would not provide any comparable results. This is why in this work for each conjugated polymer proper working conditions had to be figured out in order to compare only the best solar cell performances of the respective polymers and hence to be able to evaluate them.

#### 3.3.4.4.1 Solar cell preparation:

The device structure of the solar cells is depicted in Figure 26. ITO coated glass substrates were cleaned using deionized water and isopropanol followed by an oxygen plasma treatment. As hole transport layer a thin PEDOT:PSS layer was coated onto the ITO substrate and thermally treated on a heating plate at 150 °C for 10 minutes under inert conditions. As active layer a blend of the respective polymer, Cu- xanthate(heptyl) and In- xanthate(heptyl) was dissolved

either in chloroform, dichlorobenzene or chlorobenzene. This production step was modified using various concentrations, donor to acceptor ratios, solvents and initial weights of the ingredients to find proper compositions of the precursor materials resulting in the formation of highly efficient active layers. The respective solutions were coated onto the PEDOT:PSS layer using various adjustments of doctor blading to modify the thickness of the active layer. The thermal conversion was performed in a tube furnace heating the device up to 200 °C using a heating rate of 29 °C/min and holding the temperature for 15 minutes. The whole process was performed under vacuum conditions. Subsequently, aluminum electrodes were evaporated onto the active layer to complete the solar cell device.

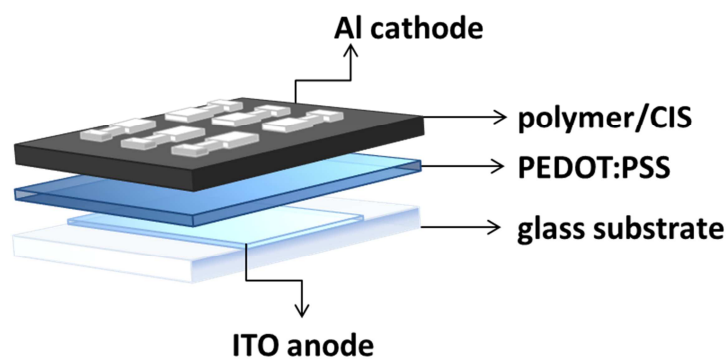


**Figure 26: Device assembly of a polymer/CIS nanocomposite solar cell**

A series of FPC/CIS and PFDMP/CIS solar cells were prepared using various donor/acceptor ratios. However, these solar cells only revealed very moderate power conversion efficiencies in combination with CIS as acceptor material and did not show much more than a diode characteristic. For the best results a chloroform solution consisting of a polymer concentration of 6 mg/mL was used. A donor to acceptor ratio of 1/4 and a copper to indium ratio of 1/1.7, which were confirmed in previous experiments to be the best ratio for the formation of indium rich and highly efficient CIS nanoparticles within the polymer matrix were used in all the experiments. The thickness of the active layers was determined taking a surface profiler and seemed to deliver the best results for active layers of about 100 – 150 nm.

F8T2 resulted in solar cells obtaining power conversion efficiencies of 0.5 %. Interestingly, the concentration of the precursor solution for the best device was 10 mg/mL of F8T2 needing a donor to acceptor ratio of 1/4. As a result of the more concentrated precursor solution layer thicknesses of more than 200 nm were determined for the best devices. In addition, a very thin interlayer of gold (1-5 nm), sandwiched between the active layer and the aluminum electrode could slightly enhance the cell performance.

The two low band gap polymers (PSBTBT and PSiFDBT) revealed power conversion efficiencies of 0.4 and 1.04 %, respectively. Both polymers showed the best results within this series of experiments with a precursor solution having a polymer concentration of 5 mg/ml, a donor to acceptor ratio of 1/7 and a copper xanthate(heptyl) to indium xanthate(heptyl) ratio of 1/1.7. Ideal active layer thickness was determined to be about 100 nm. Results of this study are summarized in Table 3 and complement I-V curves of the best solar cells of the respective polymers as depicted in Figure 27.

**Table 3: Characteristic parameters for various polymer/CIS nanocomposite solar cells**

<b>solar cell</b>	<b>Voc</b>	<b>Jsc</b>	<b>Vmpp</b>	<b>Jmpp</b>	<b>fill factor</b>	<b>efficiency</b>
	V	mA/cm <sup>2</sup>	V	mA/cm <sup>2</sup>	%	%
<b>FPC/CIS</b>	0.23	0.18	0.12	0.97	27.9	0.012
<b>PFDMB/CIS</b>	0.21	0.361	0.115	0.18	27.9	0.022
<b>F8T2/CIS</b>	0.42	3.66	0.24	2.14	33.3	0.51
<b>PSBTBT/CIS</b>	0.36	3.20	0.20	2.02	35.01	0.40
<b>PSiFDBT/CIS</b>	0.405	6.85	0.25	4.10	37.49	1.04

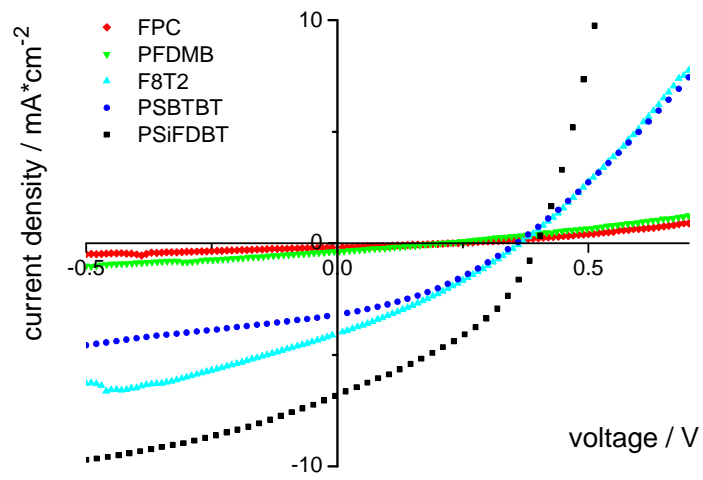


Figure 27: I-V curves of the respective polymers

The comparison of different polymers as donor materials pointed out that especially PSiFDBT seems to be a promising donor material in combination with CIS as acceptor material. Further experiments using the beneficial properties of PSiFDBT were performed in order to achieve an improvement of the device performance.

### 3.3.4.5 PSiFDBT/CIS nanocomposite solar cells

PSiFDBT is a low band gap polymer, which could already achieve power conversion efficiencies of more than 5 % with PCBM derivatives as acceptor phase. [110] Properties of PSiFDBT are illustrated in Table 2. In addition, thermal stability of PSiFDBT was analyzed using a STA apparatus, which enables simultaneous application of thermogravimetry and differential scanning calorimetry. (see Figure 28) The up and downturns of the measurement concerning the low temperature region up to 120 °C can be attributed to the measurement set up. A first real mass loss, which indicates the starting point of the decomposition of PSiFDBT was observed at a temperature of 330 °C, which is far beyond the used conversion temperature of about 200°C. Thus, this conjugated polymer is a suitable candidate for the preparation of nanocomposite solar cells via the in-situ formation of CIS particles within the polymer matrix.

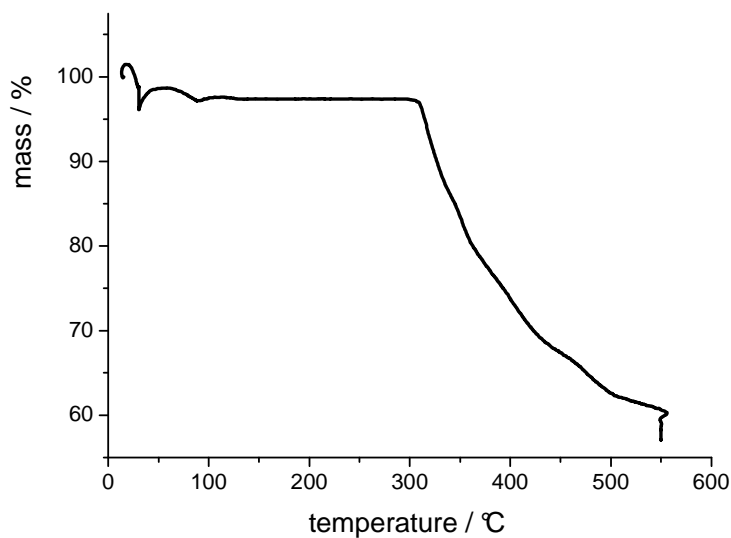


Figure 28: Thermogravimetric analysis of PSiFDBT, showing the mass loss vs. temperature

In the following chapter the formation of CIS nanoparticles, using copper and indium salt of O-2,2-dimethylpentan-3-yl dithiocarbonate, within a PSiFDBT matrix is described. Complementary investigations are presented in the diploma thesis of Dipl.-Ing. Alexander Schenk.[99]

### 3.3.4.5.1 Temperature resolved investigation of CIS formation within the polymer matrix

The formation of CIS using copper and indium salts of xanthate(heptyl) within a PSiFDBT matrix were investigated doing GIWAXS analysis with Synchrotron radiation. During these experiments the standard heating process was simulated, using a special Teflon chamber (depicted in chapter 3.2.2.1), to get reliable results.

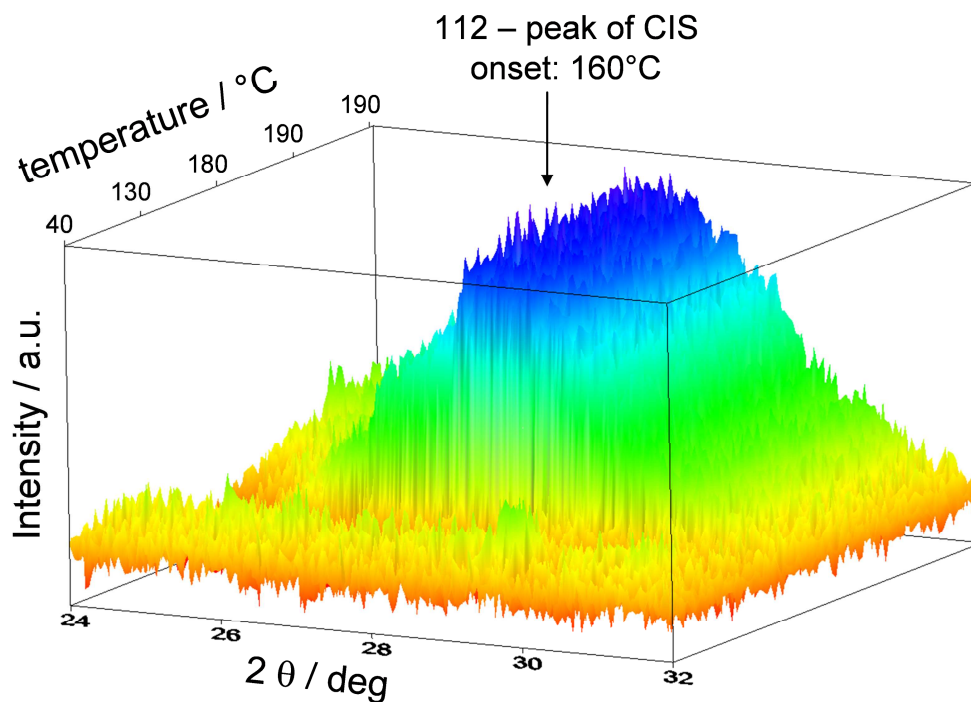


Figure 29: GIWAXS patterns of a PSiFDBT/CIS device, showing the formation of CIS via the xanthate precursor route

Obtained GIWAXS patterns are depicted in Figure 29. It shows an abrupt evolvement of an intensive reflex at 28°, which is conform to the (112) reflex of CIS chalcopyrite structure at 160 °C. The very broad signal could be attributed to the formation of a nanocrystalline CIS phase.

The integrated intensity, calculated from GIWAXS patterns, is illustrated in the following graph (Figure 30). It clearly displays a steep increase of intensity at 160 °C and consequently indicates quick formation of the CIS nanoparticles too.

Although CIS nanoparticles start to grow at temperatures of about 160 °C, for the preparation of all the solar cell devices a conversion temperature of 200 °C was chosen, in order to promote the evaporation of evolving byproducts and to ensure a total conversion of the precursor materials. Thus, pure phases of the inorganic materials can be realized and consequently a smaller amount of defects is built within the active layers. In addition, 200 °C do not destruct the conjugated polymer and could even positively influence the formation of an interpenetrating network, due to effects of phase separation.

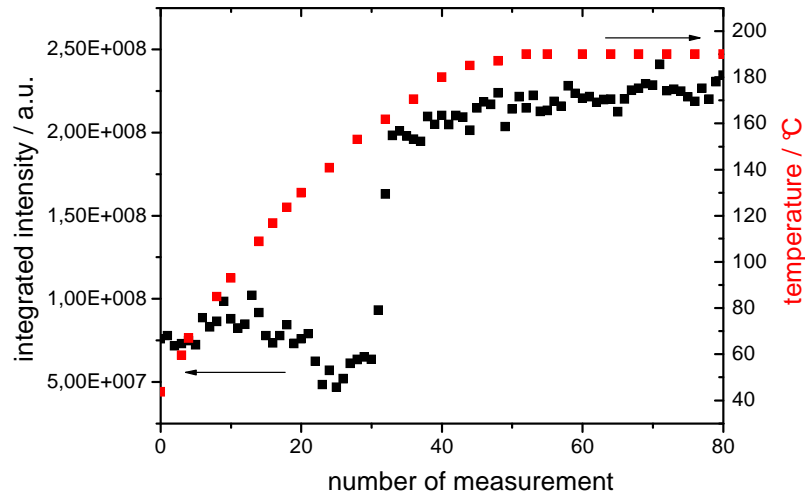


Figure 30: Integrated intensity calculated from the GIWAXS patterns in the range between 24 and 32 ° 2 $\theta$ .

Figure 31 depicts the primary crystallite size of the CIS nanoparticles. These values were determined using Scherrer equation and disclose crystallite sizes for CIS of 1.5 nm at the starting point of the formation of the nanoparticles. Subsequently, the particles grow until they reach a constant primary crystallite size of 2-2.5 nm. The constant values for the primary crystallite size are obtained when the final conversion temperature of 190-200 °C is reached.

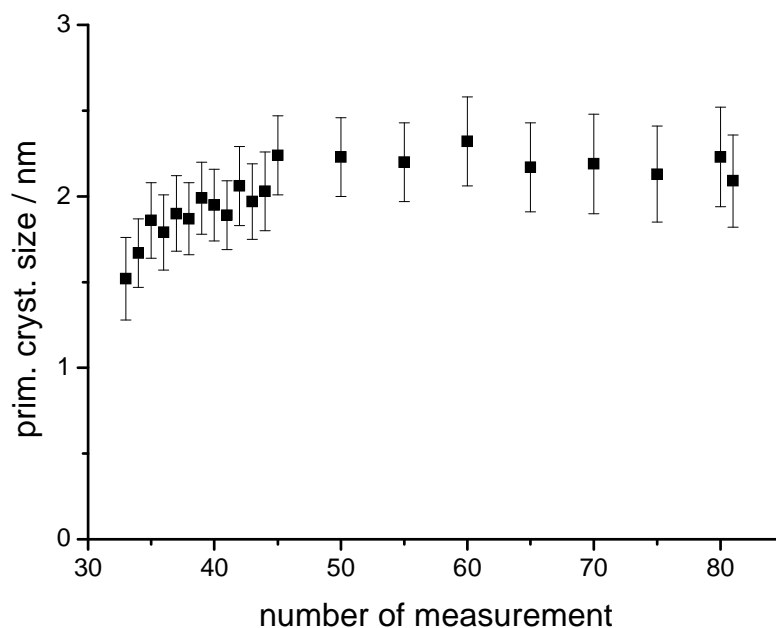


Figure 31: Determination of the primary crystallite size of the CIS nanoparticles using the Scherrer equation (Lorentz fit 24-32° 2θ)

### 3.3.4.5.2 Improvement of the performance of PSiFDBT/CIS solar cells

In the following chapter variations in production of the cell devices are described, which were done with intent to improve the performance of PSiFDBT/CIS solar cells. However, most of the modifications relate to changes of the production of the active layer. The treatment of ITO substrates, the coating and treatment of PEDOT:PSS interlayer and the evaporation of the back electrodes were kept as it is described above.

It has to be considered, that the thermal conversion step after the coating of the active solutions causes an enormous change of the deposited layer due to decomposition of the precursor materials followed by evaporation of volatile byproducts and excessive amounts of solvent. In this context, it is noteworthy that changes of the annealing temperature and especially changes of the reduced pressure, which is used during the heating step, would have a significant influence on thickness and final composition of the active materials, owing to different physical properties of the precursor materials. (see page 59) In addition, variations of



the concentration of the precursor solutions would influence the whole coating step too, affecting fluid viscosity and surface tension.

#### 3.3.4.5.2.1 1 step coating versus 2-step coating of the active layer

The introduction of a two-step coating procedure for the active layer revealed astonishing results. The power conversion efficiency could be considerably improved up to 2 %. After the deposition of the first precursor solution, which consisted of a chlorobenzene solution having a donor to acceptor ratio of 1/7, a copper xanthate(heptyl) to indium xanthate(heptyl) ratio of 1/1.7 and a polymer concentration of 5 mg/ml, onto the PEDOT:PSS coated ITO substrate the device was dried at 50 °C using a heating plate. Subsequently the second precursor solution, consisting of a chlorobenzene solution of a donor to acceptor ratio of 1/10, a copper xanthate(heptyl) to indium xanthate(heptyl) ratio of 1/1.7 and a polymer concentration of 2.5 mg/ml, was coated onto the device using doctor blading. The higher concentration of the second precursor solution should induce a gradient of the active materials within the active layer. Subsequently, thermal conversion was done via standard annealing procedure and followed by evaporation of aluminum electrodes. The device assembly is illustrated in Figure 32.

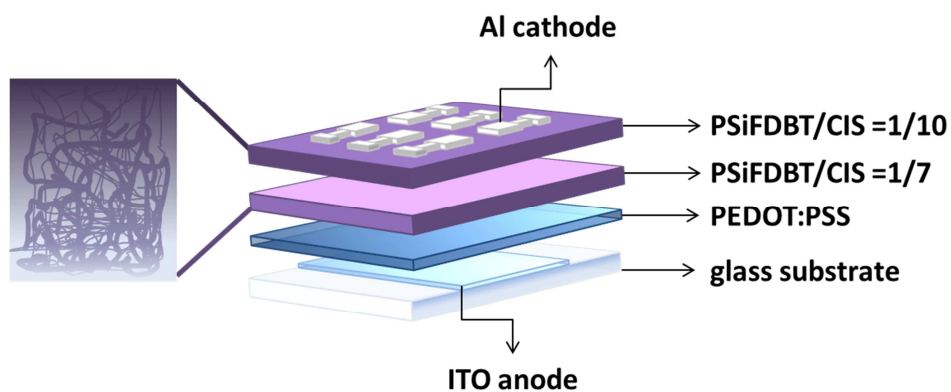


Figure 32: Device assembly of a PSiFDBT/CIS nanocomposite solar cell (two-step coating procedure)

The additional coating step led to an improvement of all characteristic cell parameters. Compared to the best results of the classical one-step coating assembly, first experiments using

the two-step coating assembly gained an improvement of the current density of more than 2 mA/cm<sup>2</sup>, an enhanced open circuit voltage and a slightly better fill factor resulting in an augmentation of the power conversion efficiency of approximately 70 %. (see Figure 33) Improvements obtained, using a two-step coating assembly, could be the result of the formation of a gradient concerning the concentrations of the active materials. An augmented accumulation of the donor material (PSiFDBT) close to the ITO anode as well as higher concentrations of CIS nanoparticles close to aluminum cathode seem to approximate a gradient of the active materials, which is known from literature to reveal good results for photovoltaic applications. In this structure the advantages of bilayer and bulk heterojunction solar cells are combined. On the one hand there is a big donor/acceptor interface, which enables efficient exciton dissociation and on the other hand this structure shows higher charge mobility owing to more ordered layers close to the electrodes. However, it has to be mentioned that the coating of two different precursor solutions did not result in the formation of two separate active layers. Transmission electron microscopy analysis confirmed the formation of only one active layer. (see page 56)

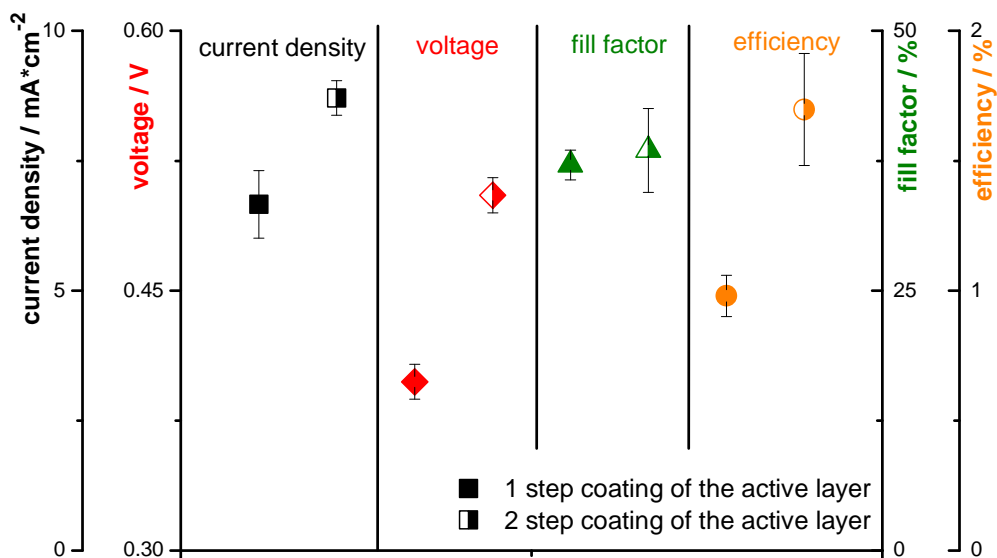


Figure 33: Comparison of solar cell parameters of a one- and a two-step coating process

#### 3.3.4.5.2.2 Investigation of coating parameters

In this chapter influences of different processing conditions during the coating process are discussed. In course of these experiments coating speed, thickness of the wet active layer and substrate temperatures have been varied and analyzed, whereas remaining processing parameters (cleaning of the substrates, coating and treatment of the PEDOT:PSS electron blocking layer, concentration of the precursor solutions, two-step coating of the active material (see page 46), temperature profile and reduced pressure during the thermal conversion step and deposition of the back electrodes) were not modified in order to prevent adulteration of obtained results. To be able to evaluate the respective coating parameters, solar cells were made to compare the characteristic cell parameters. In addition, thicknesses of the already thermally converted active layers were determined, using a surface profiler.

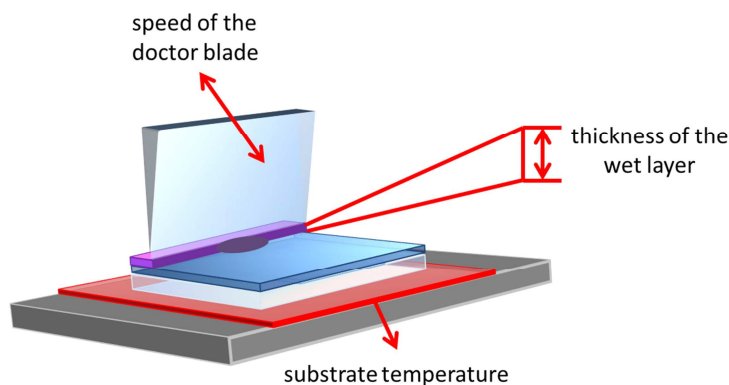


Figure 34: Variation of coating parameters

#### 3.3.4.5.2.3 Variation of the coating speed

Two different coating speeds were investigated for the preparation of solar cells based on the two-step coating procedure. The results of the surface profile analysis, which have been performed of the thermally converted samples, are illustrated in Table 4 and show that a slow coating process forms thinner active layers than a fast one. This finding can be compared to the behavior of layer formation using dip coating. A coating speed of 10 mm/s revealed layer thicknesses of about 150 nm consisting of a PEDOT:PSS layer (approximately 50 nm) and the

active layer having a layer thickness of about 100 nm, which was identified to be ideal for PSiFDBT/CIS nanocomposite solar cells. (see page 53) Using a coating speed of 25 mm/s, active layers of 200 nm were obtained.

Table 4: Thickness of converted layers using two coating speeds (two-step coating procedure)

coating speed	average height	roughness rq
mm/s	nm	nm
10	151	4
25	250	18

Although all of the devices exhibited approximately the same current densities of 7 mA/cm<sup>2</sup> and open circuit voltages of 0.45 V, slowly coated active layers could provide better cell performances due to higher fill factors. In comparison to the fast coated cell devices, which showed values for the fill factor of about 40 %, the slowly coated solar cells could reveal fill factors exceeding 50 %. (see Figure 35)

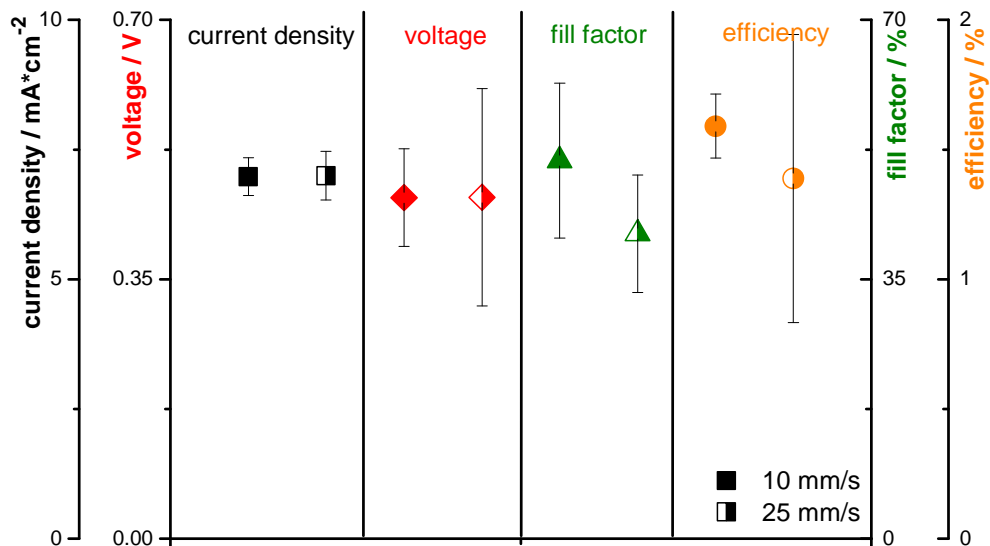


Figure 35: Comparison of characteristic cell parameters resulting from the variation of the coating speed

#### 3.3.4.5.2.4 Variation of the substrate temperature

Since surface tension of fluids and hence the wetting of substrates as well as the drying of the precursor solutions is dependent on temperature, the active materials were coated (two-step coating) onto tempered substrates, using either 30 or 40 or 50 °C. Best cell performances could be reached with a substrate temperature of 40 °C. (see Figure 36) These devices showed the best values for the current density (8 mA/cm<sup>2</sup>) as well as for the open circuit voltage (0.53 V).

**Table 5: Thickness of converted layers using different substrate temperatures (two-step coating procedure)**

<b>temperature</b>	<b>coating speed</b>	<b>average height</b>	<b>roughness rq</b>
°C	mm/s	nm	nm
30	10	151	4
40	10	136	13
50	10	106	5

According to surface profile analysis (Table 5) of the thermally converted active layers, the formation of slightly rougher surfaces could be observed for the samples coated onto substrates of 40°C. However, the observed roughness could be the reason for enhanced cell performances due to a rougher interface of the bulk material and the aluminum cathode, which implies stronger interfacial adhesion and consequently a lower contact resistance.[117] In addition, it could be shown that higher substrate temperatures lead to thinner active layers.

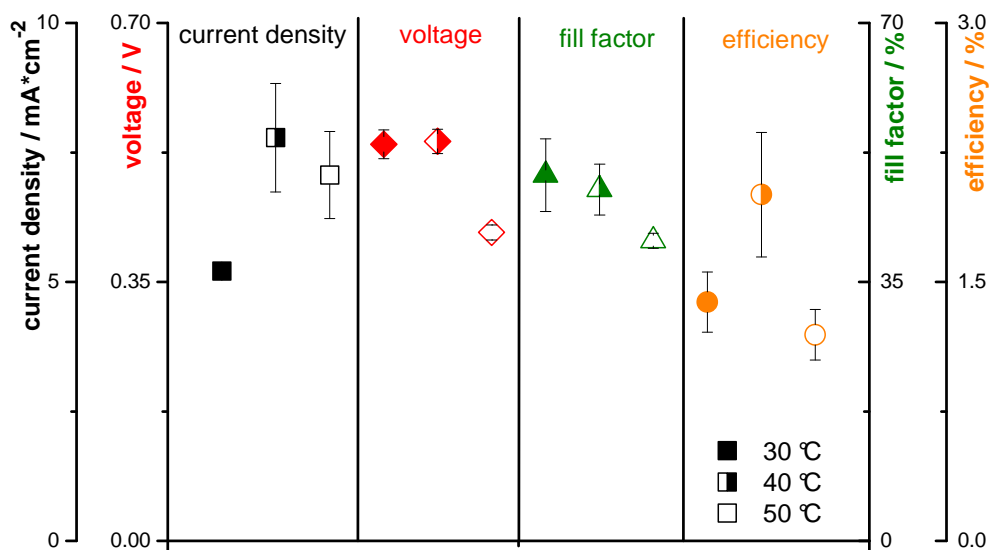


Figure 36: Comparison of characteristic cell parameters resulting from the variation of different substrate temperatures

#### 3.3.4.5.2.5 Variation of the thickness of the wet layer

The thickness of the deposited wet layer (two-step coating) was adjusted via micrometer caliper of the doctor blade. Four different alignments were performed and transformed to solar cell devices. Interestingly, all of these devices showed similar values concerning thickness as well as the roughness of the thermally converted active layers, which is described in Table 6. It even seems that lower wet layer thicknesses lead to slightly thicker thermally converted active layers. For that reason it can be supposed that the adjustment of the coating knife seems to show less influence on the thickness of the active layers than the already mentioned coating parameters. Reasons for this phenomenon could be interactions of the coating knife and the precursor solution. Thus, the knife only serves as tool for a directed wetting of the substrates and the removal of excessive precursor solution.

**Table 6: Thickness of converted layers using different wet layer thicknesses (two-step coating procedure)**

<b>micrometer adjustment</b>	<b>coating speed</b>	<b>average height</b>	<b>roughness <math>r_q</math></b>
$\mu\text{m}$	mm/s	nm	nm
30/30	10	173	7
50/50	10	156	4
70/70	10	150	10
90/90	10	145	4

Although all converted active layers revealed similar thicknesses in the range of 100 to 128 nm (without PEDO:PSS (45 nm)), there are enormous differences concerning the obtained power conversion efficiencies. Especially current density and fill factor yielded totally different results, which could be repeated in a second experiment. Best performances were achieved using a wet layer thickness of 50  $\mu\text{m}$ . Consequently, current densities of 7  $\text{mA}/\text{cm}^2$ , open circuit voltages of 0.46 V and fill factors over 50 % could be obtained. This is why for the following experiments the alignment of the micrometer caliper of the doctor blade was decided to be 50  $\mu\text{m}$ . However, further investigations should be done to explain the divergence of the gained power conversion efficiencies.

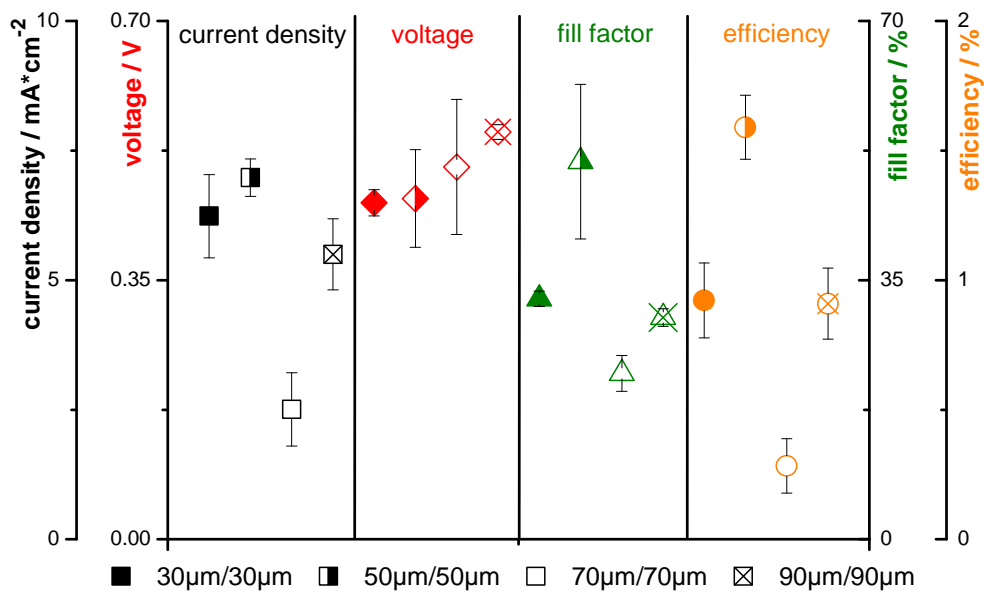


Figure 37: Comparison of characteristic cell parameters resulting from the variation of the thickness of the wet layers

### 3.3.4.5.3 Investigation of a PSiFDBT/CIS nanocomposite solar cell showing a power conversion efficiency of 2.8 %

Combining the optimized processing parameters a solar cell device revealing power conversion efficiencies up to 2.8 % could be achieved. For this device the active layer was coated using the two-step coating process, a coating speed of 10 mm/s, a substrate temperature of 40 °C and a wet layer thickness of 50 µm.

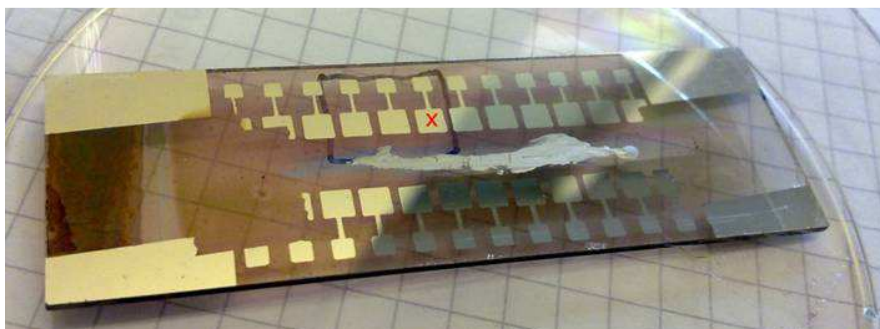


Figure 38: Device showing a power conversion efficiency of 2.8 %



The solar cells (see Figure 38) were fabricated using a blend of PSiFDBT, copper xanthate(heptyl) and indium xanthate(heptyl), which had been dissolved in chlorobenzene and were built up as depicted graphically in Figure 32. After ultrasonic cleaning of the ITO glass substrates in deionized water and isopropyl alcohol, PEDOT:PSS was deposited onto the anode material via spin coating. Subsequently, the PEDOT:PSS layer was dried at 150 °C under inert conditions. The first active layer, a blend of PSiFDBT/CIS of 1/7 having a copper/indium ratio of 1/1.7, was coated onto the PEDOT:PSS layer using the optimized parameters for the doctor blading process. (see previous chapter [coating speed: 10 mm/s; substrate temperature: 40 °C; wet-layer-thickness: 50 μm]) Afterwards the first active layer was dried on a heating plate. In order to introduce an increasing gradient of the nanoparticles towards the aluminum cathode a second active layer having a higher inorganic concentration (PSiFDBT/CIS = 1/10) was coated onto the first active layer taking the same coating parameters. Subsequently, the thermal conversion of the precursor solutions was carried out in a tube furnace under vacuum heating up to 200 °C. To complete the solar cell devices aluminum was deposited onto the active layer resulting in very well performing nanocomposite solar cells.

The best solar cells even revealed current densities exceeding 10 mA/cm<sup>2</sup> and fill factors of 50 %, which are comparable to values of the present record device for nanocomposite solar cells. [15] Only the open circuit voltage (540 mV) was low. In this context, low open circuit voltages could be a result of low shunt resistances due to penetration of PSiFDBT towards the cathode. In addition, enhanced trapping state densities of CIS, affecting its energy levels, could negatively influence the open circuit voltage. The characteristic cell parameters are depicted in Figure 39.

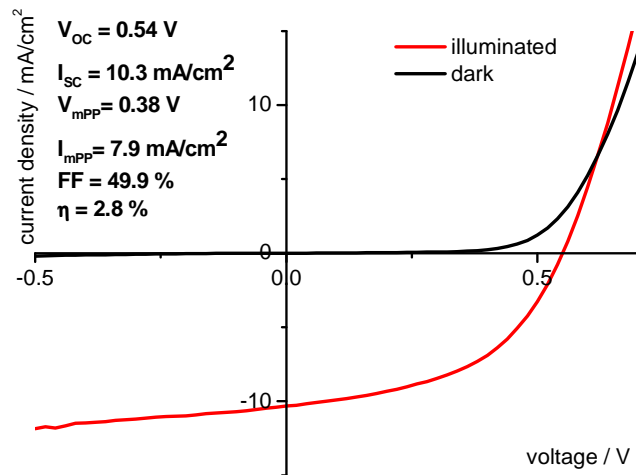


Figure 39: I-V curve of a PSiFDBT solar cell showing a power conversion efficiency of 2.8 %

A big advantage of hybrid solar cells such as PSiFDBT/CIS nanocomposite solar cells should be an additional contribution of current via the inorganic semiconductor acceptor materials. CIS offers quite good absorption behavior compared to PCBM (C60) and consequently helps to harvest photons. Incident photon to electron conversion efficiency (IPCE) measurements give the ratio of the number of charge carriers collected to the number of photons of defined energies shining to the solar cell. Thus, this type of solar cell characterization is a powerful tool to determine the percentage of electrons collected per incident photon by the used materials. Figure 40 illustrates results of an IPCE measurement and the absorption properties of a device which was prepared under optimized conditions too. The device, used, achieved a power conversion efficiency of more than 2.5 %. A comparison of the recorded IPCE curve and the UV-vis spectra of a single CIS phase, a single PSiFDBT layer and a complete solar cell clearly indicate the contribution of current due to additional absorption of CIS. Current starts to flow at wavelengths of about 820 nm, which can only be attributed to absorption of the CIS phase. PSiFDBT in contrast has a blue shifted absorption onset at wavelengths of about 690 nm. A maximum of incident photon to electron conversion efficiency is reached at 520 nm having a

constant plateau as far as 440 nm converting approximately 22 % of the incident photons. In this range PSiFDBT shows its absorption maximum at a wavelength of 530 nm.

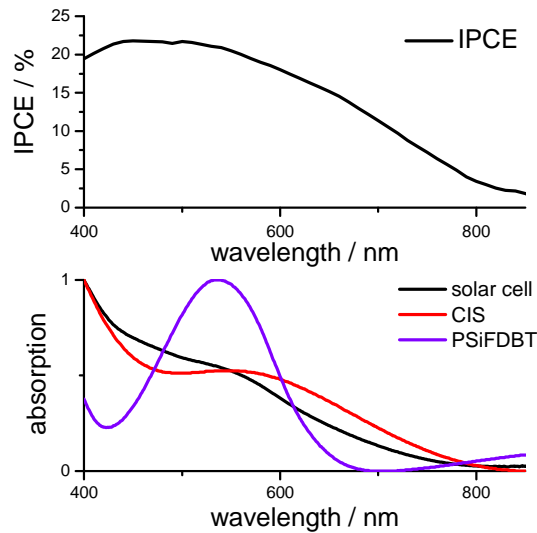
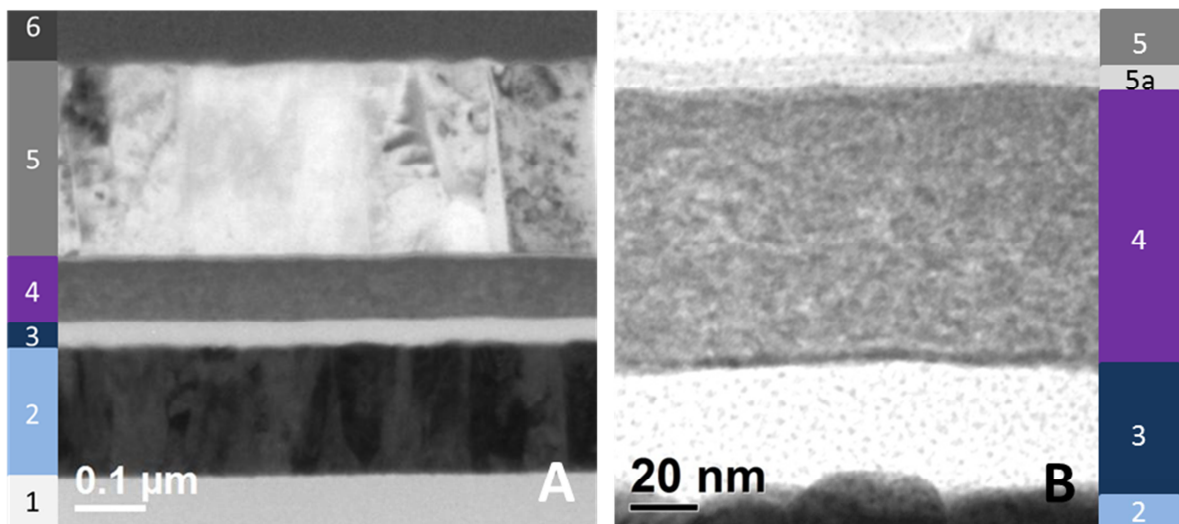


Figure 40: IPCE measurement of a PSiFDBT/CIS solar cell and UV-vis spectra of PSiFDBT, CIS and of a PSiFDBT/CIS blend

### 3.3.4.5.3.1 TEM analysis

Detailed microscopic analysis was performed to provide an insight into the nanostructured morphology of the solar cell device. In this context, a FIB lamella of the red-marked solar cell (see Figure 38) was cut out by focused ion beam (FIB) and thinned via ion milling using the lift out technique.[118] This technique allows the preparation of specimens in cross-sectional view consisting of blends of soft and hard materials such as polymer/CIS blends. Thus, it allows the investigation of layer thickness, interface quality and of the morphology of the active materials. In addition, further TEM techniques such as analytic point analysis (energy dispersive X-ray spectroscopy) and energy filtered imaging are possible and contribute to important information about the analytical composition of the specimens. [118] The bright field TEM of a cross section of the record device is pictured in Figure 41. It shows the glass substrate (1) coated with a 180 nm thick ITO electrode (2). On the ITO a thin PEDOT:PSS (3) layer of approximately 45 nm is deposited followed by the active layer consisting of homogeneous distributed inorganic CIS nanoparticles within the PSiFDBT matrix (4), the aluminum electrode (5) and a platinum

protective layer (6), which was deposited to protect the specimen from the gallium ion beam. Homogeneity of the active material is depicted in Figure 41 B, which shows the active layer in more detail. Although the active layer was prepared via a two-step coating of two differently concentrated precursor solutions, TEM images confirm the formation of one active layer with very homogeneously distributed active materials. Nanoscaled phase separation leads to percolating paths of the donor and the acceptor material resulting in an enormous interface area, which is ideal for the separation of charge carriers. Thus, nearly all of the generated excitons are able to reach a donor/acceptor interface and therefore are able to separate to free charge carriers.



**Figure 41: A, B bright field images of a cross section (FIB-lamella) of PSiFDBT/CIS nanocomposite solar cell: 1: glass; 2: ITO electrode; 3: PEDOT:PSS; 4: active layer; 5: aluminum electrode; 5a aluminum oxide 6: platinum (protective layer) (images taken by W. Haas, FELMI)**

It is also necessary to mention the evolvment of an additional aluminum oxide (5a) layer sandwiched between the active materials (4) and the back electrode (5). This very thin layer of 10 - 15 nm might be formed during the evaporation of the cathode material performed at a reduced pressure ( $10^{-5}$  mbar) due to residual amounts of oxygen remaining in the evaporation chamber. Otherwise it could be a relic owing to air-exposure after the FIB cutting procedure.

Although aluminum oxide works as insulator a very thin layer could also improve cell performances.

To gain better insight into the chemical structure and the elemental distribution of this device electron energy loss spectrum imaging (EELS) as well as energy dispersive X-ray spectrum imaging (EDX) were applied. The results of these investigations are depicted in Figure 42 and Figure 43. Energy dispersive X-ray spectroscopy is an analytical technique for the elemental analysis and chemical characterization of a sample. As a result of the interaction of the sample with the electron beam characteristic X-rays for each element are emitted and can be analyzed. In the following picture bright colors stand for high concentrations of the respective elements. On the left hand side of the illustration a schematic bar depicts the assembly of the layers. Elemental mapping was performed for indium, copper, tin, sulfur, oxygen and aluminum.

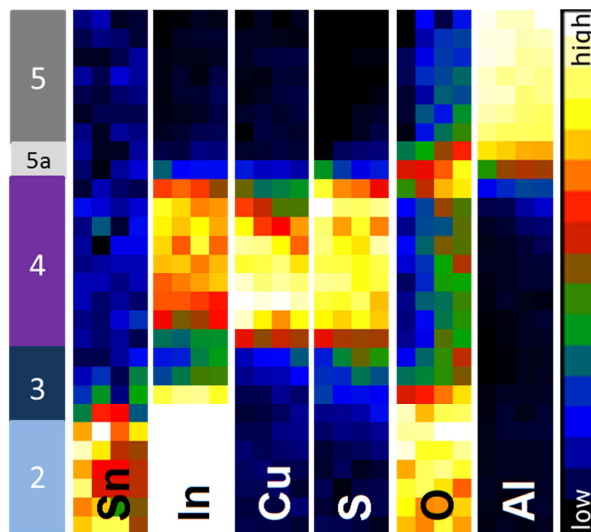


Figure 42: Elemental maps gained from EDX spectrum imaging of the cross section 2: ITO anode; 3: PEDOT:PSS; 4: active layer; 5a: aluminum oxide; 5: aluminum (W.Haas)

As expected, strong signals for indium, tin and oxygen could be detected in the district of the ITO electrode. The hole transport layer (PEDOT:PSS) discloses not only the presence of sulfur and oxygen, but also indicates indium, which can be explained by partial dissolution of the electrode material due to the strong acidic nature of PEDOT:PSS, which is able to dissolve

indium out of the ITO.[119] The active layer shows strong signals for indium, copper and sulfur resulting from the formation of the CIS nanoparticles within the Polymer matrix (PSiFDBT). In addition, it shows a quite homogeneous distribution of the inorganic elements. However, there is a slight decreasing gradient of copper towards the aluminum cathode whereas the concentration of indium and sulfur seem to be more constant. Neither the reason of this evolving gradient nor the influence on the cell performance is cleared yet and is still under investigation. EDX spectroscopy additionally confirmed the presence of the already mentioned aluminum oxide sandwiched between the active materials and the aluminum cathode.

Results of the EELS spectrum imaging are illustrated in Figure 43. Elemental mapping was performed for indium, copper and sulfur and delivers comparable results to the EDX analysis. It shows the existence of oxygen in the PEDOT:PSS layer, the distribution of copper and indium within the active layer and the additional aluminum oxide layer. Bright colors stand for high contents of the analyzed elements.

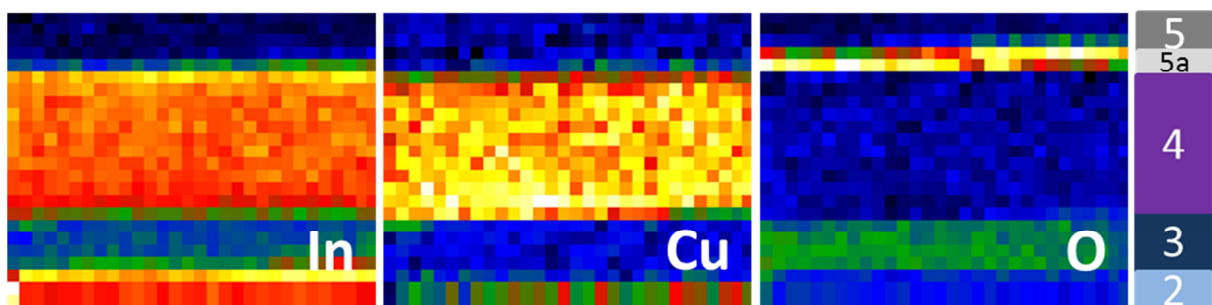
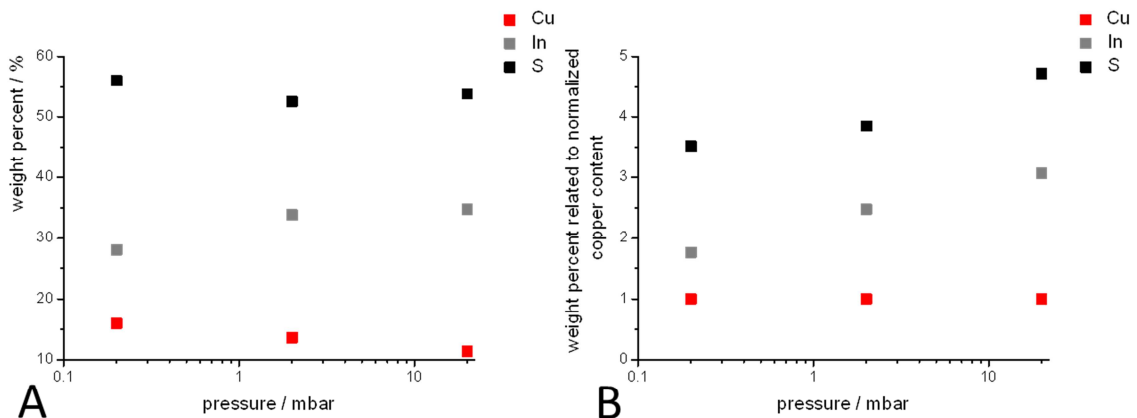


Figure 43: Elemental maps gained from EELS spectrum imaging of the cross section of the PSiFDBT/CIS solar cell 2: ITO anode; 3: PEDOT:PSS; 4: active layer; 5a: aluminum oxide; 5: aluminum (W.Haas)

#### 3.3.4.5.4 Variation of the pressure during the thermal conversion step:

All of the solar cells were thermally converted under vacuum to promote the removal of the volatile byproducts, which occur due to decomposition of the metal xanthate(heptyl) precursor materials. Loads of previous experiments indicated that better vacuum during the annealing step led to better cell performances. Consequently it can be supposed that better vacuum lead to less contaminations remaining within the active layer.

Due to an improved assembly of the heating unit the vacuum for the annealing procedure could be reduced to a pressure of 0.2 mbar compared to normally reached pressures of 1 mbar. However, better vacuum during the annealing step also means a change of the elemental composition especially of the inorganic acceptor materials due to different vapor pressures and conversion temperatures of the respective copper- and indium xanthate(heptyl). To prove the dependency of the final composition of the acceptor material on different reduced pressures thin films of PSiFDBT/CIS were produced, at 0.2, 2 and 20 mbar and investigated via TEM EDX analysis. Figure 44 plots the variation of the composition of the acceptor material versus different reduced pressures. It clearly shows the reduction of the indium content accompanied by an increased content of copper having a reduced pressure of 0.2 mbar during the thermal conversion of the precursor materials. Especially the reduction of the indium content has to be considered because only excess of indium leads to a n-type semiconductor.



**Figure 44: TEM-EDX results: Final elemental composition of the active layers depending on various reduced pressures (A: absolute values; B: normalized values)**

As a result of these experiments it could be found out, that previously optimized ratios of donor to acceptor (1/7) and copper to indium (1/1.7) may not be ideal for the in-situ formation of active materials using a reduced pressure of 0.2 mbar. In addition, it clearly shows that variation of one parameter concerning the thermal conversion step such as vacuum has a tremendous influence on the final composition of the CIS phase. Consequently, progressive improvement of

cell performances can only be assured, if all effects of the variation of one parameter are considered and iteratively checked.

Thus, a series of experiments was carried out to adjust the amounts of the precursors to the wanted ratios of the thermally converted active materials considering the new value for the reduced pressure. (0.2 mbar)

### 3.3.4.5.5 TEM-EDX investigation of various indium to copper ratios (0.2 mbar)

Since CIS is used as acceptor material in PSiFDBT/CIS nanocomposite solar cells an indium rich phase of CIS is obligatory to assure n-type conductivity of the inorganic semiconductor.[120] This is why the precursor solutions (blend of PSiFDBT, copper xanthate(heptyl) and indium xanthate(heptyl)) have to consist of high excesses of indium xanthate(heptyl). To prove the final concentration of indium and copper within the CIS phase TEM EDX measurements of converted PSiFDBT/CIS layers, taking the new reduced pressure of 0.2 mbar, were performed. The results are shown in Figure 45.

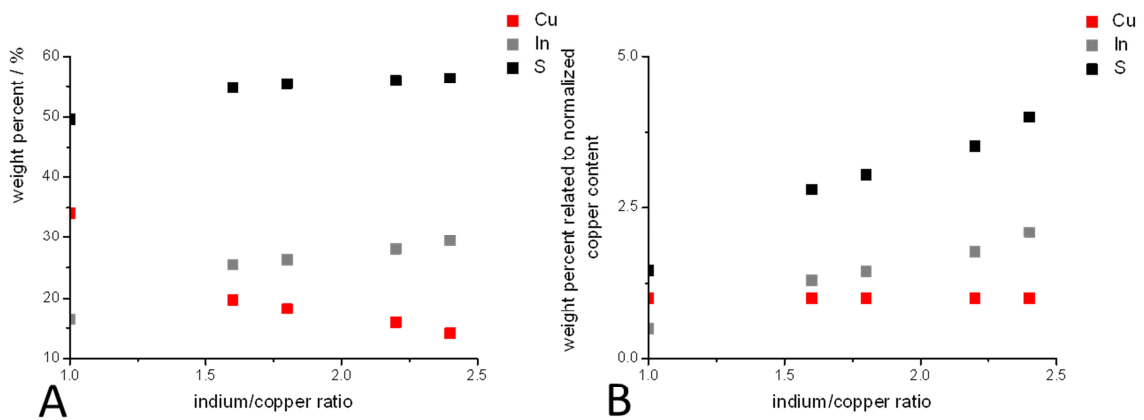


**Figure 45: TEM EDX results: Comparison of the final concentration of indium and copper of the converted active layer to the applied indium to copper ratio of the precursor materials. (A: absolut values; B: normalized values)**

Figure 45 A depicts the absolute elemental composition of converted nanocomposite layers having increasing contents of indium xanthate(heptyl). The content of indium and sulfur increases according to higher amounts of indium xanthate(heptyl), whereas the copper content decreases. Figure 45 B illustrates the same values related to normalized copper contents. This analysis clearly shows that an indium- to copper xanthate(heptyl) ratio in the range of 1.4-1.55



is necessary to obtain converted nanocomposite layers with an indium to copper ratio of 1. Even higher amounts of the indium precursor are obligatory to assure n-type conductivity of the CIS phase. Because of the necessity of high amounts of indium within the CIS phase X-ray diffraction patterns of a sample with low and with high indium content were performed to investigate the influence of additional indium concerning the formation of the chalcopyrite structure of CIS. (see Figure 46) However, both samples nearly showed identic reflection patterns, which indicate the formation of a pure chalcopyrite structure.

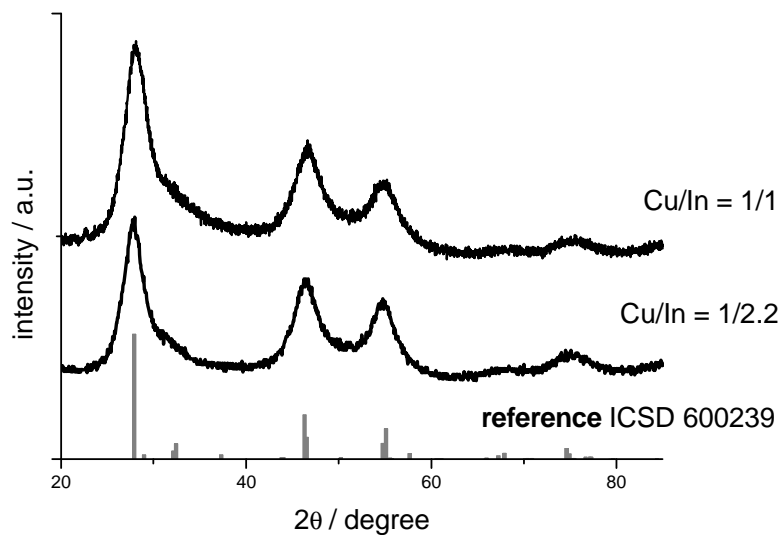


**Figure 46:** XRD of equimolar and indium rich CIS phases

#### 3.3.4.5.6 Variation of the indium to copper ratio

The following experiments were performed to find the ideal composition of the precursor solutions considering the new reduced pressure of 0.2 mbar during the thermal conversion step. Thus, a series of experiments was performed in cooperation with Stefan Moscher and Dr. Thomas Rath varying the indium to copper ratio.

The solar cells (see Figure 38) were fabricated using a blend of PSiFDBT, copper xanthate(heptyl) and indium xanthate(heptyl), which had been solved in chlorobenzene and were built up as depicted graphically in Figure 32. After ultrasonic cleaning of the ITO glass substrates in

deionized water and isopropyl alcohol, PEDOT:PSS was deposited onto the anode material via spin coating. Subsequently the PEDOT:PSS layer was dried at 150 °C under inert conditions. The first active layer, a blend of PSiFDBT/CIS of 1/5 related to a 5 mg/mL solution of PSiFDBT and having varying copper/indium ratios, was coated onto the PEDOT:PSS layer using the previously optimized parameters for the doctor blade. Afterwards the first active layer was dried on a heating plate. In the meantime the precursor solution was diluted to half of its original concentration. Using the diluted precursor solution a second active layer was coated onto the device to smooth its surface. After the thermal conversion step the solar cells were finally completed depositing aluminum back electrodes. For characterization I-V curves and UV-vis spectra were recorded. In addition, the layer thickness of the respective devices was determined using a surface profiler.

The characteristic solar cell parameters are depicted in Figure 47. The graphs show maxima of the obtained results using quite high excesses of the indium xanthate(heptyl) precursor, which was found to be necessary in order to create CIS as n-type semiconductor. Best efficiencies could be gained with an indium to copper ratio of 2, which results from the highest current densities that could be achieved during these experiments. The fill factors reveal a more or less constant level between 30 and 40 % using an indium excess in the range of 1.8-2.6. The obtained values for the open circuit voltages, however, show a continuous increase using higher amounts of indium.

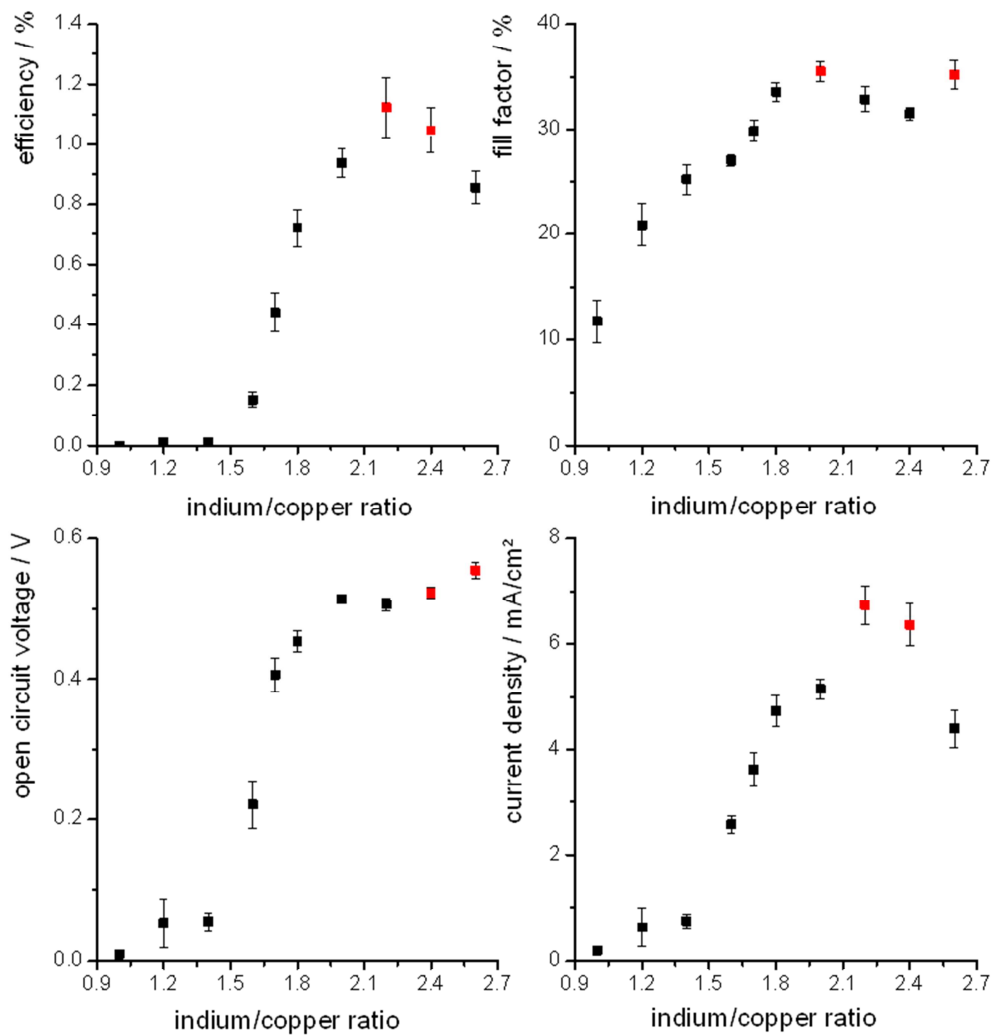


**Figure 47: Characteristic solar cell parameters of PSiFDBT/CIS solar cells having varied indium to copper ratios**

UV-vis analysis (see Figure 48) of the respective solar cells (the spectra are shifted vertically for better visibility) show a reduction of the absorption maximum at a wavelength of 520-530 nm, which is consistent to the absorption maximum of PSiFDBT and can be explained by proportional decrease of the donor material within the active layer relating to the acceptor material. In addition, a slight red-shift of the maxima can be observed, which could be the result of higher indium content of the CIS phase or the formation of an additional indium sulfide phase.

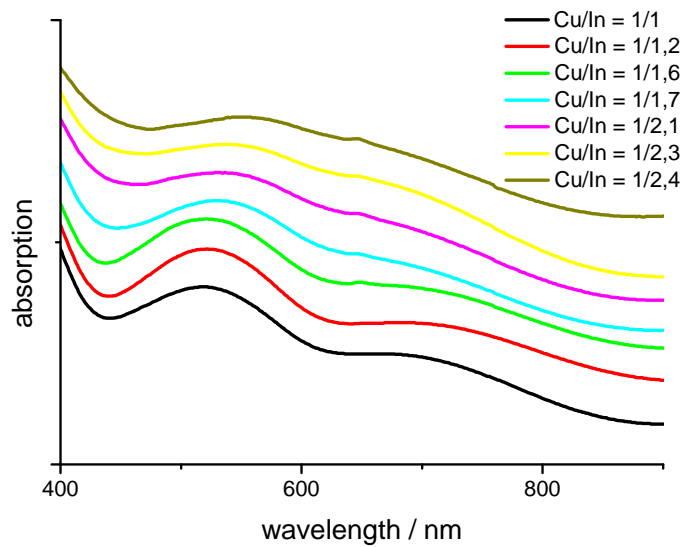


Figure 48: UV-vis spectra of PSiFDBT/CIS solar cells having varied copper to indium ratios (vertically shifted for better visibility)

The investigated solar cells showed layer thicknesses (PEDOT:PSS + active layer) in the range of 110-170 nm, which is illustrated in Table 7. Thus, all of the solar cells had active layers in the range of 70-130 nm, which approximates the preferred layer thickness of about 90-100 nm. The Divergence of the layer thickness could be a result of the solution based processing method. It is very difficult to control an exact final layer thickness of the thermally converted active materials because the wet layer film, which is in the range of 30-90  $\mu\text{m}$ , diminishes tremendously during the thermal conversion step.

Table 7: Layer thickness of solar cells having varied copper to indium ratios

<b>indium/copper</b>	-	1	1.2	1.4	1.6	1.7
<b>average height</b>	<b>nm</b>	131	154	172.5	136.5	121
<b>indium/copper</b>	-	1.8	2.0	2.2	2.4	2.6
<b>average height</b>	<b>nm</b>	169.5	147	130	121	107.9

#### 3.3.4.5.7 Variation of the acceptor to donor ratio

Already discussed changes of the preparation (new reduced pressure) of the solar cells do not only influence the preferred indium to copper ratio but will also affect the acceptor to donor ratio of the active materials. To find a beneficial composition of PSiFDBT and CIS a series of experiments was performed.

The solar cells (see Figure 38) were fabricated as described above (see page 102) However, this time the donor to acceptor ratio was varied, while the copper to indium ratio was determined to be 1/2.

The characteristic solar cell parameters are depicted in Figure 49. Best power conversion efficiencies could be achieved with high contents of the inorganic nanoparticles. However, the use of high excesses of the inorganic components is quite common in literature and resulted in high power conversion efficiencies. [16][15] Considering the density of the inorganic nanoparticles to be 4.5 times the density of PSiFDBT, an acceptor to donor ratio of 9 (weight percent) means a duplicate volume of CIS related to PSiFDBT. This ratio showed the best values for the power conversion efficiency, open circuit voltage and the fill factor. Only the current density could be enhanced via the use of 10 equivalents of the inorganic acceptor phase. Thus, power conversion efficiencies of 1.8 % could be obtained. Based on these fundamental experiments solar cells up to 3 % could be prepared by our working group.[121]

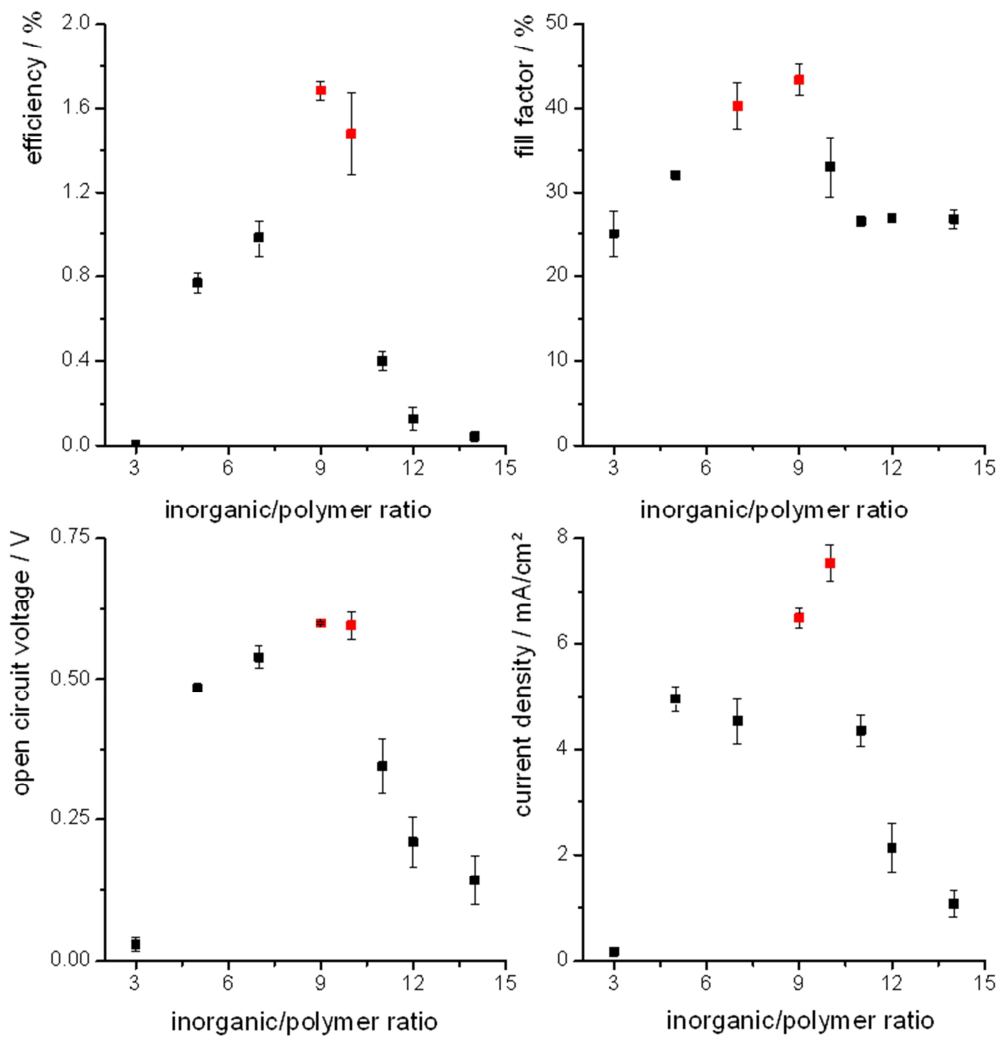


Figure 49: Characteristic solar cell parameters of PSiFDBT/CIS solar cells having varied acceptor- to donor material ratios

UV-vis analysis (see Figure 50) of the respective solar cells (the spectra are shifted vertically for better visibility) show a reduction of the absorption maximum at a wavelength of 520-530 nm, which is consistent to the absorption maximum of PSiFDBT and can be explained by proportional increase of the acceptor material within the active layer relating to the donor material.

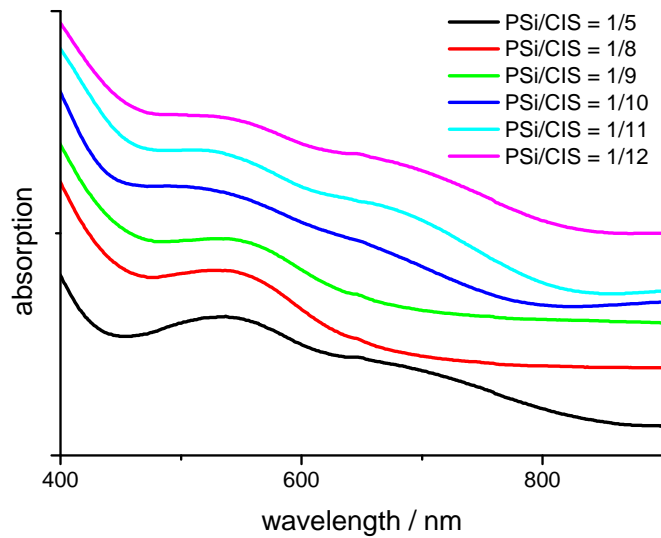


Figure 50: UV-vis spectra of PSiFDBT/CIS solar cells having varied acceptor to donor material ratios (shifted vertically for better visibility)

The results of the surface profiler reveal constant increasing layer thicknesses due to higher contents of the inorganic acceptor material. An acceptor to donor ratio of 3 resulted in quite thin layers not exceeding 100 nm (40 nm PEDOT:PSS and 60 nm active materials) whereas a ratio of 14 reached layers of 350 nm (40 nm PEDOT:PSS and 310 nm active materials). Consequently it has to be considered that the varying layer thicknesses have a serious influence on characteristic solar cell parameters. On the one hand thicker layers absorb more light according to Lambert-Beer law but on the other hand the cell performance is also influenced negatively due to increased series resistances of the device. This is why further experiments, which consider the formation of comparable thicknesses of the active layers, are under progress.

Table 8: Layer thickness of solar cells having varied acceptor to donor material ratios

<b>donor/acceptor</b>	-	3	5	7	8.0	9.0
<b>average height</b>	<b>nm</b>	100	137.6	173.5	195.5	192.5
<b>donor/acceptor</b>	-	10	11	12	14	
<b>average height</b>	<b>nm</b>	237.5	250.5	266.5	350	

### 3.3.5 Conclusion

Various production parameters of polymer/CIS nanocomposite solar cells, which were based on knowledge of previous works at our institute, were varied and investigated. Different donor materials, modified assemblies, divers compositions of the active materials and varied processing parameters were tested and analyzed to improve the power conversion efficiency of the devices. Best results could be achieved via the introduction of PSiFDBT as donor material and the two-step coating assembly. In combination with optimized conditions for the formation of the active layer, solar cells with efficiencies far beyond 2 % could be realized. The record device could even reach a power conversion efficiency of 2.8 % showing values for the current density and the fill factor comparable to the best nanocomposite solar cells, which have been published.[15] Figure 51 depicts a constant increasing trend concerning the power conversion efficiencies of the last 90 experiments. If it is possible to continue this trend via further optimization of the precursor materials and working conditions, this type of solar cells will seriously become competitive to polymer/PCBM solar cells.

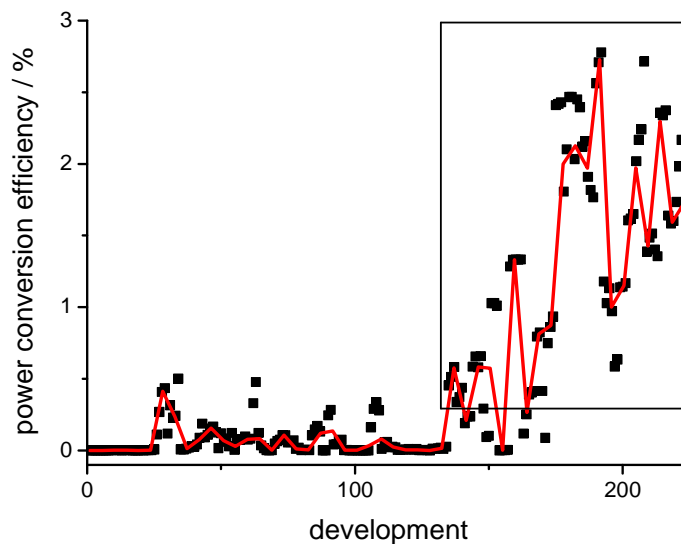


Figure 51: Improvement of the power conversion efficiencies of polymer/CIS solar cells



### **3.4 Preparation of inorganic semiconductor materials using metal salts of dialkyldithiocarbamates**

Thermal decomposition of metal salts of dialkyldithiocarbamates leads to the formation of the respective metal sulfides.[122][123][124] This is why these compounds were chosen to act as precursor material for syntheses of inorganic semiconductor materials such as copper indium sulfide and copper zinc tin sulfide, which could be used for nanocomposite solar cells.

#### **3.4.1 Dialkyldithiocarbamates**

Carbon disulfide reacts with nucleophiles such as amines to give rise to compounds known as dithio acids. The deprotonated forms of dithio acids react with metal ions to form metal salt complexes. Dialkyldithiocarbamates are half amides of the dithiocarbamic acid and belong to the group of sulfur donor ligands such as xanthates, dithiolates, dithiophosphates and dithiocarbazates. Due to their anticancer-, antiviral- and antifungal activities as well as their versatile applications in industry lots of publications have been presented, which are not topic of this thesis.[125] In this work metal salts of dialkyldithiocarbamates are used as precursor materials for the synthesis of semiconducting metal sulfides.

##### **3.4.1.1 Synthesis**

The syntheses of the homoleptic dialkyldithiocarbamate metal complexes follow a modification of literature methods [126][124].

For the preparation of sodium-dialkyldithiocarbamate respective amines (dibenzylamine, diallylamine and dihexylamine) were slowly added to a cooled stirring dispersion of sodium hydroxide, dissolved in deionized water, and CS<sub>2</sub> in benzene. The starting reaction resulted in the formation of flocculent precipitates. Hexane was poured into the reaction mixture to support precipitation and precipitates were decanted, filtered and washed with hexane to get rid of non-polar contaminations. Afterwards the product was dried under vacuum to obtain the respective sodium-dialkyldithiocarbamate as white powder, which was used in the following reaction as educt without further purification. The yield was about 70-80 %.

For the syntheses of metal-dialkyldithiocarbamates solutions of sodium-dialkyldithiocarbamate in deionized water were added to vigorously stirring solutions of appropriate metal salts ( $\text{CuCl}_2/\text{InCl}_3/\text{ZnCl}_2/\text{SnCl}_4 \cdot 5\text{H}_2\text{O}$ ) in deionized water. The resulting precipitates were filtered and washed with copious amounts of deionized water in order to remove excessive metal salts. Subsequently the precipitates were dried under vacuum for 16 hours. After further cleaning processes elemental analysis,  $^1\text{H}$ -,  $^{13}\text{C}$ -, and  $^{119}\text{Sn}$ -NMR as well as IR-spectroscopy were performed to confirm the formation as well as the purity of the desired products. The reaction scheme is depicted in Figure 53.

Most of the products could be synthesized in high yields (>80 %). Only tin dibenzylidithiocarbamate showed a poor yield of less than 30 %. However, the purity of this compound could be proved via elemental analysis, and NMR spectroscopy. The results of the syntheses are listed in the experimental part.

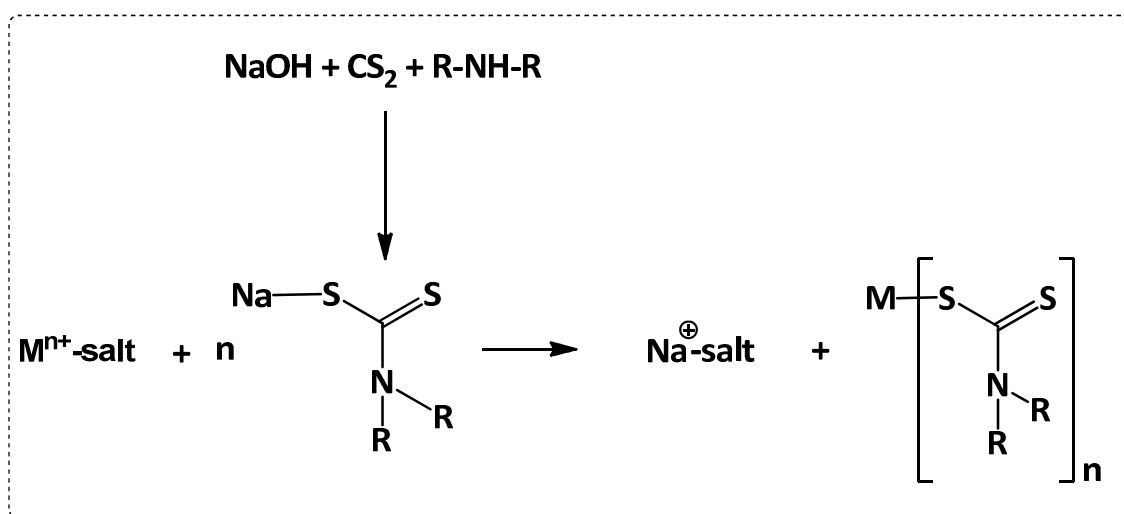


Figure 52: Synthesis of the respective metal dialkyldithiocarbamates

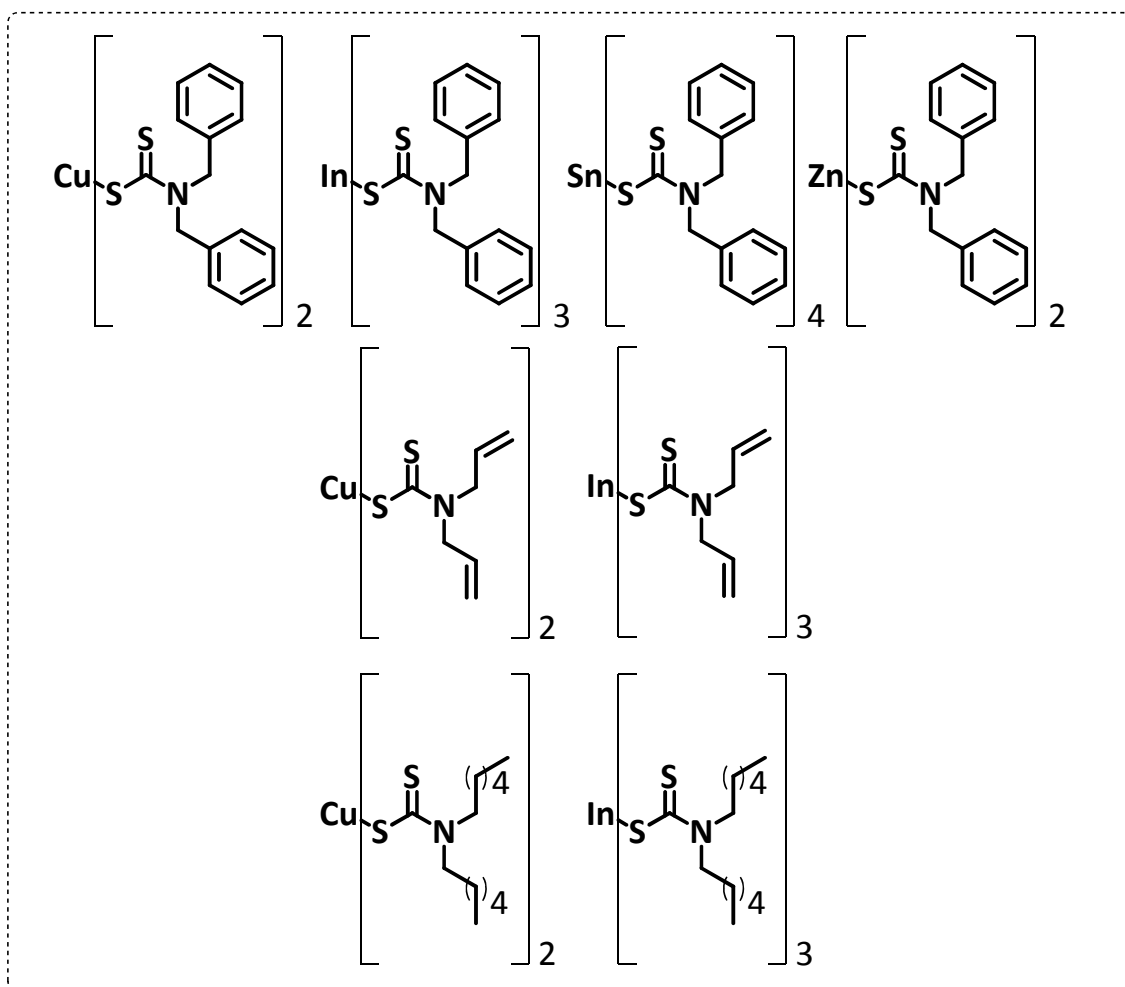


Figure 53: Synthesized metal dialkyldithiocarbamates

### 3.4.1.2 Decomposition of metal dialkyldithiocarbamates

Upon heating metal dialkyldithiocarbamates thermally decompose to release carbon disulfide and alkyl moieties into the gas phase resulting in metal sulfides. This has already been proved for a series of different combinations of metals and dialkyldithiocarbamates, mostly using chemical vapor deposition. [127][128][129] In this work metal salts of diallyl-, dibenzyl- and dihexyldithiocarbamates were chosen due to their reactive and/or big substituents, which seem to lead to easier decomposition pathways and consequently do not disappear due to volatilization, which is important to enable formation of metal sulfides directly within the coated layers.[124]

In the following chapter the decomposition of dialkyldithiocarbamates and the formation and characterization of chalcopyrite- as wells as the metastable wurtzite phase of CIS are described. CIS layers were synthesized analogously to the formation of the CZTS layers via thermal conversion of copper- (CuDTC) and indium dialkyldithiocarbamates (InDTC).

### 3.4.2 Formation of copper indium sulfide

#### 3.4.2.1 Thermogravimetry analysis

Thermogravimetric analysis (up to 500 °C) of the metal dialkyldithiocarbamate complexes show, that these complexes start to decompose in the range of 230 to 330 °C. Dialkyldithiocarbamates start to decompose at lower temperatures than the dialkyldithiocarbamates having either benzyl and or hexyl residues. (see Table 9) In addition, a slight loss of materials has to be considered due to evaporation of the precursor materials. Concerning the decomposition of indium dialkyldithiocarbamates this effect seems to be even stronger exhibiting differences of 15 % between calculated and determined values, which could be caused due to additional sublimation of indium. Indium dihexyldithiocarbamate showed a weight loss of a third of the expected value indicating that decomposition of this precursor material was not complete.

Table 9: Results of STA-analysis

metal	substituents	decomp. temperature	weight loss	calc. weight loss
		°C	%	%
Cu	allyl	231	67.9	68.9
	benzyl	256	86.2	79.1
	hexyl	290	87.2	78.3
In	allyl	293	63.2	48.4
	benzyl	300	81.1	65
	hexyl	329	21.9	63.3

### 3.4.2.2 Sample preparation

For the sample preparation precursor solutions were prepared from appropriate amounts of copper dialkyldithiocarbamate and indium dialkyldithiocarbamate either in pyridine or  $\text{CHCl}_3$ . These solutions were applied onto glass substrates by drop coating. Afterwards the precursor layers were annealed up to  $350\text{ }^\circ\text{C}$  under inert conditions, in order to form CIS layers. During the thermal conversion step only volatile organic byproducts like amines, alkyl residues and carbon disulfide are generated [130] and consequently a very pure inorganic semiconductor phase of CIS can be formed. A constant purge of nitrogen was created during the entire heating and cooling procedure, to be able to remove decomposing and evaporating by-products.

The formation of CIS was proved via powder X-ray diffraction analysis. The converted inorganic semiconductor layers were ripped off the glass substrate in order to obtain measureable powders.

### 3.4.2.3 CIS made of copper- and indium diallyldithiocarbamate

Although copper- and indium diallyldithiocarbamates offer the lowest decomposition temperatures of the tested dialkyldithiocarbamates a conversion temperature of  $350\text{ }^\circ\text{C}$  was necessary to obtain CIS.

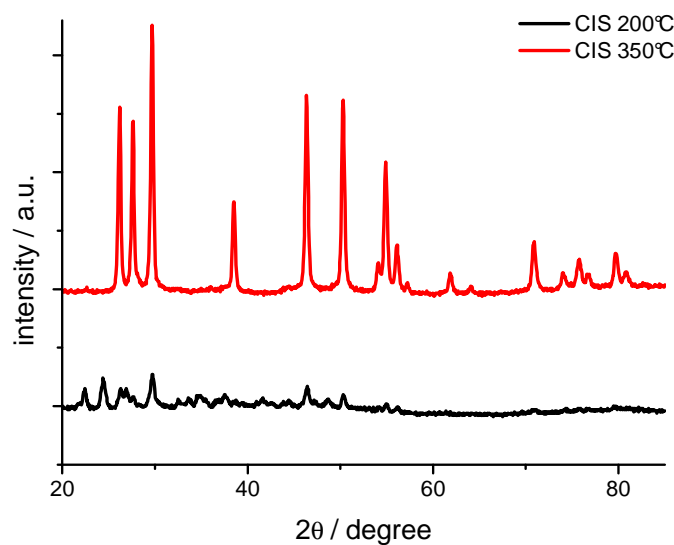


Figure 54: XRD-pattern of CIS converted at 200 and  $350\text{ }^\circ\text{C}$  (vertically shifted for better visibility)

Figure 54 depicts the results of powder X-ray diffraction analysis showing the formation of a crystalline and quite pure wurtzite phase of CIS at temperatures of 350 °C. Using a conversion temperature of 200 °C, which is more or less the maximum annealing temperature for conjugated polymers, did not result in the formation of CIS. Consequently, dialkyldithiocarbamates does not seem to be compatible to nanocomposite solar cells. However, the formation of CIS and CZTS out of dialkyldithiocarbamates is still very interesting, due to possible applications in inorganic solar cells.

Interestingly, there was no observable change of the converted CIS phase using a reduced amount of copper dialkyldithiocarbamate. Both an equimolar input of copper- and indium dialkyldithiocarbamate and a ratio of 0.75 to 1 revealed comparable XRD-patterns, which indicates the formation of a non-stoichiometric CIS phase instead of additional indium sulfide phases. (see Figure 55)

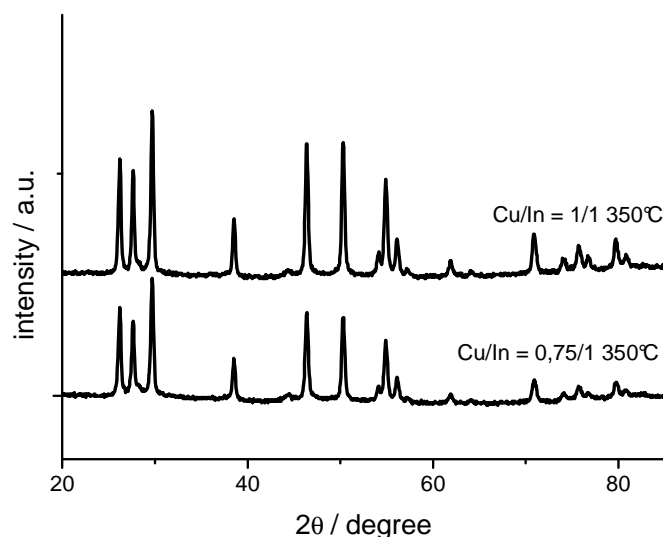


Figure 55: XRD-pattern of CIS having varied precursor ratios (vertically shifted for better visibility)

#### 3.4.2.4 CIS made of copper- and indium dibenzylthiocarbamate

Thermal conversion (350 °C) of copper- and indium dibenzylthiocarbamate resulted in the formation of thermodynamic stable chalcopyrite phase but also showed reflexes of the metastable (at room temperature) wurtzite phase, which confirms the formation of a mixture of these two phases. (see Figure 56)

#### 3.4.2.5 CIS made of copper- and indium dihexylthiocarbamate

Thermal conversion (350 °C) of copper- and indium dihexylthiocarbamate showed similar results as the conversion of dibenzylthiocarbamates. However, a higher content of arising wurtzite phase could be observed. (see Figure 56)

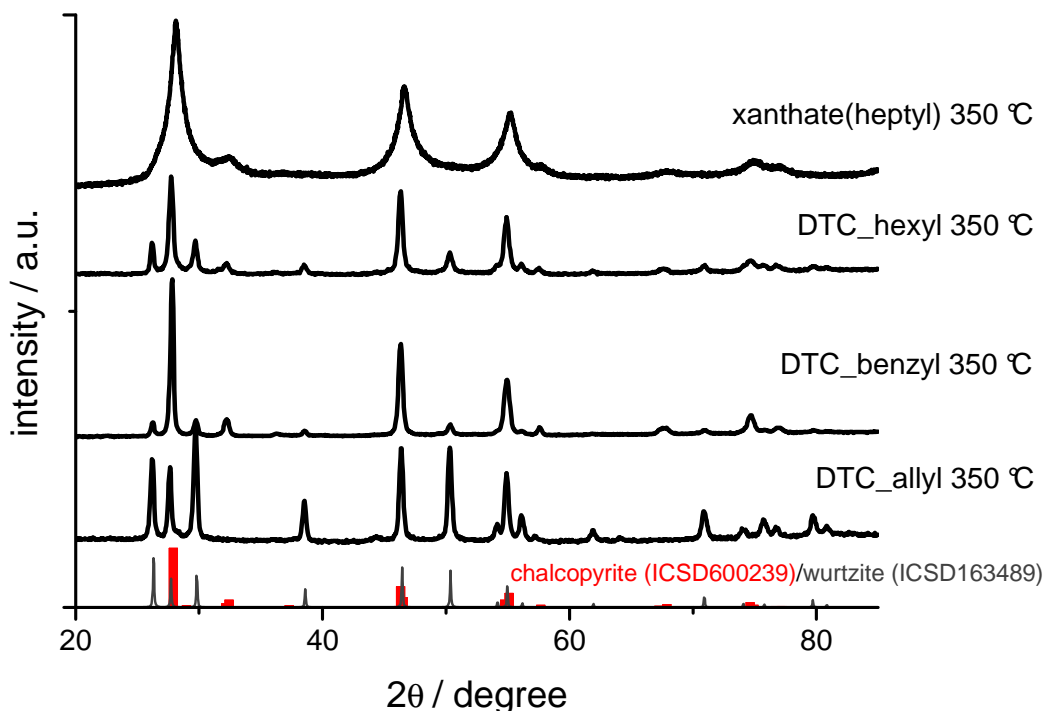


Figure 56: Comparison of XRD- patterns of various CIS phases resulting from different precursor materials. The peaks are in good agreement with the reference patterns of CIS (chalcopyrite phase ICSD600239 and the wurtzite phase ICSD163489) (vertically shifted for better visibility)

### **3.4.2.6 Comparison of wurtzite and chalcopyrite phase**

Generally CIS exists in three polymorphic forms depending on ambient temperature. Chalcopyrite is formed at temperatures lower than 980 °C, zinc blende between 980 and 1050 °C and wurtzite between 1050 °C and the melting point of the material. [131] The wurtzite phase shows more flexibility concerning the occupancy of copper and indium atoms in the lattice sites. Consequently the band gap of wurtzite phase of ternary CIS can be tuned over a wide range of energy, which is a beneficial tool for the fabrication of optoelectronic devices.[79] Depending on the precursor material, which was used, an almost pure wurtzite phase of CIS, taking dialkyldithiocarbamates, and mixtures of wurtzite and chalcopyrite, taking either dibenzyl- or dihexyldithiocarbamates could be produced. In addition, a pure chalcopyrite CIS can be obtained via metal salts of xanthate(heptyl) as it was described in previous chapters. Thus, the formation of two phases of CIS can be controlled via the utilization of respective precursor materials. However, it is worth mentioning, that the use of xanthates(heptyl) leads to the formation of smaller inorganic crystallites. Primary average crystallite sizes of the CIS nanoparticles were approximated via Scherrer relationship to be 12 nm for the CIS nanoparticles prepared with xanthates(heptyl) and 8 nm for the CIS nanoparticles prepared with dibenzylidithiocarbamates.

### **3.4.2.7 Conclusion**

The formation of CIS phases resulting from thermal conversion of dialkyldithiocarbamates could be shown. In addition, the ability to control the formation of either thermodynamically stable chalcopyrite phase of CIS or the formation of the metastable wurtzite phase of CIS could be realized using various precursor materials.

However, due to high temperatures of 350 °C, which are necessary to convert the used dialkyldithiocarbamates, these precursor materials are not suitable for nanocomposite solar cells but could be applied for the formation of pure inorganic CIS layers, which could be used for inorganic photovoltaic devices.



### **3.4.3 Formation of copper zinc tin sulfide thin layers**

#### **3.4.3.1 Introduction**

This chapter deals with the formation of pure inorganic CZTS thin layers using metal salts of dibenzylidithiocarbamates as precursor materials.

Chalcogenide semiconductors, such as copper indium disulfide have attracted attention because of their beneficial optical and electrical properties for photovoltaic and optoelectronic applications. However, indium is an expensive and scarce element, and consequently hard to combine with large scale production. In order to overcome these limitations high potential semiconductor materials, in which indium is replaced, for example, by zinc and tin in copper zinc tin sulfide (CZTS), are of great interest. [132][133] CZTS has a direct band gap of 1.5 eV, shows p-type electrical conductivity and indicates a good absorption behavior. [80][81][82] For the formation of CZTS layers several techniques such as vacuum-based approaches like sputtering [134][135][136][137][138] and co-evaporation procedures [139][80][140] have been performed successfully. The prevention of vacuum based production steps, however, could lead to an enormous simplification of the entire manufacturing and consequently to a remarkable price reduction. That is why non vacuum based CZTS approaches like electro-deposition[82][141][142][143], spray pyrolysis [144][145] and especially ink based coating methods [146][147][148], which are particularly compatible to high throughput deposition techniques, such as printing and casting, have attracted great interest in recent years. In this work we present a solution processed formation of nanocrystalline CZTS microspheres using metal-dialkyldithiocarbamate precursors. These precursor systems have the advantage, that solubility as well as decomposition temperature of the dialkyldithiocarbamates can be tuned by varying the residues of their alkyl chains.[149] Thus, a wide range of possible solvents and the ability to tune the conversion temperature via special dialkyldithiocarbamates could lead to a simplification of respective production steps. Up to now various metal sulfides have been synthesized using dialkyldithiocarbamate based precursor materials. Nomura et al., for instance, presented the formation of copper sulfide [150] and copper indium sulfide [151] semiconductor materials. Ngo and coworkers described the decomposition of copper-dithiocarbamate

derivatives resulting in copper sulfide as well. [124] Pike et al. showed the formation of zinc sulfide thin films out of zinc-diethyldithiocarbamate complexes via ultrasonic spray pyrolysis [130] and Menezes et al. reported about tin sulfide powders made of tin-dialkyldithiocarbamates.[127] Even CZTS, made of dialkyldithiocarbamates has recently been published by Ramasamy, who prepared semiconductor layers via chemical vapour deposition.[152] However, these semiconductor materials made by low throughput sputtering or vapor deposition techniques are very expensive [153], which is their major roadblock for industrial applications. Consequently Zou et al. reported about a facile and inexpensive solution processed preparation of CZTS nanoparticles, in which a dialkyldithiocarbamate  $[\text{Cu}_2\text{ZnSn}(\text{S}_2\text{CNET}_2)_{10}]$ , oleylamine and oleic acid were used as precursor, activation and capping agent, respectively.[154] To the best of our knowledge, no scientific article has reported about a dialkyldithiocarbamate-solution processed direct formation of nanocrystalline CZTS thin layers, without using any capping agents, so far. In order to enable the solution based direct formation of CZTS metal salts of the dibenzylidithiocarbamate were chosen because of their appropriate decomposition behavior as result of the benzyl residue.[124] The CZTS thin films were characterized using X-ray diffraction (XRD), transmission electron microscopy (TEM), scanning electron microscopy (SEM), energy dispersive-X-ray spectroscopy (EDX), X-ray photoelectron spectroscopy (XPS), Raman- and UV-vis spectroscopy.

### **3.4.3.2 Results and discussion**

In the last few years, we have focused our work on the development of direct and simple preparation methods for inorganic metal sulfides with intention to prevent the need of stabilizing cappers in order to be able to obtain pure semiconductor phases. [96] [51] [52] Thus, we developed a precursor solution based technique, which is compatible to high throughput reel to reel modes like spraying, printing and slot coating. Figure 57 depicts homoleptic metal complexes (CuDTC), (ZnDTC) and (SnDTC), which were used as metal and sulfur sources for the formation of CZTS. To obtain CZTS-layers via a solution based fabrication method, evaporation of the precursor material has to be prevented as much as possible. Otherwise the thermal conversion step would accompany an enormous waste of the precursors. This is why in this

work metal salts of dibenzylthiocarbamates, instead of the more volatile dialkyldithiocarbamates having n-propyl or n-butyl residues were used (see thermogravimetry analysis). Ngo et al., who reported about thermal and structural characterization of a series of homoleptic Cu(II) dialkyldithiocarbamate complexes, suppose, that the reactive substituents in copper salts of dibenzylthiocarbamates seem to lead to easier decomposition pathways and consequently takes place before a possible sublimation occurs. [124]

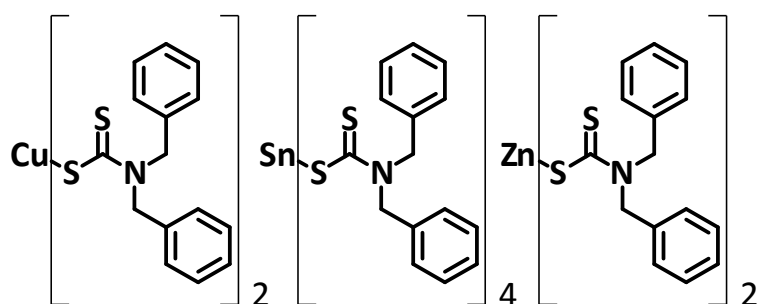


Figure 57: Structures of the prepared metal-dibenzylthiocarbamates

#### 3.4.3.2.1 Sample preparation

Precursor solutions were prepared from appropriate amounts of (CuDTC), (ZnDTC) and (SnDTC) either in pyridine or  $\text{CHCl}_3$ . These solutions were applied onto glass substrates either by drop coating, spin coating or doctor-blading. Afterwards the precursor layers were annealed under inert conditions, in order to form the CZTS. The procedure, which is illustrated in Figure 58, depicts this simple, direct and therefore very economic route to CZTS not using any energy consuming vacuum based production steps.

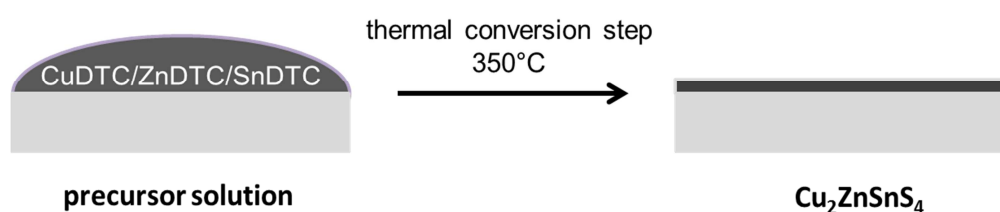


Figure 58: Scheme of the preparation of the nanostructured CZTS layers

During the thermal conversion step only volatile organic by-products like amines, alkyl residues and carbon disulfide are generated [130] and consequently a very pure inorganic semiconductor phase can be formed. A constant purge of nitrogen was created during the entire heating and cooling procedure, to be able to remove decomposing and evaporating by-products.

#### 3.4.3.2.2 Characterization

Thermogravimetry analysis of the dialkyldithiocarbamate complexes show, that these complexes start to decompose in the range of 200 to 317 °C. (CuDTC) decomposes at 252, (ZnDTC) at 317 and (SnDTC) shows a binary decomposition behavior having two temperatures of the maximum rate of the weight loss at 200 and 320°C. (see Figure 59) However, concerning metal salts of dialkyldithiocarbamates it has to be considered, that weight loss can either be associated with decomposition or vaporization of the complexes. Hereby, it has to be mentioned that the observed amounts of residues of the thermogravimetric analysis are quite close to that predicted to the corresponding metal sulfides  $\text{Cu}_2\text{S}$ ,  $\text{ZnS}$  and  $\text{SnS}/\text{SnS}_2$  and so the evaporation of these compounds can be neglected. Moreover, these investigations point out that an annealing temperature of at least 350 °C is required for a successful formation of CZTS.

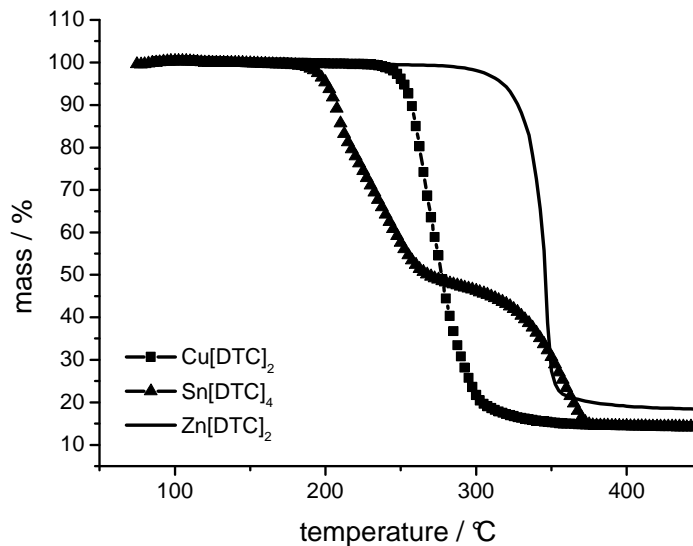


Figure 59: TGA-analysis of copper-, zinc- and tin- dibenzylidithiocarbamates

The use of stoichiometric amounts of (CuDTC) (2 equiv.), (ZnDTC) (1 equiv.) and (SnDTC) (1 equiv.) in the precursor solution did not result in the formation of one pure inorganic phase. (see Figure 60) Especially the additional formation of a copper sulfide, digenite, phase, which is marked by red frameworks in Figure 60 has to be mentioned. So we tried to convert a series of precursor solutions consisting of various ratios of the precursor materials. Only the reduction of the input of (CuDTC) and (SnDTC) led to promising results. Figure 60 depicts the X-ray diffraction patterns, which are vertically shifted for better visibility, of a series of samples with a varying content of (CuDTC). Only samples with a precursor content of a maximum input of 1.3 equivalents of (CuDTC) do not show the additional copper sulfide phase. We suppose that the different decomposition temperatures of the respective precursor materials are responsible for this phenomenon. Due to earlier thermal breakup of (CuDTC) and (SnDTC), they might show a faster conversion to the inorganic metal sulfides and consequently less volatilization of the precursor materials compared to (ZnDTC), whose decomposition does not start below a temperature of 317°C. The conversion of proper ratios of the precursor materials ((CuDTC)/(ZnDTC)/(SnDTC) = 1.3/1/0.55) lead to the formation of an inorganic phase, showing a diffraction pattern, which is in good agreement with the high intensity reflections of crystalline CZTS (kesterite), according to the Powder Diffraction File (PDF) 26-0575 of the International Centre for Diffraction Data. The respective sample exhibits broad peaks at approximately 28.4 °, 32.9 °, 47.3 °, 56.1 °, 69.1 ° and 76.3° 2Theta. Hereby the broadening of the characteristic peaks is dedicated to the nanostructural build-up of the investigated sample. The average primary crystallite sizes of the samples ( $D_{XRD}$ ) were determined according to the broadening of the diffraction peaks using the Scherrer relationship and resulted in particles of about 10 nm.

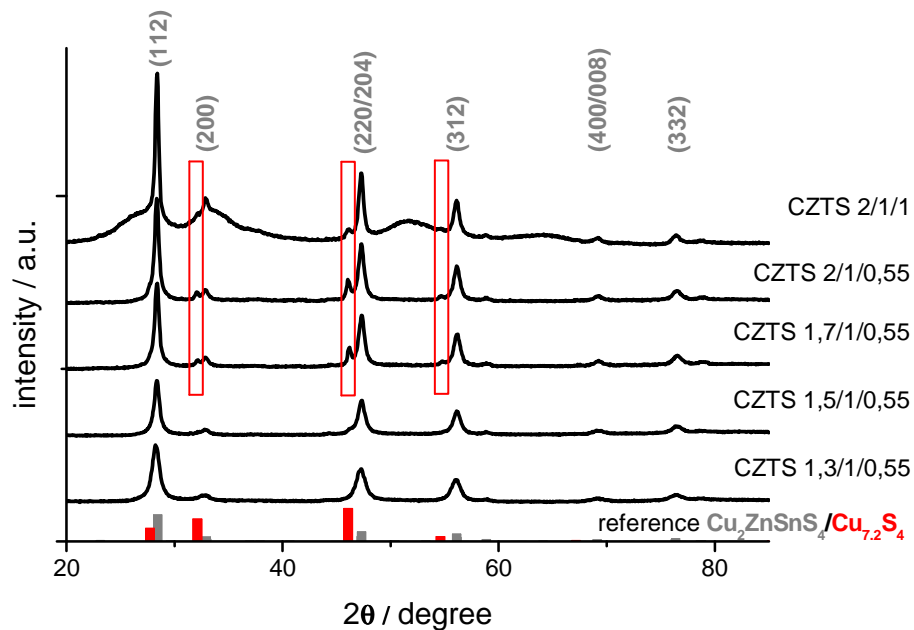


Figure 60: X-ray diffraction patterns of the CZTS layers prepared with different precursor ratios. The peaks are in good agreement with the reference pattern of CZTS (PDF 26-0575, sharp grey lines at the bottom). The corresponding indexation is given. As reference for the additionally arising peaks of the CuDTC rich samples a copper sulfide digenite phase PDF 24-0061 (sharp red lines at the bottom) fits well. (vertically shifted for better visibility)

However, due to their very similar crystal structures neither the presence of stannite as possible modification of  $\text{Cu}_2\text{ZnSnS}_4$  nor the presence of cubic sphalerite (ZnS) and  $\text{Cu}_2\text{SnS}_3$  (CTS) can fully be excluded based on XRD-measurements. This is why TEM-EDX investigations as well as additional XPS, Raman and UV-vis spectroscopy measurements were performed to obtain supplementary information about the samples.

More information about the structure and the chemical composition of the converted inorganic powders could be gained via energy dispersive X-ray analysis. Transmission electron microscopy was performed on the sample ((CuDTC)/(ZnDTC)/(SnDTC) = 1.3/1/0.55). This sample was prepared from  $\text{CHCl}_3$  dispersions casted onto TEM grids. A TEM- as well as SEM images are shown in Figure 61.

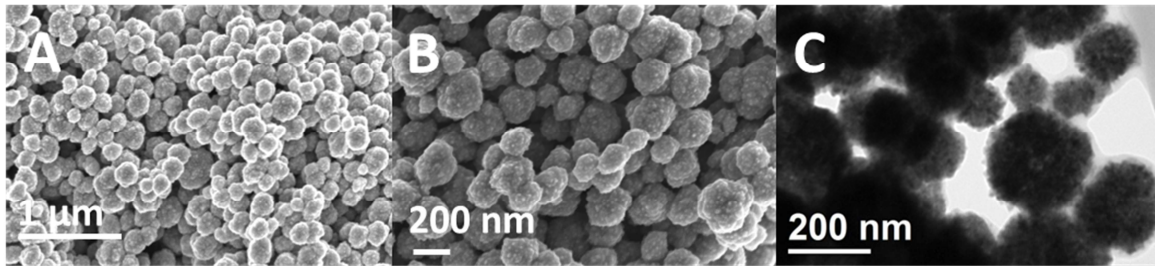


Figure 61: SEM- images of the CZTS layer with different magnifications (A,B) and a TEM micrograph (C) indicating that the microspheres consist of smaller crystallites with diameters of 10-20 nm. (W.Haas)

These images show the formation of agglomerates of microspheres, which have a diameter in the range of one hundred nanometers. These agglomerates seem to consist of nanoparticle based substructures, which are in good agreement with the results for the crystallite size obtained via Scherrer's equation (10 nm). The chemical composition of the samples was analyzed by energy dispersive X-ray spectrum imaging (EDX). The EDX-spectrum of the sample is depicted in Figure 62.

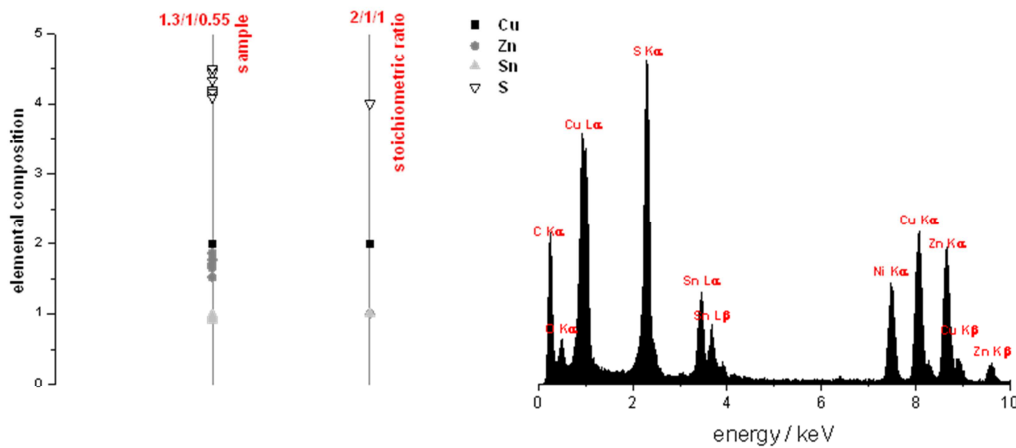


Figure 62: Summary of the EDX results and EDX spectrum of the CZTS sample (1.3/1/0.55)

Besides the emission lines of nickel, stemming from the TEM grid, the most intense emission peaks can be assigned to Cu, Zn, Sn, and S. The atom percentages of these elements were

calculated using the Cu K, Zn K, Sn L, and S K peaks using the Cliff-Lorimer approximation.[155] The obtained relative atom percentages in the material were normalized to the expected copper value (Cu=2 for  $\text{Cu}_2\text{ZnSnS}_4$ ) At least ten measurements were taken into account, to get reasonable results and to be able to confirm constant values for the composition of the CZTS. The results are illustrated in the Figure 62, which compares the maintained data of the sample with calculated values for  $\text{Cu}_2\text{ZnSnS}_4$ . The precursor solution with the precursor ratio of  $\text{CuDTC}/\text{ZnDTC}/\text{SnDTC} = 1.3/1/0.55$  led to the formation of well-defined nanoparticles of constant elemental composition, exhibiting a notable excess of zinc and a small excess of sulfur. According to literature zinc rich stoichiometries of CZTS are attracting attention because high power conversion efficiencies could be achieved in photovoltaic devices with compositional phases, having a slight excess of Zn ( $[\text{Zn}]/[\text{Sn}]=1.25$ ) [83].

The  $[\text{Zn}]/[\text{Sn}]$  ratio was about 1.8 in the investigated sample, which is a quite high excess of Zn and this is why the formation of additional zinc sulfide has to be considered.

In order to find out, whether the excess of zinc results in the formation of a zinc rich CZTS phase or leads to an additional zinc sulfide phase, raman spectroscopy measurements were performed. (see Figure 63)

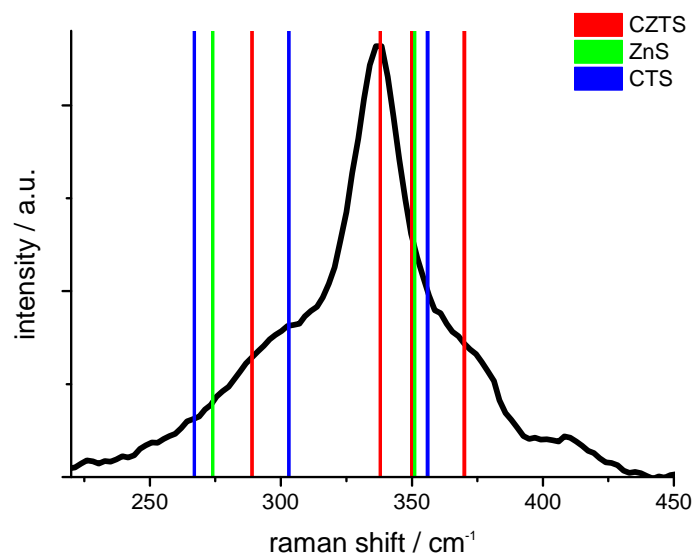


Figure 63: Raman Spectrum of the sample ((CuDTC)/(ZnDTC)/(SnDTC) = 1.3/1/0.55).



The existence of CZTS as main phase is confirmed by the most intense peak at  $338\text{ cm}^{-1}$ , which is in agreement with values reported in literature for CZTS thin films. [156][83] However, the investigations show a very broad peak of the raman spectrum, which is presumably caused by the nano-crystalline substructure of the CZTS microspheres. Thus, neither the presence of cubic sphalerite zinc sulfide showing its characteristic peaks at  $351$  and  $274\text{ cm}^{-1}$  nor the presence of cubic CTS, having its main raman signals at  $267$ ,  $303$  and  $356\text{ cm}^{-1}$  can fully be excluded by raman analysis. [157]

Consequently, further studies were necessary to proof or to exclude the presence of zinc sulfide. This is why X-ray photoelectron spectroscopy experiments were performed. In a controlled experiment a sample of CZTS as well as a sample of pure zinc sulfide were produced and analyzed. Hereby the Zn2p peaks of the CZTS sample should be shifted compared to those of pure zinc sulfide, because zinc atoms in zinc sulfide are only linked to sulfur and are not additionally surrounded by copper and tin atoms. Thus, the chemical circumstances of zinc atoms in CZTS are different from those in zinc sulfide and affect their binding energies. Zou et al.[154] ruled out that their CZTS nanocrystals were a mixture of copper tin sulfide and zinc sulfide because of an emerging shift difference of about  $1.2\text{ eV}$ . Our samples displayed a shift difference of about  $0.4\text{ eV}$  (see Figure 64), showing values for Zn $2p_{3/2}$  and Zn $2p_{1/2}$  of  $1022.3$  and  $1045.4\text{ eV}$  in the CZTS sample and  $1021.8$  and  $1044.8$  in pure zinc sulfide. Using high resolution XPS, the oxidation states could be determined for Cu2p, Zn2p, Sn3d and S2p (see Figure 65). Cu2p showed two peaks at  $932.4$  and  $952.4\text{ eV}$ , which is indicative for monovalent copper. Zn2p, having two peaks at  $1021.8$  and  $1044.8\text{ eV}$ , is known for bivalent zinc. Sn3d confirmed its tetravalent character via arising peaks at  $487.0$  and  $495.5\text{ eV}$  and S2p (sulfur) showed a peak splitting of  $1.2\text{ eV}$  ( $161.7$  and  $162.9\text{ eV}$ ). All these values are consistent with literature. According to our results of the XPS measurements and literature reports[154][158][159] we can disclose that there is a shift difference between the CZTS- and the pure zinc sulfide- sample of about  $0.4\text{ eV}$ . However, this observed shift is considerably smaller than shifts known in literature and this is why we cannot explicitly exclude that zinc sulfide may exist in the sample.

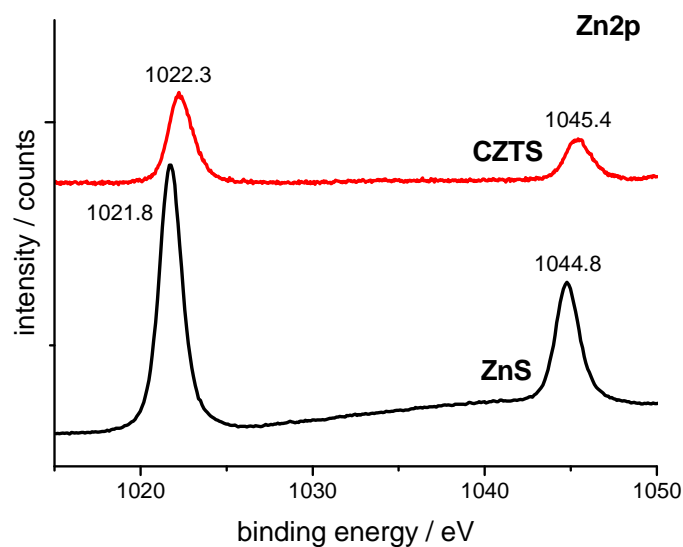


Figure 64: XPS-Spectra of CZTS compared to ZnS

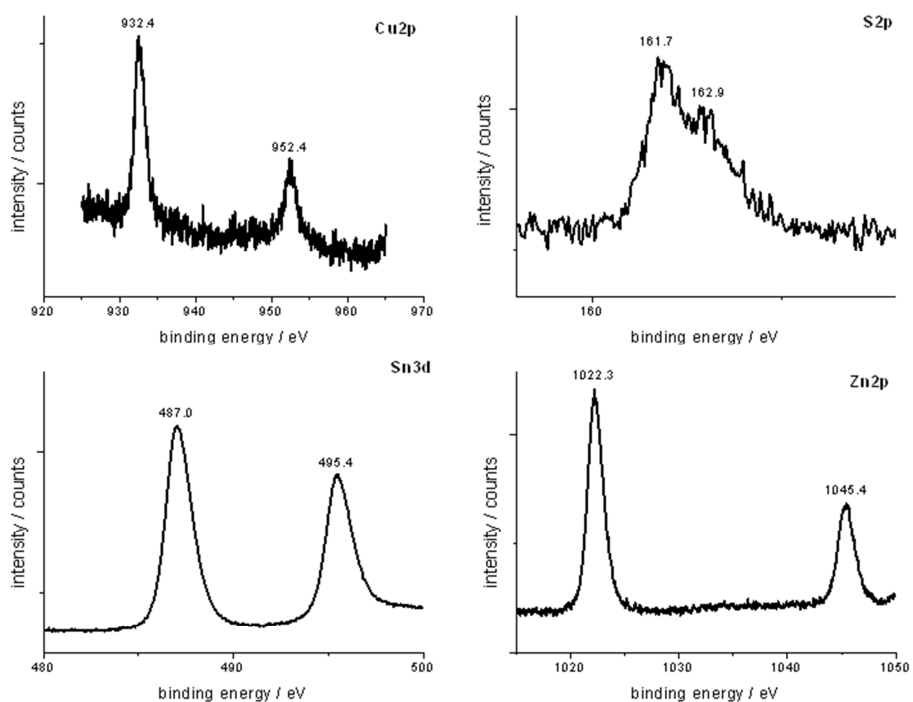


Figure 65: XPS-Spectra. (a) Cu 2p: binding energy at 932.4 eV and 952.4 eV with a peak splitting of 20.0 eV from Cu(I); (b) S 2p: binding energy at 161.7 eV and 162.9 eV with a peak splitting of 1.2 eV; (c) Sn 3d: binding energy at 487.0 eV and 495.4 eV with a splitting of 8.4 eV from Sn(IV); and (d) Zn 2p: binding energy at 1022.3 eV and 1045.4 eV with a peak splitting of 23.0 eV from Zn(II);

The optical band gap and the absorption coefficient ( $\alpha$ ) of the CZTS nanostructured particles were studied via transmittance and reflectance measurements. For these measurements thin CZTS films were prepared using the fabrication method as described before. The thickness of the layers was determined by a surface profiler and showed values in the range of 100 nanometer. To obtain the absorption coefficient the following equation

$$\alpha = \frac{1}{d} * \ln\left(\frac{1 - R}{T}\right)$$

was used, which is an accredited method in accordance with literature.[96][160] R stands for the reflectance, T for the transmittance and d for the thickness of the thin film. The film indicates a high absorption coefficient larger than  $1 \times 10^4 \text{ cm}^{-1}$ . Figure 66 plotting the absorption coefficient versus the wavelength and  $(\alpha h\nu)^2$  versus  $h\nu$  as insert discloses an optical band gap of about 1.6 eV which is consistent with the bulk value for CZTS in the range of 1.45 – 1.6 eV. [80][161] The band gap values were estimated from the  $(\alpha h\nu)^2$  versus  $h\nu$  by extrapolating the linear part of the depicted function.

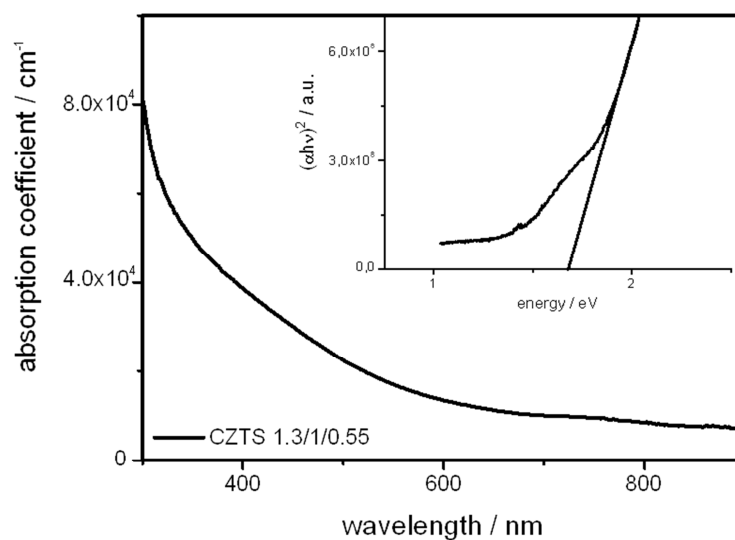


Figure 66: Absorption spectrum of sample CZTS 1.3/1/0.55. The  $(\alpha h\nu)^2$  vs.  $h\nu$  – plot for band gap determination is given in the insert.

### 3.4.3.3 Conclusion

In this work we present a dialkyldithiocarbamate solution processed direct formation of layers of nanocrystalline CZTS. For the formation of a kesterite copper zinc tin sulfide phase appropriate amounts of the respective dialkyldithiocarbamate precursors including an excess of ZnDTC were necessary. In addition, the content of CuDTC had to be reduced to avoid the formation of an additional copper sulfide phase.

EDX measurements disclosed a high excess of zinc within the CZTS powders resulting from the applied amounts of the precursor materials. Thus, the excessive zinc could either stand for a zinc rich phase of CZTS or for the formation of an additional zinc sulfide phase. That is why Raman- and XPS-studies were performed to be able to distinguish between a pure CZTS phase and a blend of CZTS, CTS and zinc sulfide. Although the results of both analysis methods trend to display the formation of a pure zinc rich CZTS phase, they could not exclude an additional formation of a zinc sulfide phase, which shows the complexity of this nanostructured quaternary CZTS semiconductor material.

## 4 Experimental part

### 4.1 Chemicals and materials

Table 10: Chemicals and materials

chemicals and materials	purity and description	supplier
Acetone	puriss	Sigma Aldrich
Aluminum	99.98%	Umicore
Benzene	≤ 99.9 %	Aldrich
Carbon disulfide	> 99.9 % S47702	Sigma Aldrich
Chlorobenzene	99.9 % Chromasolv	Sigma Aldrich
Chloroform	puriss. P.a.	Sigma Aldrich
Chloroform	> 99.8 %	Sigma Aldrich
Copper(I) iodide	>99 %, purum	Sigma Aldrich
Copper(II)chloride	> 99.99+ % metal basis	Sigma Aldrich
Deionized water	Purelab Prima water purification	water line
Diallylamine	99%	Aldrich
Dibenzylamine	97%	aldrich
Diethyl ether	puriss.	Sigma Aldrich
Dihexylamine	97 % LOT S43281-040	aldrich
Ethanol	>99.9 %, absolut	Sigma Aldrich
F8T2		ADS
FPC		Sigma Aldrich
Hexane	Art.Nr.: 52767	Fluka
Hydrochloric acid	37 %,puriss. p.a.	Sigma Aldrich
Indium (III) chloride	99.999%	Aldrich
Isopropyl alcohol	99.8 %, p.a.	Roth
ITO covered glass substrates	Rs = 15-25 Ω	Delta Technologies
MDMO-PPV		H.W. Sands
Methanol	> 99 %	Roth
Nitric acid	70%	Sigma Aldrich
PEDOT:PSS		HC Starck
PFDMB		Sigma Aldrich
Poly(p-xylene tetrahydrothiophenium chloride)	0.25 %W solution in water	Aldrich
PSBTBT	OS1001	1-Material
PSiFDBT	OS0927G1	1-Material
Pyridine	≥99.9 % Chroma solv.	Sigma Aldrich
Sodium hydroxide	> 99 % Art.Nr.: 9356.1	Roth
Thioacetamide	≥99.0 %	Fluka
Tin(IV)chloride penta-hydrate	> 98 %	Sigma Aldrich
Zinc chloride	> 98 %	Sigma Aldrich
Zinc powder	98+ %, dust	Sigma Aldrich

## **4.2 PPV/CIS – nanocomposite solar cells**

### **4.2.1 Preparation of PPV/CIS solar cells**

For the preparation of nanocomposite solar cells (see figure 2) ITO coated glass substrates were used as translucent anode material. In order to avoid shorts, which could be caused by the measuring tip during I-V characterization, parts of the ITO had to be etched. For this purpose zinc powder and hydrochloric acid were used. After an accurate cleaning of the structured ITO glass substrates using deionized water and isopropyl alcohol, the first PPV layer serving as hole transport layer was drop coated onto the substrate. Therefore a commercial acquired Pre-PPV (p-xylylene-bis-(triphenylphosphonium chloride) solution, based on water, was diluted with ethanol (1/4) to give a final concentration of 0.5 mg/ml of the precursor polymer. The coated layer was then converted to PPV under inert conditions in a programmable heating plate, holding the devices at 250 °C for 30 minutes. To form the active PPV/CIS layer the working instructions for the best results of the PPV/CIS solar cells made by Alejandro Santis [20] were adopted and only slightly modified. Thus, a solution of pyridine, containing 1 equivalent (equiv.) copper iodide (82.4 mmol), 2 equiv. indium chloride (164.8 mmol) and 5 equiv. TAA (412.4 mmol), was blended with the Pre-PPV solution to give a final weight ratio of PPV/CIS of 1/11. This solution was drop coated onto the PPV layer and thermally treated like the single PPV layer. Finally aluminum electrodes were thermally evaporated at a final air pressure of  $3 \cdot 10^{-5}$  mbar using a Baltec Med020 evaporation unit.

### **4.2.2 Preparation of the samples for Grazing Incidence Wide Angle X-ray Scattering (GIWAXS) analysis**

The samples for GIWAXS analysis were prepared like the solar cell devices using the same weighed portions. Only the second heating step and the evaporation of the aluminum electrodes were skipped. At the synchrotron in Trieste a special measuring setup was chosen to be able to perform experiments and to observe the in-situ formation of the CIS nanoparticles within the polymer matrix simulating the original annealing program of the solar cell devices.

## **4.3 PSiFDBT/CIS – nanocomposite solar cells**

### **4.3.1 General preparation of nanocomposite solar cells**

#### **4.3.1.1 Etching**

In order to avoid shorts during I-V characterization, parts of the ITO electrode had to be etched. Structuring of the ITO was performed via adhesive tape. Non covered parts of the translucent electrode material were removed using hydrochloric acid and zinc powder.

#### **4.3.1.2 Cleaning**

After the etching the adhesive tape was removed from the substrate. Subsequently the substrates were cleaned with water and acetone to get rid of residues stemming from the adhesive tape. In addition, the substrates were cleaned by ultrasonic treatment in deionized water and isopropyl alcohol. (20 min at room temperature/VWR ultrasonic cleaner) Further cleaning was performed via a plasma etching unit, produced by Diener Electronics. Oxygen was chosen as working gas. For the plasma a constant flow of oxygen was adjusted to be 8 sccm. The plasma (100 % power) was generated for two minutes to clean/etch the ITO substrates.

#### **4.3.1.3 Hole transport layer (optional)**

As hole transport layer, which is sandwiched between the anode and the active layer, PEDOT:PSS was used. A commercially available solution of PEDOT:PSS (HC Starck Clevios P VP.AI4083) in water was diluted with deionized water at a ratio of 1:1. This solution was coated onto the ITO glass substrates using a CT62 spin-coater produced by Karl Suss Technique S.A. (300 rpm/s; 2500 rpm; 30 s). The PEDOT:PSS layers were finally heated up to 150 °C for 10 minutes under inert conditions via a heating plate of a magnetic stirrer positioned in a glove box.

#### **4.3.1.4 Active layer**

For the preparation of the active layer(s) appropriate amounts of conducting polymers were dissolved either in chloroform or chlorobenzene and transferred into a glass vial containing the calculated amounts of copper- and indium xanthate. These solutions were stirred for a few minutes on a magnetic stirrer at elevated temperatures up to 50 °C in order to guarantee a

homogeneous precursor solution. Afterwards the precursor solution was coated onto the pretreated ITO glass (PEDOT:PSS) substrates using an Erichsen doctor blading machine. After the coating the substrates were dried on the heating plate for 20 seconds at a temperature of 60 °C. For the fabrication of a two-step coating assembly the coating and drying step was repeated once again. However, the second precursor solution was either prepared with reduced concentration of the polymer and higher inorganic content or just taking a 1:1 diluted version of the first precursor solution. The whole coating procedure was performed under inert conditions using a glove box.

#### **4.3.1.5 Thermal conversion step**

The thermal conversion of the precursor solution was carried out in a tube furnace produced by the company Heraeus. The coated substrates were annealed up to 200 °C using a heating rate of 28.5 °C/min and holding the final temperature at 200 °C for 15 minutes. The whole process was performed under vacuum.

#### **4.3.1.6 Deposition of the back electrodes**

To complete the nanocomposite solar cells, back electrodes consisting of aluminum were evaporated onto the active layers via the coating unit MED020 from Baltec, which is also equipped with a thickness measurement unit. The deposition of the aluminum electrodes was started at air pressures of  $5 \cdot 10^{-5}$  mbar.

### **4.3.2 Pretreatment of the ITO substrates**

After standard cleaning of the substrates via deionized water and isopropyl alcohol, they were either treated with potassium hydroxide, hydrochloric acid, aqua regia, nitric acid or oxygen plasma for a few minutes.

Potassium hydroxide: Potassium hydroxide (10 %W) was dissolved in isopropyl alcohol and heated up to 50 °C. The ITO substrates were put inside the solution and were treated for 10 minutes.

Hydrochloric acid: The ITO substrates were treated with an aqueous solution of hydrochloric acid (12 %mol) for 15 minutes.



Aqua regia: A diluted version of aqua regia was obtained by the mixture of fuming hydrochloric acid, nitric acid and deionized water at a ratio of 3:1:12. The substrates were treated for 5 minutes. Undiluted aqua regia totally removed the whole ITO layer of the glass substrates.

Nitric acid: The ITO substrates were put into a bath consisting of nitric acid (2 mol/L) for 20 minutes.

Oxygen plasma: The substrates were treated with oxygen plasma using a plasma etcher produced by Diener Electronics. Oxygen was chosen as working gas. Constant flow of oxygen was adjusted to be 8 sccm. The plasma (100 % power) was generated for two minutes to clean/etch the ITO substrates.

### 4.3.3 Preparation of the samples for Grazing Incidence Wide Angle X-ray Scattering (GIWAXS) analysis

Glass substrates were cleaned as it is described above. The active layer (PSiFDBT/CIS=1/7; Cu/In=1/1.7 see Table 11) was coated onto the PEDOT:PSS layer via drop coating. At the synchrotron in Trieste a special measuring setup was chosen to be able to perform experiments and to observe the in-situ formation of the CIS nanoparticles within the polymer matrix simulating the original annealing program of the solar cell devices.

Table 11: Weighed portion of polymer and xanthates for the preparation synchrotron samples

	PSiFDBT	Cu xanthate(heptyl)	In xanthate(heptyl)	chlorobenzene
<b>molar mass / g/mol</b>	2540-60910*	254.9	688.7	112.6
<b>mass / mg</b>	2.5	12.5	58.4	0.555
<b>concentration / mg/mL</b>	5	25	116.8	-
<b>equivalent P/CIS</b>	1	7		-
<b>volume / mL</b>	-	-	-	0.5

\*bimodal distribution

#### 4.3.4 Iterative improvement of the efficiency of polymer/CIS solar cells

##### 4.3.4.1 Influence of a PEDOT:PSS hole transport layer

For this purpose, blends of PSiFDBT, copper xanthate(heptyl) and indium xanthate(heptyl) were dissolved in chlorobenzene, solar cells were produced as described above (see general preparation of nanocomposite solar cells) and I-V curves were recorded. Detailed data for the amounts of the ingredients are listed in Table 12 and Table 13.

Table 12: Weighed portion of polymer and xanthates for the preparation of nanocomposite solar cells (1.active layer/PEDOT:PSS)

	Polymer	Cu xanthate(heptyl)	In xanthate(heptyl)	chlorobenzene
molar mass / g/mol	2540-60910*	254.9	688.7	112.6
mass / mg	2.5	12.5	57.5	0.555
concentration / mg/mL	5	25	115	-
equivalent P/CIS	1	7		-
volume / mL	-	-	-	0.5

\*bimodal distribution

Table 13: Weighed portion of polymer and xanthates for the preparation of nanocomposite solar cells (2.active layer/PEDOT:PSS)

	Polymer	Cu xanthate(heptyl)	In xanthate(heptyl)	chlorobenzene
molar mass / g/mol	2540-60910*	254.9	688.7	112.6
mass / mg	1.25	8.9	41	0.555
concentration / mg/mL	2.5	17.8	82	-
equivalent P/CIS	1	10		-
volume / mL	-	-	-	0.5

\*bimodal distribution

##### 4.3.4.2 DLS analysis of the precursor solutions

For DLS-analysis three types of precursor solutions were prepared. A solution of MDMO-PPV, copper xanthate(hexyl) and indium xanthate(hexyl) in chloroform as well as precursor solutions of MDMO-PPV, copper xanthate(heptyl) and indium xanthate(heptyl) dissolved either in chloroform or chlorobenzene. The solutions had a polymer concentration of 5 mg/mL having a donor- to acceptor ratio of 1/5 (CIS content refers to thermally converted CIS) and a copper to indium ratio of 1/1.7. In order to avoid influences of dust particles, the precursor solutions, which had been stirred all over the time, were centrifugalized after they had been transferred into the measuring vessels.

#### 4.3.4.3 Comparison of various conjugated polymers as donor materials

For the evaluation of five conjugated polymers a one-step coating assembly was chosen:

glass-ITO/PEDOT:PSS/polymer+CIS/aluminum.

##### 4.3.4.3.1 Poly[(9,9-dioctylfluorenyl-2,7-diyl)-co-bithiophene] (F8T2):

The ITO substrates were cleaned and coated with PEDOT:PSS as described above. The active layer (F8T2/CIS=1/4; Cu/In=1/1.7 see Table 14) was spin coated onto the PEDOT:PSS layer using the following parameters: 300 rpm/s; 700 rpm; 55 s. Afterwards the thermal conversion was performed with the standard annealing procedure (28.5 °C/min; 200 °C; 22 min). Sandwiched between the active layer and the back electrodes a very thin interlayer (1-5 nm) made of gold was deposited via the coating unit MED020 at an air pressure of  $2.8 \cdot 10^{-6}$  mbar. The back electrodes (aluminum) were deposited at a reduced pressure of  $1.1 \cdot 10^{-5}$  mbar.

Table 14: Weighed portion of polymer and xanthates for the preparation of nanocomposite solar cells (F8T2)

	F8T2	Cu xanthate(heptyl)	In xanthate(heptyl)	chlorobenzene
molar mass / g/mol	12400-90844*	254.9	688.7	112.6
mass / mg	15	42.9	197.7	1.665
concentration / mg/mL	10	28.6	131.8	-
equivalent P/CIS	1		4	-
volume / mL	-	-	-	1.5

\*bimodal distribution

##### 4.3.4.3.2 Poly[(9,9-N-dihexyl-2,7-fluorene-alt-9-phenyl-3,6-carbazole) (FPC):

The ITO substrates were cleaned and coated with PEDOT:PSS as described above. The active layer (FPC/CIS=1/4; Cu/In=1/1.7 see Table 15) was spin coated onto the PEDOT:PSS layer using the following parameters: 300 rpm/s; 700 rpm; 2\*18 s. Afterwards the thermal conversion was performed with a heating rate of 28.5 °C/min, final temperature of 210 °C and a holding time of 22 min. The back electrodes (aluminum) were deposited at a reduced pressure of  $5 \cdot 10^{-5}$  mbar.

**Table 15: Weighed portion of polymer and xanthates for the preparation of nanocomposite solar cells (FPC)**

	<b>FPC</b>	<b>Cu xanthate(heptyl)</b>	<b>In xanthate(heptyl)</b>	<b>chloroform</b>
<b>molar mass / g/mol</b>	4778	254.9	688.7	119.4
<b>mass / mg</b>	6	17.2	78.8	1.48
<b>concentration / mg/mL</b>	6	17.2	78.8	-
<b>equivalent P/CIS</b>	1	4		-
<b>volume / mL</b>	-	-	-	1

#### 4.3.4.3.3 Poly[(9,9-dioctylflourenyl-2,7-diyl)-alt-(2,5dimethyl-1,4-phenylene)] (PFDMB):

The ITO substrates were cleaned and coated with PEDOT:PSS as described above. The active layer (PFDMB/CIS=1/4; Cu/In=1/1.7 see Table 16) was spin coated onto the PEDOT:PSS layer using the following parameters: 300 rpm/s; 700 rpm; 40 s. Afterwards the thermal conversion was performed with the standard annealing procedure (28.5 °C/min; 200 °C; 22 min). The back electrodes (aluminum) were deposited at a reduced pressure of  $5 \cdot 10^{-5}$  mbar.

**Table 16: Weighed portion of polymer and xanthates for the preparation of nanocomposite solar cells (PFDMB)**

	<b>PFDMB</b>	<b>Cu xanthate(heptyl)</b>	<b>In xanthate(heptyl)</b>	<b>chloroform</b>
<b>molar mass / g/mol</b>	27659	254.9	688.7	119.4
<b>mass / mg</b>	6	17.1	78.7	0
<b>concentration / mg/mL</b>	6	17.1	78.7	-
<b>equivalent P/CIS</b>	1	4		-
<b>volume / mL</b>	-	-	-	1

#### 4.3.4.3.4 Poly[(4,4'-bis(2-ethylhexyl)-dithieno[3,2-b:2',3'-d]silole)-2,6-diyl-alt-(2,1,3-benzothiadiazole)4,7-diyl] (PSBTBT):

The ITO substrates were cleaned and coated with PEDOT:PSS as described above. The active layer (PSBTBT/CIS=1/7; Cu/In=1/1.7 see Table 17) was coated onto the PEDOT:PSS layer via doctor blading. The following parameters were used: wet layer thickness = 50  $\mu$ m; 80  $\mu$ L of the precursor solution; coating speed = 10 mm/s; at room temperature. After that the thermal conversion was performed with the standard annealing procedure (28.5 °C/min; 200 °C; 22 min). The back electrodes (aluminum) were deposited at a reduced pressure of  $2.9 \cdot 10^{-5}$  mbar.

Table 17: Weighed portion of polymer and xanthates for the preparation of nanocomposite solar cells (PSBTBT)

	PSBTBT	Cu xanthate(heptyl)	In xanthate(heptyl)	chlorobenzene
molar mass / g/mol	8500	254.9	688.7	112.6
mass / mg	2.5	12.5	57.5	0.555
concentration / mg/mL	5	25	115	-
equivalent P/CIS	1	7		-
volume / mL	-	-	-	0.5

4.3.4.3.5 Copolymer of 2,7-silafluorene and 4,7-di(2'-thienyl)-2,1,3-benzothiadiazole (PSiFDBT): The ITO substrates were cleaned and coated with PEDOT:PSS as described above. The active layer (PSiFDBT/CIS=1/7; Cu/In=1/1.7 see Table 18) was coated onto the PEDOT:PSS layer via doctor blading. The following parameters were used: wet layer thickness = 50  $\mu\text{m}$ ; 30  $\mu\text{L}$  of the precursor solution; coating speed = 10 mm/s; at room temperature. Afterwards the thermal conversion was performed with the standard annealing procedure (28.5  $^{\circ}\text{C}/\text{min}$ ; 200  $^{\circ}\text{C}$ ; 22 min). The back electrodes (aluminum) were deposited at a reduced pressure of  $5 \cdot 10^{-5}$  mbar.

Table 18: Weighed portion of polymer and xanthates for the preparation of nanocomposite solar cells (PSiFDBT)

	PSiFDBT	Cu xanthate(heptyl)	In xanthate(heptyl)	chlorobenzene
molar mass / g/mol	2540-60910*	254.9	688.7	112.6
mass / mg	2.5	12.5	58.4	0.555
concentration / mg/mL	5	25	116.8	-
equivalent P/CIS	1	7		-
volume / mL	-	-	-	0.5

\*bimodal distribution

## 4.3.5 Iterative improvement of the efficiency of PSiFDBT/CIS solar cells

### 4.3.5.1 1 step coating versus 2 step coating of the active layer

The ITO substrates were cleaned and coated with PEDOT:PSS as described above. The active layer (PSiFDBT/CIS=1/7; Cu/In=1/1.7 see Table 19) was coated onto the PEDOT:PSS layer via doctor blading. The following parameters were used: wet layer thickness = 50  $\mu\text{m}$ ; 30  $\mu\text{L}$  of the precursor solution; coating speed = 10 mm/s; at room temperature. After the coating the substrates were dried on the heating plate for 20 seconds at a temperature of 60  $^{\circ}\text{C}$ . Then the second precursor solution (PSiFDBT/CIS=1/10; Cu/In=1/1.7 see Table 20) was coated onto the

active layer. (only for the two-step coating assembly) Afterwards the thermal conversion was performed with the standard annealing procedure (28.5 °C/min; 200 °C; 22 min). The back electrodes (aluminum) were deposited at a reduced pressure of  $1 \cdot 10^{-5}$  mbar.

Table 19: Weighed portion of polymer and xanthates for the preparation of nanocomposite solar cells (1. active layer)

	PSiFDBT	Cu xanthate(heptyl)	In xanthate(heptyl)	chlorobenzene
molar mass / g/mol	2540-60910*	254.9	688.7	112.6
mass / mg	2.5	12.5	58.4	0.555
concentration / mg/mL	5	25	116.8	-
equivalent P/CIS	1	7		-
volume / mL	-	-	-	0.5

\*bimodal distribution

Table 20: Weighed portion of polymer and xanthates for the preparation of nanocomposite solar cells (2. active layer)

	PSiFDBT	Cu xanthate(heptyl)	In xanthate(heptyl)	chlorobenzene
molar mass / g/mol	2540-60910*	254,9	688,7	112,6
mass / mg	1,25	8,9	41	0,555
concentration / mg/mL	2,5	17,8	82	-
equivalent P/CIS	1	10		-
volume / mL	-	-	-	0,5

\*bimodal distribution

#### 4.3.5.2 Parameter adjustments for doctor blading

The ITO substrates were cleaned and coated with PEDOT:PSS as described above. All of these experiments were performed with the same precursor solutions as mentioned on the previous page. The active layer (PSiFDBT/CIS=1/7; Cu/In=1/1.7 see Table 19) was coated onto the PEDOT:PSS layer via doctor blade varying its parameters such as wet layer thickness, coating speed and the substrate temperature. After coating, the substrates were dried on the heating plate for 20 seconds at a temperature of 60 °C. Then the second precursor solution (PSiFDBT/CIS=1/10; Cu/In=1/1.7 see Table 20) was coated onto the active layer using the same parameters. Afterwards the thermal conversion was performed with the standard annealing

procedure (28.5 °C/min; 200 °C; 22 min). The back electrodes (aluminum) were deposited at an air pressure of  $1 \cdot 10^{-5}$  mbar.

#### 4.3.5.2.1 Variation of the coating speed

Both active layers were coated either with a coating speed of 10 or 25 mm/s.

#### 4.3.5.2.2 Variation of the substrate temperature:

The active layers were coated onto the substrates either at substrate temperatures of 30, 40 or 50 °C.

#### 4.3.5.2.3 Variation of the thickness of the wet layer

The thickness of the deposited wet layer was adjusted via micrometer caliper of the doctor blade to be either 30, 50, 70 or 90  $\mu\text{m}$ . For both layers the same adjustment was selected.

#### 4.3.5.3 Devices showing a power conversion efficiencies up to 2.8 %

The ITO substrate was cleaned and coated with PEDOT:PSS as described above. The first precursor solution, a blend of PSiFDBT/CIS of 1/7 having a copper/indium ratio of 1/1.7 (see Table 21), was coated onto the PEDOT:PSS layer using following parameters of the doctor blade: coating speed = 10 mm/s; substrate temperature = 40 °C; wet layer thickness = 50 µm. After the coating the substrate was dried on the heating plate for 20 seconds at a temperature of 60 °C. Then the second precursor solution (PSiFDBT/CIS=1/10; Cu/In=1/1.8 see Table 22) was coated onto the active layer using the same coating parameters. Afterwards the thermal conversion was performed with the standard annealing procedure (28.5 °C/min; 200 °C; 22 min). The back electrodes (aluminum) were deposited at an air pressure of  $5 \cdot 10^{-5}$  mbar.

Table 21: Weighed portion of polymer and xanthates for the preparation of nanocomposite solar cells (1. active layer)

	PSiFDBT	Cu xanthate(heptyl)	In xanthate(heptyl)	chlorobenzene
molar mass / g/mol	2540-60910*	254.9	688.7	112.6
mass / mg	2.5	12.5	59	0.555
concentration / mg/mL	5	25	118	-
equivalent P/CIS	1	7.1		-
volume / mL	-	-	-	0.5

\*bimodal distribution

Table 22: Weighed portion of polymer and xanthates for the Preparation of nanocomposite solar cells (2. active layer)

	PSiFDBT	Cu xanthate(heptyl)	In xanthate(heptyl)	chlorobenzene
molar mass / g/mol	2540-60910*	254.9	688.7	112.6
mass / mg	1.25	8.6	42	0.555
concentration / mg/mL	2.5	17.2	84	-
equivalent P/CIS	1	10		-
volume / mL	-	-	-	0.5

\*bimodal distribution



#### 4.3.5.4 Variation of the indium to copper ratio

The ITO substrates were cleaned and coated with PEDOT:PSS as described above. The first precursor solution, a blend of PSiFDBT/CIS of 1/5 related to a 5 mg/mL solution of PSiFDBT and having varying copper/indium ratios (1/1; 1/1.2; 1/1.4; 1/1.6; 1/1.7; 1/1.8; 1/2; 1/2.2; 1/2.4; 1/2.6), was coated onto the PEDOT:PSS layer using optimized parameters for doctor blading (coating speed = 10 mm/s; substrate temperature = 40 °C; wet layer thickness = 50 μm). Weighed portions of the compounds, which were used, are listed in Table 23. After coating the substrates were dried on the heating plate for 20 seconds at a temperature of 60 °C. In the meantime the precursor solution was diluted to half of its original concentration. Then the second coating step (using the diluted precursor solution) was performed using the same coating parameters. Afterwards, the thermal conversion was performed with the standard annealing procedure (28.5 °C/min; 200 °C; 22 min). The back electrodes (aluminum) were deposited at a reduced pressure of  $3 \times 10^{-5}$  mbar.

Table 23: Weighed portion for the preparation of nanocomposite solar cells having varied Cu/In ratio

	PSiFDBT	Cu xanthate(heptyl)	In xanthate(heptyl)
<b>molar mass / g/mol</b>	2540-60910	254.9	688.7
<b>ratio</b>	PSiFDBT/CIS =1/5; Cu/In =1/1		
<b>concentration / mg/mL</b>	5	26.4	70.9
<b>ratio</b>	PSiFDBT/CIS =1/5; Cu/In =1/1.2		
<b>concentration / mg/mL</b>	5	23.2	75.2
<b>ratio</b>	PSiFDBT/CIS =1/5; Cu/In =1/1.4		
<b>concentration / mg/mL</b>	5	20.7	78.5
<b>ratio</b>	PSiFDBT/CIS =1/5; Cu/In =1/1.6		
<b>concentration / mg/mL</b>	5	18.5	80.9
<b>ratio</b>	PSiFDBT/CIS =1/5; Cu/In =1/1.7		
<b>concentration / mg/mL</b>	5	17.9	82.1
<b>ratio</b>	PSiFDBT/CIS =1/5; Cu/In =1/1.8		
<b>concentration / mg/mL</b>	5	17.1	83.1
<b>ratio</b>	PSiFDBT/CIS =1/5; Cu/In =1/2		
<b>concentration / mg/mL</b>	5	15.8	85.2
<b>ratio</b>	PSiFDBT/CIS =1/14; Cu/In =1/2.2		
<b>concentration / mg/mL</b>	5	14.6	86.6
<b>ratio</b>	PSiFDBT/CIS =1/5; Cu/In =1/2.4		
<b>concentration / mg/mL</b>	5	13.5	87.8
<b>ratio</b>	PSiFDBT/CIS =1/14; Cu/In =1/2.2		
<b>concentration / mg/mL</b>	5	12.7	88.9

#### 4.3.5.5 Variation of the acceptor to donor ratio

The ITO substrates were cleaned and coated with PEDOT:PSS as described above. The first precursor solution, blends of varying PSiFDBT/CIS ratios (1/3; 1/5; 1/7; 1/9; 1/10; 1/11; 1/12; 1/14) related to a 5 mg/mL solution of PSiFDBT and having an indium to copper ratio of 2, was coated onto the PEDOT:PSS layer using the optimized parameters for the doctor blading (coating speed = 10 mm/s; substrate temperature = 40 °C; wet layer thickness = 50 μm). Weighed portions of the compounds, which were used, are listed in Table 24. After coating, the substrates were dried on the heating plate for 20 seconds at a temperature of 60 °C. In the meantime the precursor solution was diluted to half of its original concentration. Then the second coating step (using the diluted precursor solution) was performed using the same coating parameters. Afterwards the thermal conversion was performed with the standard annealing procedure (28.5 °C/min; 200 °C; 22 min). The back electrodes (aluminum) were deposited at reduced pressure of  $3 \times 10^{-5}$  mbar.

Table 24: Weighed portion for the preparation of nanocomposite solar cells having varied PSiFDBT/CIS ratio

	PSiFDBT	Cu xanthate(heptyl)	In xanthate(heptyl)
<b>molar mass / g/mol</b>	2540-60910	254.9	688.7
<b>ratio</b>	PSiFDBT/CIS =1/3; Cu/In =1/2		
<b>concentration / mg/mL</b>	5	9.4	51.1
<b>ratio</b>	PSiFDBT/CIS =1/5; Cu/In =1/2		
<b>concentration / mg/mL</b>	5	15.8	85.2
<b>ratio</b>	PSiFDBT/CIS =1/7; Cu/In =1/2		
<b>concentration / mg/mL</b>	5	22.2	119
<b>ratio</b>	PSiFDBT/CIS =1/9; Cu/In =1/2		
<b>concentration / mg/mL</b>	5	28.4	152.9
<b>ratio</b>	PSiFDBT/CIS =1/10; Cu/In =1/2		
<b>concentration / mg/mL</b>	5	31.4	169.9
<b>ratio</b>	PSiFDBT/CIS =1/11; Cu/In =1/2		
<b>concentration / mg/mL</b>	5	34.6	186.9
<b>ratio</b>	PSiFDBT/CIS =1/12; Cu/In =1/2		
<b>concentration / mg/mL</b>	5	37.7	203.8
<b>ratio</b>	PSiFDBT/CIS =1/14; Cu/In =1/2		
<b>concentration / mg/mL</b>	5	44	237.8

### **4.3.6 Sample preparation for TEM EDX analysis**

#### ***4.3.6.1 Various reduced air pressures during the thermal conversion step***

The precursor solution was prepared using a blend of PSiFDBT/CIS of 1/9 related to a 5 mg/mL solution of PSiFDBT and having a copper/indium ratio of 1/2.2. The ingredients were dissolved in chloroform and stirred for 10 minutes on the magnetic stirrer to guarantee a homogeneous precursor solution. Afterwards the precursor solution was spin-coated onto NaCl single crystals using the following parameters: 300 rpm/s; 800 rpm; 30 s. The precursor solution was converted with the standard annealing procedure (28.5 °C/min; 200 °C; 22 min). However, the reduced pressure was varied during the thermal conversion step using a reduced pressure of either 0.2, 2 or 20 mbar. Further preparation of the samples was performed at the institute for electron microscopy and fine structure research. The NaCl single crystal was dissolved in deionized water and the floating thin film was caught with a TEM-nickel-grid.

#### ***4.3.6.2 Various copper to indium ratios***

Precursor solutions were prepared using a blend of PSiFDBT/CIS of 1/9 related to a 5 mg/mL solution of PSiFDBT and having copper to indium ratios of either 1/1, 1/1.6, 1/1.8, 1/2.2 or 1/2.4. The ingredients were dissolved in chloroform and stirred for 10 minutes on the magnetic stirrer to guarantee homogeneous precursor solutions. Afterwards the precursor solutions were spin-coated onto NaCl single crystals using the following parameters: 300 rpm/s; 800 rpm; 30 s. The precursor materials were converted with the standard annealing procedure (28.5 °C/min; 200 °C; 22 min). Further preparation of the samples was performed at the institute for electron microscopy and fine structure research. The NaCl single crystal was dissolved in deionized water and the floating thin film was caught with a TEM-nickel-grid. Detailed data for the preparation of the respective thin films are listed in Table 25.

Table 25: Weighed portions of the chemicals for the preparation of PSiFDBT/CIS nanocomposite thin films on NaCl-crystals

	<b>PSiFDBT</b>	<b>Cu xanthate(heptyl)</b>	<b>In xanthate(heptyl)</b>
<b>molar mass / g/mol</b>	2540-60910	254.9	688.7
<b>ratio</b>	PSiFDBT/CIS =1/9; Cu/In =1/1		
<b>concentration / mg/mL</b>	5	47.2	127.8
<b>ratio</b>	PSiFDBT/CIS =1/9; Cu/In =1/1.6		
<b>concentration / mg/mL</b>	5	33.8	145.72
<b>ratio</b>	PSiFDBT/CIS =1/9; Cu/In =1/1.8		
<b>concentration / mg/mL</b>	5	30.8	149.8
<b>ratio</b>	PSiFDBT/CIS =1/9; Cu/In =1/2.2		
<b>concentration / mg/mL</b>	5	26.2	155.6
<b>ratio</b>	PSiFDBT/CIS =1/9; Cu/In =1/2.4		
<b>concentration / mg/mL</b>	5	24.4	158.2

## 4.4 Synthesis of metal-dialkyldithiocarbamates

The syntheses of the homoleptic dithiocarbamate metal complexes follow a modification of literature methods [126][124].

### 4.4.1 Sodium diallyldithiocarbamate

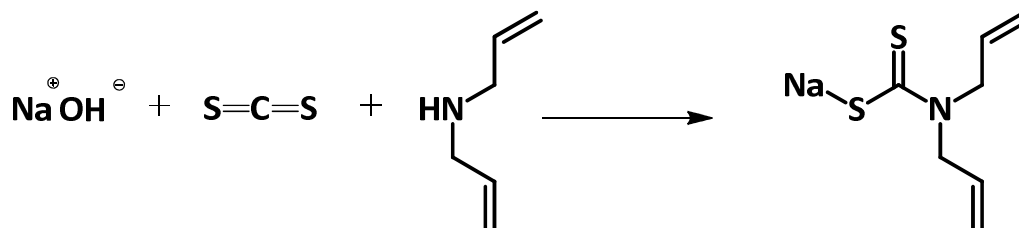


Figure 67: Reaction scheme for the synthesis of sodium diallyldithiocarbamate

Sodium hydroxide (NaOH / 1999 mg/ 1 equiv./ 50 mmol) was dissolved in deionized water (3 mL) and poured into a flask. Afterwards the flask was cooled down to 0 °C using a cooling bath and carbon disulfide (CS<sub>2</sub> / 6043 mL / 2 equiv. / 100 mmol), which had been dispersed in benzene (20 mL), was slowly added to the NaOH-solution. The addition of CS<sub>2</sub> was accompanied with the formation of white precipitates. Subsequently diallylamine (6.219 mL/ 1 equiv. / 50 mmol) was added to the cooled and vigorously stirred dispersion. The starting reaction resulted in the formation of an orange viscous solution showing intermediate precipitates, which disappeared again. After 90 minutes hexane was poured into the reaction mixture and slightly yellow flocs were built. These precipitates were decanted, filtered and washed well with hexane. Afterwards, the product was dried under vacuum to obtain sodium diallyldithiocarbamate as pale yellow powder, which was used in the following reactions as educt without further purification. The yield was about 80 %.

Sodium diallyldithiocarbamate: yield, 80%; colorless to pale yellow powder; analytical calculated for : %C, 43.05; %H, 5.16; %N, 7.17; %S, 32.85; Found: %C, 37.43; %H, 5.59; %N, 6.41; %S, 29.24.

#### 4.4.2 Sodium dihexyldithiocarbamate

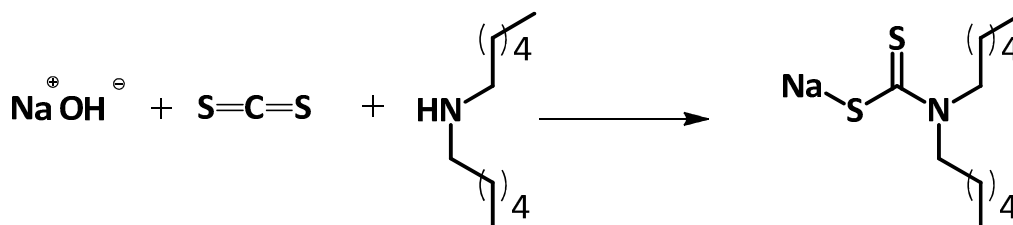


Figure 68: Reaction scheme for the synthesis of sodium dihexyldithiocarbamate

Sodium hydroxide (NaOH / 1919 mg/ 1.2 equiv./ 48 mmol) was dissolved in deionized water (3 mL) and poured into a flask. Afterwards the flask was cooled down to 0 °C using a cooling bath and carbon disulfide ( $\text{CS}_2$  / 2901 mL / 1.2 equiv. / 48 mmol), which had been dispersed in benzene (20 mL), was slowly added to the NaOH-solution. Subsequently dihexylamine (9614 mL/ 1 equiv. / 40 mmol) was added to the cooled and vigorously stirring dispersion using a dropping funnel. After two hours the product was extracted with diethyl ether using a separatory funnel. Subsequently, this solution was filtered and the solvent was evaporated resulting in the formation of yellow to orange residues, which were dried for 16 hours under vacuum. The yield was 95 %.

Sodium dihexyldithiocarbamate: yield, 95%; yellow to orange solid residues; analytical calculated for : %C, 55.08; %H, 9.24; %N, 4.94; %S, 22.62; Found: %C, 50.99; %H, 4.46; %N, 4.71; %S, 21.26.

#### 4.4.3 Sodium dibenzylidithiocarbamate

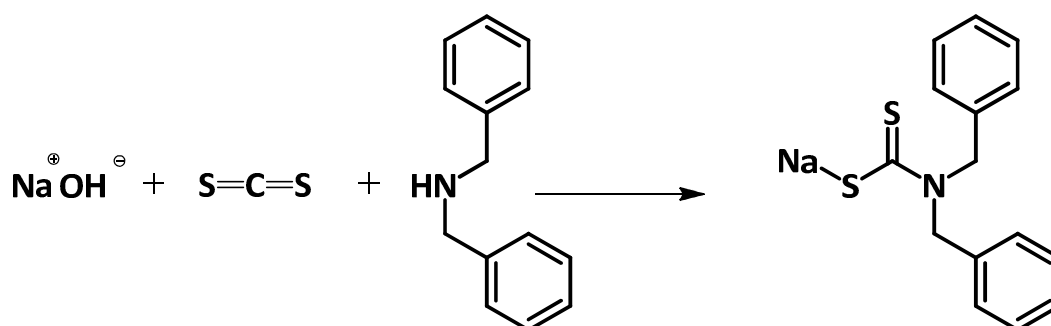


Figure 69: Reaction scheme for the synthesis of sodium dibenzylidithiocarbamate

Sodium dibenzylidithiocarbamate was synthesized analogously to sodium diallyldithiocarbamate. Thus, sodium hydroxide (NaOH / 1999 mg/ 1 equiv./ 50 mmol) was dissolved in deionized water (3 mL) and poured into a flask. Afterwards the flask was cooled down to 0 °C using a cooling bath and carbon disulfide (CS<sub>2</sub> / 6043 mL / 2 equiv. / 100 mmol), which had been dispersed in benzene (20 mL), was slowly added to the NaOH-solution. Subsequently dibenzylamine (10169 mg/ 1 equiv. / 50 mmol) was added to the cooled and vigorously stirring dispersion using a dropping funnel. After the solution had been stirred for one hour hexane was poured into the reaction mixture. The gained product was decanted, filtered and washed well with hexane. Afterwards the product was dried under vacuum to obtain sodium dibenzylidithiocarbamate as colorless powder, which was used in the following reactions as educt without further purification. The yield was about 88 %.

Sodium dihexylidithiocarbamate: yield, 88%; colorless powder; analytical calculated for : %C, 55.08; %H, 9.24; %N, 4.94; %S, 22.62; Found: %C, 50.99; %H, 4.46; %N, 4.71; %S, 21.26.

#### 4.4.4 Syntheses of metal dialkyldithiocarbamates

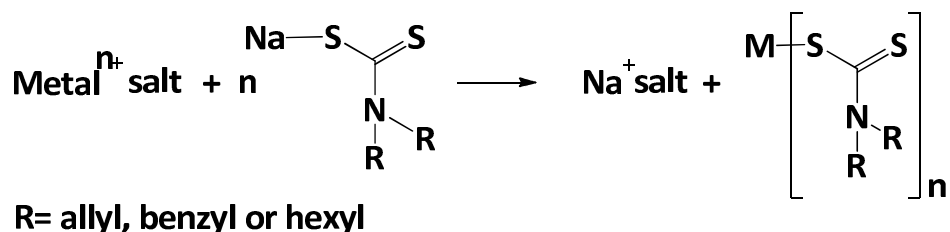


Figure 70: Reaction scheme for the synthesis of metal dialkyldithiocarbamates

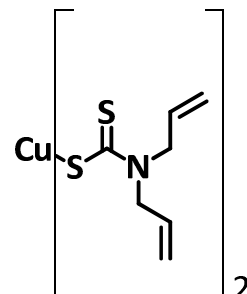
All dialkyldithiocarbamates were synthesized analogously. A solution of the respective dialkyldithiocarbamate in deionized water was added to a stirred solution of the appropriate metal salts ( $\text{CuCl}_2/\text{InCl}_3/\text{ZnCl}_2/\text{SnCl}_4 \cdot 5\text{H}_2\text{O}$ ) in deionized water. The reactions lasted for 3 to 5 hours. The resulting precipitates were filtered and washed with copious amounts of deionized water. Subsequently the precipitates were dried under vacuum for 16 hours. Afterwards the crude product was dissolved in  $\text{CHCl}_3$ , filtered and separated from all insoluble contaminations. Then the  $\text{CHCl}_3$  solution was concentrated and the product was precipitated in methanol. The solids were filtered and desiccated under vacuum. For characterization elemental analysis and IR-spectroscopy were performed. The indium, zinc and tin dialkyldithiocarbamates were additionally investigated using  $^1\text{H}$ -,  $^{13}\text{C}$ -, and  $^{119}\text{Sn}$ -NMR spectroscopy.

The weighed portions of the respective materials, the yields, and results of the characterization are illustrated in the following tables.



#### 4.4.4.1 Copper diallyldithiocarbamate $\text{Cu}[\text{DTC}]_2(\text{allyl})$

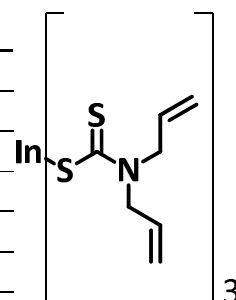
	$\text{CuCl}_2$	$\text{NaDTC}(\text{allyl})$	$\text{Cu}[\text{DTC}]_2(\text{allyl})$
molar mass / g/mol	176.5	195.28	408.13
equivalent	1.0	2.0	-
amount of substance / mmol	3.7	7.5	-
mass / mg	660.0	1460.6	-
theoretical yield / mg	-	-	1526.4
yield / mg	-	-	1315.0



Results of the characterization: yield, 86.2%; brown to black crystals; elemental analysis: analytical calculated for  $\text{C}_{14}\text{H}_{20}\text{N}_2\text{S}_4\text{Cu}$ : %C, 41.2; %H, 4.94; %N, 6.86; %S, 31.43; Found: %C, 41.74; %H, 4.85; %N, 6.96; %S, 31.88. IR (silicon waver) 3082-2928, 1641, 1478, 1412, 1232, 1179, 985, 942, 695.

#### 4.4.4.2 Indium diallyldithiocarbamate $\text{In}[\text{DTC}]_3(\text{allyl})$

	$\text{InCl}_3$	$\text{NaDTC}(\text{allyl})$	$\text{In}[\text{DTC}]_3(\text{allyl})$
molar mass / g/mol	221.2	195.28	631.69
equivalent	1.0	3.0	-
amount of substance / mmol	2.6	7.8	-
mass / mg	570.0	1523.2	-
theoretical yield / mg	-	-	1642.4
yield / mg	-	-	1100.0



Results of the characterization: yield, 67%; colorless crystals; elemental analysis: analytical calculated for  $\text{C}_{21}\text{H}_{30}\text{N}_3\text{S}_6\text{In}$ : %C, 39.93; %H, 4.79; %N, 6.65; %S, 30.46; Found: %C, 39.61; %H, 4.78; %N, 6.60; %S, 30.34. IR (silicon waver) 3080-2926, 1641, 1478, 1415, 1229, 1183, 985, 939, 692.

#### 4.4.4.3 Copper dihexyldithiocarbamate $\text{Cu}[\text{DTC}]_2(\text{hexyl})$

	$\text{CuCl}_2$	$\text{NaDTC}(\text{hexyl})$	$\text{Cu}[\text{DTC}]_2(\text{hexyl})$
molar mass / g/mol	176.5	283.5	584.5
equivalent	1.0	2.0	-
amount of substance / mmol	1.6	3.2	-
mass / mg	282.4	907.1	-
theoretical yield / mg	-	-	935.2
yield / mg	-	-	659.4

Results of the characterization: yield, 70.5%; black crystals; elemental analysis: analytical calculated for  $\text{C}_{26}\text{H}_{52}\text{N}_2\text{S}_4\text{Cu}$ : %C, 53.43; %H, 8.97; %N, 4.79; %S, 21.94; Found: %C, 53.36; %H, 8.94; %N, 4.79; %S, 21.90. IR (silicon waver) 2954-2852, 1501, 1426, 1369, 1290, 1192, 977, 726.

#### 4.4.4.4 Indium dihexyldithiocarbamate $\text{In}[\text{DTC}]_3(\text{hexyl})$

	$\text{InCl}_3$	$\text{NaDTC}(\text{hexyl})$	$\text{In}[\text{DTC}]_3(\text{hexyl})$
molar mass / g/mol	221.2	283.5	896.3
equivalent	1.0	3.0	-
amount of substance / mmol	1.6	4.8	-
mass / mg	361.0	1362.0	-
theoretical yield / mg	-	-	1434.0
yield / mg	-	-	1420.0

Results of the characterization: yield, 99%; colorless powder; elemental analysis: analytical calculated for  $\text{C}_{39}\text{H}_{78}\text{N}_3\text{S}_6\text{In}$ : %C, 52.26; %H, 8.77; %N, 4.69; %S, 21.47; Found: %C, 50.26; %H, 8.50; %N, 4.52; %S, 20.23.  $^1\text{H}$  NMR ( $\text{CDCl}_3$ )  $\delta$ : 0.88 (6H,  $-\text{CH}_3$ ); 1.290-1.765 (16H,  $-\text{CH}_2-$ ); 3.706 (4H, N- $\text{CH}_2$ ). IR (silicon waver) 2951-2855, 1501, 1428, 1369, 1293, 1189, 981, 726.

#### 4.4.4.5 Copper dibenzylthiocarbamate $\text{Cu}[\text{DTC}]_2(\text{benzyl})$

	$\text{CuCl}_2$	$\text{NaDTC}(\text{benzyl})$	$\text{Cu}[\text{DTC}]_2(\text{benzyl})$
molar mass / g/mol	176.5	295.4	608.36
equivalent	1.0	2.0	-
amount of substance / mmol	2.5	5.1	-
mass / mg	447.9	1500.0	-
theoretical yield / mg	-	-	1544.0
yield / mg	-	-	1325.0

Results of the characterization: yield, 85.8%; brown powder; analytical calculated for  $\text{C}_{30}\text{H}_{28}\text{N}_2\text{S}_4\text{Cu}$ : %C, 59.23; %H, 4.64; %N, 4.6; %S, 21.08; Found: %C, 58.8; %H, 4.63; %N, 4.59; %S, 21.12. IR (NaCl) 3085-2923, 1494-1452, 1428, 1357, 1220, 1150, 990, 752, 690.

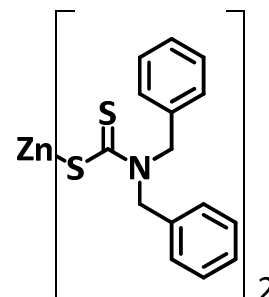
#### 4.4.4.6 Indium dibenzylthiocarbamate $\text{In}[\text{DTC}]_3(\text{benzyl})$

	$\text{InCl}_3$	$\text{NaDTC}(\text{benzyl})$	$\text{In}[\text{DTC}]_3(\text{benzyl})$
molar mass / g/mol	221.2	295.4	932.04
equivalent	1.0	3.0	-
amount of substance / mmol	1.7	5.1	-
mass / mg	374.4	1500.0	-
theoretical yield / mg	-	-	1577.6
yield / mg	-	-	1440.0

Results of the characterization: yield, 91,3%; colorless crystals; analytical calculated for  $\text{C}_{45}\text{H}_{43}\text{N}_3\text{S}_6\text{Cu}$ : %C, 57.99; %H, 4.54; %N, 4.51; %S, 20.64; Found: %C, 57.50; %H, 4.52; %N, 4.49; %S, 20.69.  $^1\text{H}$  NMR ( $\text{CDCl}_3$ )  $\delta$ : 5.05 (8H,  $-\text{CH}_2-$ ); 7.22-7.4 (20H,  $-\text{CH}_{\text{aromat.}}$ ).  $^{13}\text{C}$  NMR ( $\text{CDCl}_3$ )  $\delta$ : 56 (N-C-Phenyl); 128.0-129.0 (C2-C5/aromat); 135.0 (C1/aromat); 206.1 ( $-\text{CS}_2$ ). IR (NaCl) 3085-3060, 3024, 2914, 1496-1448, 1426, 1356, 1219, 1148, 983, 752, 701.

#### 4.4.4.7 Zinc dibenzylthiocarbamate Zn[DTC]<sub>2</sub>(benzyl)

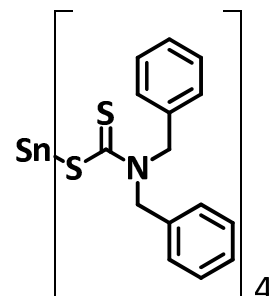
	ZnCl <sub>2</sub>	NaDTC(benzyl)	Zn[DTC] <sub>2</sub> (benzyl)
molar mass / g/mol	183.5	295.4	610.2
equivalent	1.0	2.0	-
amount of substance / mmol	2.5	5.0	-
mass / mg	465.8	1500.0	-
theoretical yield / mg	-	-	1549.3
yield / mg	-	-	1250.0



Results of the characterization: yield, 80,7%; colorless to pale rose crystals; analytical calculated for C<sub>30</sub>H<sub>28</sub>N<sub>2</sub>S<sub>4</sub>Zn: %C, 59.05; %H, 4.63; %N, 4.59; %S, 21.02; Found: %C, 59.0; %H, 4.61; %N, 4.62; %S, 21.06. <sup>1</sup>H NMR (CDCl<sub>3</sub>) δ: 5.05 (8H, -CH<sub>2</sub>-); 7.32-7.4 (20H, -CH<sub>aromat.</sub>-). <sup>13</sup>C NMR (CDCl<sub>3</sub>) δ: 55.7 (N-C-Phenyl); 128.0-129.0 (C2-C5/aromat); 134.5 (C1/aromat); 206.1 (-CS<sub>2</sub>). IR (NaCl) 3104-2928, 1495-1454, 1427, 1356, 1220, 1143, 981, 753, 699.

#### 4.4.4.8 Tin dibenzylthiocarbamate Sn[DTC]<sub>4</sub>(benzyl)

	SnCl <sub>4</sub>	NaDT(benzyl)	Sn[DTC] <sub>4</sub> (benzyl)
molar mass / g/mol	350.6	295.4	1208.34
equivalent	1.0	4.0	-
amount of substance / mmol	1.3	5.1	-
mass / mg	445.1	1500.0	-
theoretical yield / mg	-	-	1533.9
yield / mg	-	-	450.0



Results of the characterization: yield, 29%; orange powder; analytical calculated for C<sub>60</sub>H<sub>56</sub>N<sub>4</sub>S<sub>8</sub>Sn: %C, 59.64; %H, 4.67; %N, 4.64; %S, 21.23; Found: %C, 58.9; %H, 4.65; %N, 4.59; %S, 21.14. <sup>1</sup>H NMR (CDCl<sub>3</sub>) δ: 5.04 (8H, -CH<sub>2</sub>-); 7.27-7.34 (20H, -CH<sub>aromat.</sub>-). <sup>13</sup>C NMR (CDCl<sub>3</sub>) δ: 56.4 (N-C-Phenyl); 128.0-129.0 (C2-C5/aromat); 135.0 (C1/aromat); 203.0 (-CS<sub>2</sub>). <sup>119</sup>Sn NMR(CDCl<sub>3</sub>) δ: -845.263. IR (NaCl) 3105-2925, 1495-1452, 1429, 1355, 1219, 1147, 1000, 753, 698.

## 4.5 Preparation of CIS layers via metal-dialkyldithiocarbamates

Appropriate amounts of copper dialkyldithiocarbamate and indium dialkyldithiocarbamate were dissolved either in pyridine or chloroform. The molar concentration standing for 1 equivalent was 0.1 mol/l. Detailed data are depicted in the following tables (see Table 26, Table 27, Table 28, Table 29). The solution was drop coated onto the glass substrates, which had been cleaned in an ultrasonic water bath followed by an ultrasonic isopropanol bath each for 20 minutes. The coated substrates were annealed in a tube furnace under nitrogen atmosphere. Two different heating programs were used:

- The precursor materials were annealed up to 200 °C using a heating rate of 29 °C/min and were baked for 15 min at 200 °C.
- The precursor materials were annealed up to 350 °C using a heating rate of 23 °C/min and were baked for 15 min at 350 °C.

After the heating step the substrates were cooled down to room temperature under nitrogen atmosphere.

Table 26: Weighed portion of dibenzylthiocarbamates for the synthesis of CIS layers

	<b>Cudtc(benzyl)</b>	<b>Indtc(benzyl)</b>
<b>molar mass / g/mol</b>	608.4	932.0
<b>mass / mg</b>	60.8	93.2
<b>concentration / mmol/ml</b>	0.1	0.1
<b>equivalent</b>	1.0	1.0

Table 27: Weighed portion of dihexylthiocarbamates for the synthesis of CIS layers

	<b>Cudtc(hexyl)</b>	<b>Indtc(hexyl)</b>
<b>molar mass / g/mol</b>	583.3	896.3
<b>mass / mg</b>	58.3	89.6
<b>concentration / mmol/ml</b>	0.1	0.1
<b>equivalent</b>	1.0	1.0

**Table 28: Weighed portion of diallyldithiocarbamates for the synthesis of CIS layers**

	<b>Cudtc(allyl)</b>	<b>Indtc(allyl)</b>
<b>molar mass / g/mol</b>	408.1	631.7
<b>mass / mg</b>	40.8	63.2
<b>concentration / mmol/ml</b>	0.1	0.1
<b>equivalent</b>	1.0	1.0

**Table 29: Weighed portion of diallyldithiocarbamates for the synthesis of CIS layers**

	<b>Cudtc(allyl)</b>	<b>Indtc(allyl)</b>
<b>molar mass / g/mol</b>	408.1	631.7
<b>mass / mg</b>	30.6	63.2
<b>concentration / mmol/ml</b>	0.075	0.1
<b>equivalent</b>	0.75	1.0

## 4.6 Preparation of CZTS layers

The CZTS layers were fabricated analogous to CIS layers as described above. For solubility reasons the concentrations of the metal dialkyldithiocarbamate solutions were reduced to be 0.025 mol/L (1 equivalent). Detailed data are illustrated in the following tables. (Table 30, Table 31, Table 32, Table 33) In addition, all of the CZTS samples were annealed up to 350 °C corresponding to the annealing program of the CIS samples.

For the reflectance and transmission spectroscopy as well as XPS studies the coated substrates were used without further pretreatment. However, for XRD-measurements, TEM-EDX investigations, SEM studies and Raman spectroscopy the metal sulfide layers were scratched off the substrates to obtain metal sulfide powders.

Table 30: Weighed portion of dibenzylthiocarbamates for the synthesis of CZTS (2/1/0.55) layers

	<b>Cudtc(benzyl)</b>	<b>Zndtc(benzyl)</b>	<b>Sndtc(benzyl)</b>
<b>molar mass / g/mol</b>	608.36	610.23	1208.34
<b>mass / mg</b>	30.4	15.3	16.6
<b>concentration / mmol/ml</b>	0.050	0.025	0.014
<b>equivalent</b>	2	1	0.55

Table 31: Weighed portion of dibenzylthiocarbamates for the synthesis of CZTS (1.7/1/0.55) layers

	<b>Cudtc(benzyl)</b>	<b>Zndtc(benzyl)</b>	<b>Sndtc(benzyl)</b>
<b>molar mass / g/mol</b>	608.36	610.23	1208.34
<b>mass / mg</b>	25.9	15.3	16.6
<b>concentration / mmol/ml</b>	0.0425	0.025	0.014
<b>equivalent</b>	1.7	1	0.55

Table 32: Weighed portion of dibenzylthiocarbamates for the synthesis of CZTS (1.5/1/0.55) layers

	<b>Cudtc(benzyl)</b>	<b>Zndtc(benzyl)</b>	<b>Sndtc(benzyl)</b>
<b>molar mass / g/mol</b>	608.36	610.23	1208.34
<b>mass / mg</b>	22.8	15.3	16.6
<b>concentration / mmol/ml</b>	0.0375	0.025	0.014
<b>equivalent</b>	1.5	1	0.55

Table 33: Weighed portion of dibenzylthiocarbamates for the synthesis of CZTS (1.3/1/0.55) layers

	<b>Cudtc(benzyl)</b>	<b>Zndtc(benzyl)</b>	<b>Sndtc(benzyl)</b>
<b>molar mass / g/mol</b>	608.36	610.23	1208.34
<b>mass / mg</b>	19.8	15.3	16.6
<b>concentration / mmol/ml</b>	0.0325	0.025	0.014
<b>equivalent</b>	1.3	1	0.55

## 4.7 Characterization techniques

### 4.7.1 X-ray powder diffraction analysis

XRD patterns of the respective CIS and CZTS powders were recorded with a Siemens D 501 Diffractometer. The patterns were recorded using Bragg Brentano Geometry operated at 40 kV and 30 mA. As radiation CuK $\alpha$  emission ( $\lambda = 1.54178 \text{ \AA}$ ) was used at a scan rate of 0.05  $^{\circ}$ .

Primary average crystallite sizes of the CZTS nanoparticles were approximated via Scherrer relationship:

$$L \approx \frac{k * \lambda}{\Delta(2\theta) * \cos(\theta)}$$

L: crystallite size

$\Delta(2\theta)$ : broadening of the reflexes

k: form factor  $\approx 1$

$\lambda$ : wavelength

$\theta$ : diffraction angle

This approximation, however, is only acceptable for crystal sizes below 100 nm and reveals best results for spherical crystals. The experimental line width was defined to be 0.12  $^{\circ}$  at the 2 $\theta$  - position using a Si-reference standard (NIST 640c)

### 4.7.2 Scanning electron microscopy (SEM)

Scanning electron microscopy images were recorded at 3 kV either with a Zeiss-Ultra 55 or a Zeiss Gemini DSM 982 using an InLens detector.

### 4.7.3 Transmission electron microscopy (TEM)

TEM investigations of the PSiFDBT/CIS nanocomposite solar cell were conducted on a Tecnai F 20 microscope (FEI company, 200 kV, Schottky emitter). A FIB lamella of the solar cell device had



to be prepared. Therefore platinum was deposited onto the solar cell as protective layer and a lamella was milled using a gallium ion beam. Subsequently the lamella was transferred to a sample holder grid and thinned to a thickness of about 50 nm.

TEM images of the CZTS nanoparticles and CIS thin films were conducted on a CM20/STEM instrument operated at 200 kV with a LaB<sub>6</sub> cathode.

The CZTS powders, which had been scratched off the substrates after their thermal conversion, were suspended in ethanol and transferred onto a Ni-TEM- grid. Subsequently, the solvent was evaporated.

After the precursor solution had been spin coated onto a NaCl single crystal and thermally converted, the CIS thin films were floated off the single crystal and were attached to a Ni-TEM-grid.

#### ***4.7.3.1 Energy dispersive X-ray spectrum imaging (EDX)***

A Philips CM20/STEM operated at 200 kV with a LaB<sub>6</sub> cathode equipped with a Noran HPGe detector was used for the EDX analysis of the CZTS powders and the CIS thin films. Spectra were recorded in scanning transmission electron microscopy mode (STEM). The Cu-K, Zn-K, Sn-L and S-K lines were used for quantification with the thin film technique.[155]

#### ***4.7.3.2 Energy electron loss spectrum imaging (EELS)***

A Tecnai F 20 microscope (FEI company, 200 kV, Schottky emitter, Gatan GIF Quantum energy filter system) was used for EELS analysis of the cross section of the PSiFDBT/CIS solar cell.

#### **4.7.4 Raman spectroscopy**

Raman images were collected using a HORIBA LabRAM HR 800 confocal Raman microscope.

#### **4.7.5 Reflectance and transmission measurements**

Reflectance and transmission measurements of CZTS thin films were performed using a lambda 900 spectrometer from Perkin Elmer having an optional, external integrating sphere (PELA 1000).

#### **4.7.6 Surface profiler**

The layer thicknesses as well as the surface morphology of the CZTS layers were analyzed with a Veeco Dektak 150 surface profiler.

#### **4.7.7 X-Ray photoelectron spectroscopy**

XPS studies were performed with a K-Alpha photoelectron spectrometer (Thermo Scientific). For the radiation an aluminum K $\alpha$  source was used. Further parameters: spot size of the sample (400  $\mu\text{m}$ ), pass energy (20 eV) and step size energy (0.1 eV).

#### **4.7.8 Elemental analysis**

Elemental analyses of the metal dialkyldithiocarbamates were studied on a Universal CHNS Elemental Analyzer (Vario El III)

#### **4.7.9 Fourier transform infrared spectroscopy (FTIR)**

The respective metal dialkyldithiocarbamates were dissolved in chloroform and coated onto a silicon wafer or sodium chloride single crystals. After the evaporation of the solvent FTIR measurements were carried out with a Perkin Elmer Spectrum One apparatus using the transmission mode.

#### **4.7.10 Nuclear magnetic resonance spectroscopy (NMR)**

For NMR analyses the sodium dialkyldithiocarbamates had to be dissolved in deuterated acetone whereas the dialkyldithiocarbamate of all other metals could be dissolved in deuterated chloroform.  $^1\text{H}$ - and  $^{13}\text{C}$ - NMR spectroscopy was performed using a Bruker Ultrashield 300.

#### **4.7.11 Dynamic light scattering analysis (DLS)**

DLS measurements of the precursor solutions, containing MDMO-PPV, copper- and indium xanthate, were performed using a laser with a wavelength of 632.8 nm (power: 25-35 mW). All measurements were carried out at 25 °C and the light scattering was measured for 30 seconds at a scattering angle of 90 °. Each measurement was repeated ten times. The signals were detected and recorded taking an ALV/SO-SIPD/DUAL photomultiplier and an ALV 5000/E correlator.

#### **4.7.12 I-V characterization**

I-V characteristics of the nanocomposite solar cells were determined via a Keithley-2400 sourcemeter controlled by special Lab VIEW software. The devices were measured in a glove box and illuminated with a halogen bulb (150 W) through a borosilicate window, integrated to the glove box. The incoming light was currently checked via a pyranometer unit to ensure an irradiance of 1000 W/m<sup>2</sup>.

#### **4.7.13 IPCE measurements**

For IPCE measurements devices were transferred into a measurement chamber to be able to record the IPCE spectra under inert conditions. The measurement set up consists of an AMKO xenon lamp, an AMKO grating monochromator (multimode-4 monochromator), a light guide leading the photons to the solar cells, a reference diode (produced by Hamamatsu) to

determine the incoming light and a Keithley-2400 sourcemeter to record the photocurrent which is generated at a defined wavelength.

#### **4.7.14 Contact angle analysis**

The wetting behavior of the differently pretreated ITO substrates was derived from the investigation of contact angles of water touching the ITO surface via a Kruss DSA 100 analysis instrument.

#### **4.7.15 Grazing Incidence Wide Angle X-ray Scattering (GIWAXS) analysis**

Gracing incident wide-angle X-ray scattering (GIWAXS) measurements were performed at the Austrian SAXS Beamline 5.2 L of the electron storage ring ELETTRA (Italy). The beamline was adjusted to resolve the angular range ( $2\theta$ ) between  $21.1^\circ$  and  $41.8^\circ$  using X-ray energy of 8 keV. The precursor-substrates (glass, glass/ITO) were placed in a custom-made sample cell with a grazing angle of about  $0.18^\circ$  and were heated from  $40^\circ\text{C}$  up to  $180^\circ\text{C}$  at a heating rate of approximately  $8^\circ\text{C}/\text{min}$  in vacuum. During the temperature scan, data were recorded with 10 s resolution.

## 5 Summary and outlook

This thesis deals with the investigation of various preparation routes for nanocomposite solar cells. Therefore, a series of active materials and processing parameters was studied. In addition, dialkyldithiocarbamates were synthesized as possible precursor materials for the formation of semiconducting metal sulfides.

The first part of this work had its focus on temperature resolved investigations of the formation of CIS within a PPV matrix. PPV as well as CIS were obtained via thermal conversion of precursor materials (p-xylylene-bis-(triphenylphosphonium chloride/copper iodide/ indium trichloride/ thioacetamide). The required results could be obtained with GIWAXS analysis using Synchrotron radiation. These in-situ investigations, which were performed during the thermal conversion step of the precursor materials, show the starting temperature of the formation of CIS to be about 100 °C. For the preparation of the PPV/CIS solar cells, however, temperatures of 250 °C were chosen to ensure complete conversion of both, the donor and the acceptor precursors. In addition, IPCE (incident photon to current efficiency) measurements were conducted and confirmed an enhancement of the external quantum efficiency due to additional absorption of the CIS nanoparticles. Thus, power conversion efficiencies up to 1 % could be obtained. These cell performances, however, were difficult to reproduce, which could be the result of complex active-layer-forming-mechanisms resulting from the decomposition of the precursors for the donor as well as the acceptor materials.

The topic of the second chapter was about PSiFDBT/CIS solar cells. PSiFDBT is a low band gap polymer that could achieve power conversion efficiencies up to 5 % taking PCBM as acceptor material and therefore proved to be a promising polymer for organic photovoltaics. For these solar cells CIS was obtained via thermal conversion of copper and indium xanthate(heptyl) directly within the polymer matrix. Xanthates are known to decompose at low temperatures and to release only volatile byproducts. For this purpose xanthates seemed to be ideal candidates for a copper agent free synthesis of highly pure CIS nanoparticles within the polymer matrix. In general, the active layers of the PSiFDBT/CIS solar cells were prepared as it is shown in the following scheme. (see Figure 71) A blend of PSiFDBT and the appropriate amounts of

copper and indium xanthate(heptyl), dissolved in chlorobenzene, were coated on glass/ITO/PEDOT:PSS substrates either by spin coating or doctor blading. Subsequently the precursor layers were thermally converted under reduced pressure. To complete the solar cells counter electrodes were evaporated onto the active materials and hence a glass/ITO/PEDOT:PSS/active layer/Al assembly was obtained.

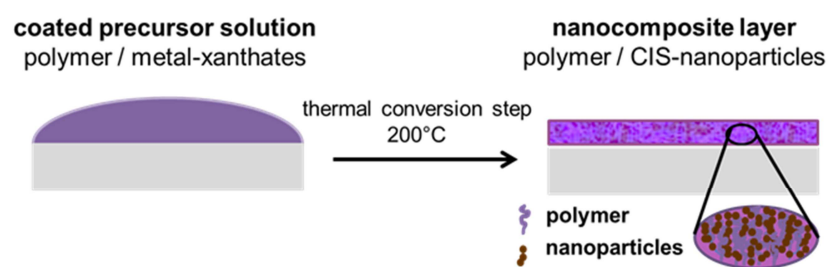


Figure 71: Precursor route to nanocomposite solar cells

In order to improve the power conversion efficiency a series of parameters was tested. Pretreatment of the ITO substrates, comparison of different conjugated polymers, solubility of two types of xanthate precursors, investigation of various precursor compositions, testing of coating parameters and comparison of various reduced pressures during the thermal conversion step were analyzed. Combining the optimized parameters, solar cells could be prepared showing power conversion efficiencies up to 2.8 %. These devices displayed values for the characteristic solar cell parameters, which were close to those presented for the current record device of nanocomposite solar cells having a power conversion efficiency of 3.13 %. Besides the testing of various processing parameters, detailed analyses of the device, which disclosed a power conversion efficiency of 2.8 % were performed including TEM, TEM-EDX and TEM-EELS investigations. (see Figure 72)

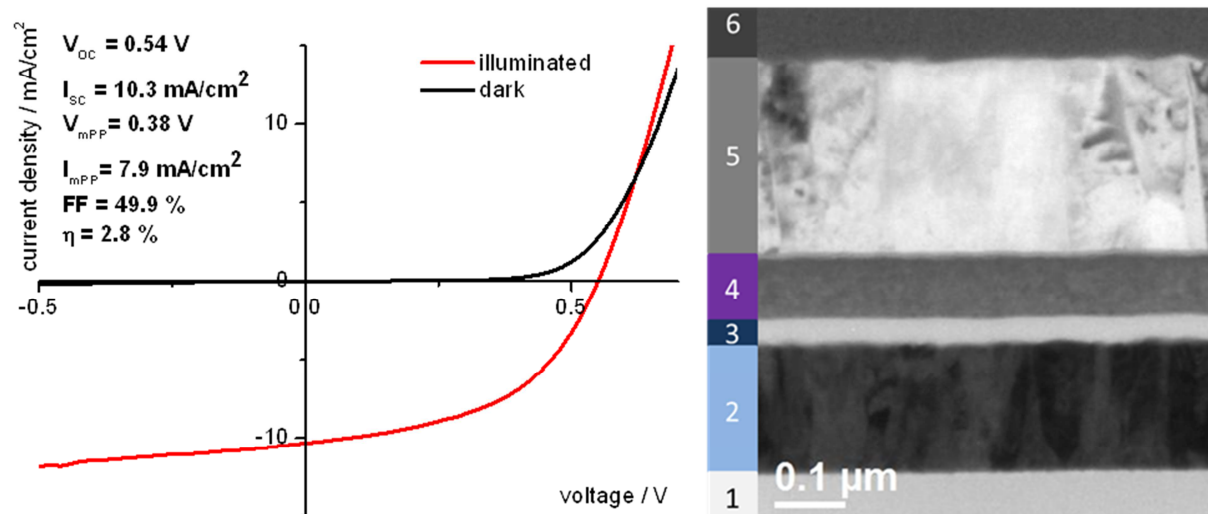


Figure 72: IV-plot (left) and TEM image of the cross-section of a PSiFDBT/CIS solar cell showing a power conversion efficiency of 2.8 %

Metal salts of dialkyldithiocarbamates were synthesized to obtain alternative precursors for the formation of CIS. Although these precursor materials were not suitable for nanocomposite solar cells, due to their high decomposition temperatures up to 350 °C, they were used for the formation of inorganic semiconducting metal sulfides, which could be applied in thin film solar cells. Thus the third main topic was focused on the preparation of CIS- and especially of copper zinc tin sulfide layers (CZTS), using metal salts of dialkyldithiocarbamates. It could be shown that kesterite structure of CZTS could be prepared via blends of dibenzylthiocarbamates. CZTS layers were prepared via drop coating and subsequent thermal conversion of solutions of appropriate amounts of copper, zinc and tin dibenzylthiocarbamate. However, pure kesterite phases (in accordance with XRD-analysis) could only be reached for samples, which were produced with a high excess of the zinc precursor. Thus, a very high content of zinc could be detected via TEM-EDX spectrum imaging. As a consequence the formation of additional sphalerite zinc sulfide, which shows identical XRD reflexes to the kesterite phase of CZTS, had to be considered and further investigations had to be performed. Although Raman spectroscopy is a quite powerful tool to distinguish between CZTS and sphalerite, only a very broad absorption peak could be obtained for the amorphous CZTS samples. This is why the presence of zinc sulfide could not be totally excluded.

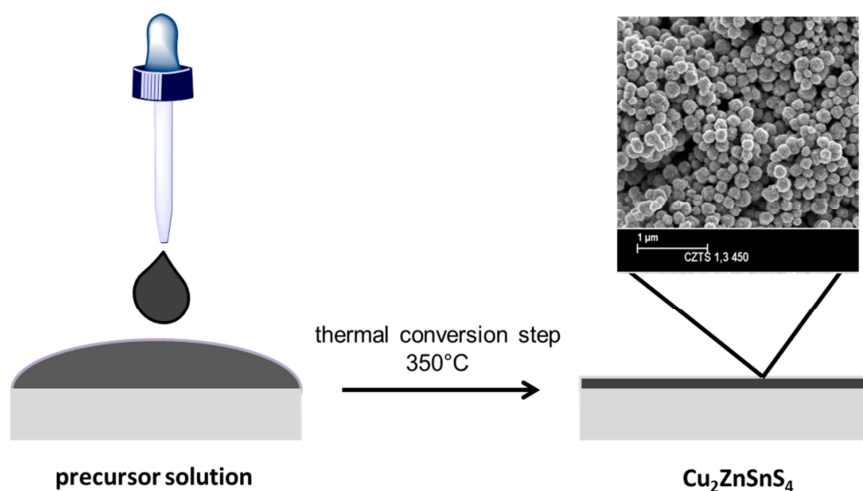


Figure 73: production scheme for the preparation of CZTS layers using metal dialkyldithiocarbamates as precursor materials

## Outlook

PSiFDBT/CIS solar cells, however, revealed very promising results. In the last three years our working group could improve the efficiencies of polymer/CIS solar cells from 0.6 to 3 %, which is a tremendous success. If this trend continues, this type of solar cells could become an alternative to the polymer fullerene solar cells. Further improvement of the power conversion efficiencies could be achieved via the introduction of special hole - and/or electron blocking layers. In addition, the inner morphology could be positively influenced using other solvents, solvent mixtures or special additives, which could promote the formation of interpenetrating networks. Different electrode materials could show a significant improvement as well.

The formation of CZTS precursor layers via solution processed precursor routes could be shown. Since the use of dibenzylidithiocarbamates is not suitable for nanocomposite solar cells, these precursor materials could be applied in inorganic thin film solar cells. Consequently further experiments have to be performed to prove their potential for inorganic photovoltaic devices.



## 6 Bibliography

- [1] Key World Energy Statistics 2009, OECD Publishing, 2009.
- [2] Global Status Report Renewables 2011, 2011.
- [3] M. Graetzel, *Nature* 414 (2001) 338-344.
- [4] F. Krebs, *Polymeric Solar Cells: Materials, Design, Manufacture*, DEStech Publications, Inc., 2010.
- [5] M. Green, *Prog. Photovolt.* 17 (2009) 320-326.
- [6] W. Shockley, H.J. Queisser, *Journal of Applied Physics* 32 (1961) 510-519.
- [7] [Http://www.solarmer.com](http://www.solarmer.com) (2011).
- [8] [Http://www.heliatek.com](http://www.heliatek.com) (2011).
- [9] M.A. Green, K. Emery, Y. Hishikawa, W. Warta, *Progress in Photovoltaics* 19 (2011) 84-92.
- [10] [Http://www.konarka.com](http://www.konarka.com) (2011).
- [11] Y. Liang, Z. Xu, J. Xia, S.-T. Tsai, Y. Wu, G. Li, C. Ray, L. Yu, *Advanced Materials* 22 (2010) 135-138.
- [12] S. Cho, N. Coates, M. Leclerc, K. Lee, A.J. Heeger, *Nature Photonics* 3 (2009) 297-303.
- [13] Y. Liang, L. Yu, *Accounts of Chemical Research* 43 (2010) 1227-1236.
- [14] R. Po, M. Maggini, N. Camaioni, *The Journal of Physical Chemistry C* 114 (2010) 695-706.
- [15] S. Dayal, N. Kopidakis, D.C. Olson, D.S. Ginley, G. Rumbles, *Nano Letters* 10 (2010) 239-242.
- [16] Y. Zhou, M. Eck, S. Yilmaz, I. Dumsch, S. Allard, U. Scherf, *Solar Energy Materials and Solar Cells* 95 (2011) 1232-1237.
- [17] J. Seo, M.J. Cho, D. Lee, a N. Cartwright, P.N. Prasad, *Advanced Materials* (2011).
- [18] E. Maier, *Dissertation*, 2010.
- [19] M. Pieber, *Dissertation*, 2007.

- [20] A. Santis, Diploma Thesis, 2009.
- [21] J. Chandrasekaran, D. Nithyaprakash, K.B. Ajjan, S. Maruthamuthu, D. Manoharan, S. Kumar, *Renewable and Sustainable Energy Reviews* 15 (2011) 1228-1238.
- [22] A.E. Becquerel, *Acad Sci Paris* 9 (1839) 561.
- [23] H. Shirakawa, A.G. Macdiarmid, *Physical Review Letters* 39 (1977) 1098-1101.
- [24] C.W. Tang, *Applied Physics Letters* 48 (1986) 183-185.
- [25] N.S. Sariciftci, D. Braun, C. Zhang, *Applied Physics Letters* 62 (1993) 585-587.
- [26] Y. Zhou, M. Eck, M. Krüger, *Energy & Environmental Science* 3 (2010) 1851-1864.
- [27] L.E. Brus, *The Journal of Chemical Physics* 80 (1984) 4403-4409.
- [28] A.L. Briseno, T.W. Holcombe, A.I. Boukai, E.C. Garnett, S.W. Shelton, J.J.M. Fréchet, P. Yang, *Nano Letters* 10 (2010) 334-340.
- [29] D.J.D. Moet, L.J.A. Koster, B. de Boer, P.W.M. Blom, *Chemistry of Materials* 19 (2007) 5856-5861.
- [30] L.J. a Koster, W.J. van Strien, W.J.E. Beek, P.W.M. Blom, *Advanced Functional Materials* 17 (2007) 1297-1302.
- [31] W.J.E. Beek, M.M. Wienk, R. a J. Janssen, *Advanced Functional Materials* 16 (2006) 1112-1116.
- [32] W.J.E. Beek, M.M. Wienk, R. a J. Janssen, *Advanced Materials* 16 (2004) 1009-1013.
- [33] L. Baeten, B. Conings, H.-G. Boyen, J. D'Haen, A. Hardy, M. D'Olieslaeger, J.V. Manca, M.K. Van Bael, *Advanced Materials (Deerfield Beach, Fla.)* 23 (2011) 2802-2805.
- [34] K. Vandewal, L. Goris, I. Haeldermans, M. Nesladek, K. Haenen, P. Wagner, J. Manca, *Thin Solid Films* 516 (2008) 7135-7138.
- [35] Y. Lin, L. Wang, W. Chiu, *Thin Solid Films* 511-512 (2006) 199-202.
- [36] Y.-M. Chang, W.-F. Su, L. Wang, *Macromolecular Rapid Communications* 29 (2008) 1303-1308.
- [37] S. Günes, N. Marjanovic, J.M. Nedeljkovic, N.S. Sariciftci, *Nanotechnology* 19 (2008) 424009.
- [38] L.H. Slooff, J.M. Kroon, J. Loos, M.M. Koetse, J. Sweelssen, *Advanced Functional Materials* 15 (2005) 689-694.

- [39] Z. Wang, S. Qu, X. Zeng, J. Liu, C. Zhang, M. Shi, F. Tan, Z. Wang, *Current Applied Physics* 9 (2009) 1175-1179.
- [40] Z. Wang, S. Qu, X. Zeng, C. Zhang, M. Shi, F. Tan, Z. Wang, J. Liu, Y. Hou, F. Teng, *Polymer* 49 (2008) 4647-4651.
- [41] M. Bredol, K. Matras, A. Szatkowski, J. Sanetra, A. Prodi-Schwab, *Solar Energy Materials and Solar Cells* 93 (2009) 662-666.
- [42] Y.-Y. Lin, D.-Y. Wang, H.-C. Yen, H.-L. Chen, C.-C. Chen, C.-M. Chen, C.-Y. Tang, C.-W. Chen, *Nanotechnology* 20 (2009) 405207.
- [43] Y. Zhou, Y. Li, H. Zhong, J. Hou, Y. Ding, C. Yang, Y. Li, *Nanotechnology* 17 (2006) 4041-4047.
- [44] L. Han, D. Qin, X. Jiang, Y. Liu, L. Wang, J. Chen, Y. Cao, *Nanotechnology* 17 (2006) 4736-4742.
- [45] L. Wang, Y. Liu, X. Jiang, D. Qin, Y. Cao, *Journal of Physical Chemistry C* 111 (2007) 9538-9542.
- [46] J. Liu, T. Tanaka, K. Sivula, a P. Alivisatos, J.M.J. Fréchet, *Journal of the American Chemical Society* 126 (2004) 6550-6551.
- [47] S.-H. Choi, H. Song, I.K. Park, J.-H. Yum, S.-S. Kim, S. Lee, Y.-E. Sung, *Journal of Photochemistry and Photobiology A: Chemistry* 179 (2006) 135-141.
- [48] D. Verma, a Ranga Rao, V. Dutta, *Solar Energy Materials and Solar Cells* 93 (2009) 1482-1487.
- [49] S. Dayal, N. Kopidakis, D.C. Olson, D.S. Ginley, G. Rumbles, *Journal of the American Chemical Society* 131 (2009) 17726-17727.
- [50] S. Dowland, T. Lutz, A. Ward, S.P. King, A. Sudlow, M.S. Hill, K.C. Molloy, S. a Haque, *Advanced Materials* (2011).
- [51] E. Maier, T. Rath, W. Haas, O. Werzer, R. Saf, F. Hofer, D. Meissner, O. Volobujeva, S. Bereznev, E. Mellikov, *Solar Energy Materials and Solar Cells* 95 (2011) 1354-1361.
- [52] E. Maier, A. Fischereeder, W. Haas, G. Mauthner, J. Albering, T. Rath, F. Hofer, E.J.W. List, G. Trimmel, *Thin Solid Films* 519 (2011) 4201-4206.
- [53] Y.-Y. Yu, W.-C. Chien, C.-Y. Ciou, H.-C. Wu, *Thin Solid Films* 519 (2011) 4721-4730.
- [54] E. Martínez-Ferrero, J. Albero, E. Palomares, *The Journal of Physical Chemistry Letters* 1 (2010) 3039-3045.

- [55] Y. Zhou, F.S. Riehle, Y. Yuan, H.-F. Schleiermacher, M. Niggemann, G. a Urban, M. Krüger, *Applied Physics Letters* 96 (2010) 013304.
- [56] Q. Zhang, T.P. Russell, T. Emrick, *Chemistry of Materials* 19 (2007) 3712-3716.
- [57] J. Seo, W.J. Kim, S.J. Kim, K.-S. Lee, a N. Cartwright, P.N. Prasad, *Applied Physics Letters* 94 (2009) 133302.
- [58] H.-C. Liao, S.-Y. Chen, D.-M. Liu, *Macromolecules* 42 (2009) 6558-6563.
- [59] H.C. Leventis, S.P. King, A. Sudlow, M.S. Hill, K.C. Molloy, S. a Haque, *Nano Letters* 10 (2010) 1253-1258.
- [60] B. a Gregg, M.C. Hanna, *Journal of Applied Physics* 93 (2003) 3605-3614.
- [61] B.R. Saunders, M.L. Turner, *Advances in Colloid and Interface Science* 138 (2008) 1-23.
- [62] J.-michel Nunzi, *Polymer International* 55 (2006) 583-600.
- [63] S.C.J. Meskers, J. Hübner, M. Oestreich, H. Bässler, *The Journal of Physical Chemistry B* 105 (2001) 9139-9149.
- [64] M. Gruber, B. Stickler, G. Trimmel, F. Schürerer, K. Zojer, *Organic Electronics* 11 (2010) 1999-2011.
- [65] D. Woehrle, D. Meissner, *Advanced Materials* 3 (1991) 129-138.
- [66] H. Hoppe, N.S. Sariciftci, *Journal of Materials Research* 19 (2004) 1924-1945.
- [67] P.W.M. Blom, V.D. Mihailetschi, L.J. a Koster, D.E. Markov, *Advanced Materials* 19 (2007) 1551-1566.
- [68] G. Yua, A.J. Heeger, *J. Applied Phys* 78 (1995) 4510-4515.
- [69] J. Halls, *Nature* 376 (1995) 498-500.
- [70] C.J. Brabec, *Advanced Functional Materials* 11 (2001) 374-380.
- [71] E. Arici, D. Meissner, F. Schäffler, N.S. Sariciftci, *International Journal of Photoenergy* 5 (2003) 199-208.
- [72] A. Goetzberger, *Materials Science and Engineering: R: Reports* 40 (2003) 1-46.
- [73] J.H. Burroughes, *Nature* 347 (1990) 539-541.
- [74] Y.-J. Cheng, S.-H. Yang, C.-S. Hsu, *Chemical Reviews* 109 (2009) 5868-5923.

- [75] S. Schorr, *Thin Solid Films* 515 (2007) 5985-5991.
- [76] W. Calvet, Dissertation, 2002.
- [77] H. Hahn, *Zeitschrift Für Anorganische Und Allgemeine Chemie* 271 (1952) 153-170.
- [78] F.M. Courtel, R.W. Paynter, B. Marsan, M. Morin, *Chemistry of Materials* 21 (2009) 3752-3762.
- [79] P. Bera, S. Il Seok, *Journal of Solid State Chemistry* 183 (2010) 1872-1877.
- [80] H. Katagiri, *Solar Energy Materials and Solar Cells* 65 (2001) 141-148.
- [81] K. Tanaka, N. Moritake, H. Uchiki, *Solar Energy Materials and Solar Cells* 91 (2007) 1199-1201.
- [82] J.J. Scragg, P.J. Dale, L.M. Peter, G. Zoppi, I. Forbes, *Physica Status Solidi (B)* 245 (2008) 1772-1778.
- [83] D.B. Mitzi, O. Gunawan, T.K. Todorov, K. Wang, S. Guha, *Solar Energy Materials and Solar Cells* 95 (2011) 1421-1436.
- [84] F.C. Krebs, T. Tromholt, M. Jørgensen, *Nanoscale* 2 (2010) 873-886.
- [85] N. Greenham, X. Peng, A. Alivisatos, *Physical Review. B, Condensed Matter* 54 (1996) 17628-17637.
- [86] B. Sun, N.C. Greenham, *Physical Chemistry Chemical Physics : PCCP* 8 (2006) 3557-3560.
- [87] J. Albero, E. Martínez-Ferrero, J. Ajuria, C. Waldauf, R. Pacios, E. Palomares, *Physical Chemistry Chemical Physics : PCCP* 11 (2009) 9644-9647.
- [88] M.M. Alam, S. a Jenekhe, *Chemistry of Materials* 14 (2002) 4775-4780.
- [89] R.A. Wessling, *Polym. Sci., Polym. Symp.* 72 (1985) 55.
- [90] P.L. Burn, A. Kraft, D.R. Baigentf, D.D.C. Bradley, A.R. Brown, R.H. Friend, R.W. Cymer, A.B. Holmes, R.W. Jackson, *Journal of the American Chemical Society* 115 (1993) 10117-10124.
- [91] L. Lutsen, P. Adriaensens, H. Becker, A.J.V. Breemen, D. Vanderzande, J. Gelan, *Macromolecules* 32 (1999) 6517-6525.
- [92] G. Padmanaban, S. Ramakrishnan, *Journal of the American Chemical Society* 122 (2000) 2244-2251.

- [93] M. Bjerring, J.S. Nielsen, A. Siu, N.C. Nielsen, F.C. Krebs, *Solar Energy Materials and Solar Cells* 92 (2008) 772-784.
- [94] O. Hagemann, M. Bjerring, N.C. Nielsen, F.C. Krebs, *Solar Energy Materials and Solar Cells* 92 (2008) 1327-1335.
- [95] T. Rath, Dissertation, 2008.
- [96] A. Fischereeder, T. Rath, W. Haas, H. Amenitsch, J. Albering, D. Meischler, S. Larissegger, M. Edler, R. Saf, F. Hofer, G. Trimmel, *Chemistry of Materials* 22 (2010) 3399-3406.
- [97] H.-C. Li, K. Koteswara Rao, J.-Y. Jeng, Y.-J. Hsiao, T.-F. Guo, Y.-R. Jeng, T.-C. Wen, *Solar Energy Materials and Solar Cells* 95 (2011) 2976-2980.
- [98] L. Tschugaeff, *Berichte Der Deutschen Chemischen Gesellschaft* 3 (1899) 3332-3335.
- [99] A. Schenk, Diploma Thesis, 2011.
- [100] M. Yamaguchi, K. Ando, *J. Applied Phys.* 63 (1988) 5555-5562.
- [101] Manivannan, *J. Phys. D: Appl. Phys.* 26 (1993) 1510-1515.
- [102] Eftekhari, *Semiconductor Science and Technology* 10 (1995) 707 - 710.
- [103] G. Wantz, L. Hirsch, N. Huby, L. Vignau, J.F. Silvain, a S. Barrière, J.P. Parneix, *Thin Solid Films* 485 (2005) 247-251.
- [104] J. Chaney, *Applied Surface Science* 218 (2003) 258-266.
- [105] B. Low, *Thin Solid Films* 417 (2002) 116-119.
- [106] C.N. Li, a B. Djurišić, C.Y. Kwong, P.T. Lai, W.K. Chan, S.Y. Liu, *Applied Physics A* 80 (2003) 301-307.
- [107] T. Nguyen, *Surface and Coatings Technology* 180-181 (2004) 646-649.
- [108] M. Skompska, *Synthetic Metals* 160 (2010) 1-15.
- [109] M. Svensson, F. Zhang, S.C. Veenstra, W.J.H. Verhees, J.C. Hummelen, J.M. Kroon, O. Inganäs, M.R. Andersson, *Advanced Materials* 15 (2003) 988-991.
- [110] E. Wang, L. Wang, L. Lan, C. Luo, W. Zhuang, J. Peng, Y. Cao, *Applied Physics Letters* 92 (2008) 033307.
- [111] H.-Y. Chen, J. Hou, A.E. Hayden, H. Yang, K.N. Houk, Y. Yang, *Advanced Materials* 22 (2010) 371-375.

- [112] K.R. Choudhury, J. Subbiah, S. Chen, P.M. Beaujuge, C.M. Amb, J.R. Reynolds, F. So, *Solar Energy Materials and Solar Cells* 95 (2011) 2502-2510.
- [113] E. Lim, B.-J. Jung, H.-K. Shim, *Macromolecules* 36 (2003) 4288-4293.
- [114] P.M. Beaujuge, W. Pisula, H.N. Tsao, S. Ellinger, K. Müllen, J.R. Reynolds, *Journal of the American Chemical Society* 131 (2009) 7514-7515.
- [115] J. Hou, H.-Y. Chen, S. Zhang, G. Li, Y. Yang, *Journal of the American Chemical Society* 130 (2008) 16144-16145.
- [116] W.-Y. Wong, L. Liu, D. Cui, L.M. Leung, C.-F. Kwong, T.-H. Lee, H.-F. Ng, *Macromolecules* 38 (2005) 4970-4976.
- [117] Y. Shen, K. Li, N. Majumdar, J.C. Campbell, M.C. Gupta, *Solar Energy Materials and Solar Cells* 95 (2011) 2314-2317.
- [118] B. Schaffer, C. Mitterbauer, A. Schertel, A. Pogantsch, S. Rentenberger, E. Zojer, F. Hofer, *Ultramicroscopy* 101 (2004) 123-128.
- [119] M. Jong, M. Voigt, *Applied Physics Letters* 77 (2000) 2255-2257.
- [120] H. Lewerenz, *Solar Energy Materials and Solar Cells* 83 (2004) 395-407.
- [121] Ongoing Work by Dr Thomas Rath, 2011.
- [122] D. Pan, L. An, Z. Sun, W. Hou, Y. Yang, Z. Yang, Y. Lu, *Journal of the American Chemical Society* 130 (2008) 5620-5621.
- [123] D. Pan, D. Weng, X. Wang, Q. Xiao, W. Chen, C. Xu, Z. Yang, Y. Lu, *Chemical Communications* (2009) 4221-4223.
- [124] S. Ngo, *Polyhedron* 22 (2003) 1575-1583.
- [125] K. Sharma, *Thermochimica Acta* 104 (1986) 339-372.
- [126] A. Uhlin, *Acta Chemica Scandinavica* 25 (1971) 393-410.
- [127] D. Menezes, G. Delima, a Porto, C. Donnici, J. Ardisson, a Doriguetto, J. Ellena, *Polyhedron* 23 (2004) 2103-2109.
- [128] D. Hehemann, J. Lau, J. Harris, M. Hoops, N. Duffy, P. Fanwick, O. Khan, M. Jin, a Hepp, *Materials Science and Engineering B* 116 (2005) 381-389.
- [129] B. Ali, *Thermochimica Acta* 419 (2004) 39-43.

- [130] R. Pike, H. Cui, R. Kershaw, K. Dwight, a Wold, T. Blanton, a Wernberg, H. Gysling, *Thin Solid Films* 224 (1993) 221-226.
- [131] L.J. Giling, J. Bloem, I. Introduction, *Journal of Crystal Growth* 50 (1980) 429-436.
- [132] T. Dittrich, A. Belaidi, A. Ennaoui, *Solar Energy Materials and Solar Cells* 95 (2011) 1527-1536.
- [133] C. Wadia, a P. Alivisatos, D.M. Kammen, *Environmental Science & Technology* 43 (2009) 2072-2077.
- [134] J. Seol, S. Lee, J. Lee, H. Nam, K. Kim, *Solar Energy Materials and Solar Cells* 75 (2003) 155-162.
- [135] K. Jimbo, R. Kimura, T. Kamimura, S. Yamada, W. Maw, H. Araki, K. Oishi, H. Katagiri, *Thin Solid Films* 515 (2007) 5997-5999.
- [136] H. Yoo, J. Kim, *Thin Solid Films* 518 (2010) 6567-6572.
- [137] H. Yoo, J. Kim, *Solar Energy Materials and Solar Cells* 95 (2011) 239-244.
- [138] P. a Fernandes, P.M.P. Salomé, a F. da Cunha, *Thin Solid Films* 517 (2009) 2519-2523.
- [139] H. Katagiri, *Solar Energy Materials and Solar Cells* 49 (1997) 407-414.
- [140] K. Wang, O. Gunawan, T. Todorov, B. Shin, S.J. Chey, N. a Bojarczuk, D. Mitzi, S. Guha, *Applied Physics Letters* 97 (2010) 143508.
- [141] J.J. Scragg, D.M. Berg, P.J. Dale, *Journal of Electroanalytical Chemistry* 646 (2010) 52-59.
- [142] A. Ennaoui, M. Lux-Steiner, A. Weber, D. Abou-Ras, I. Kötschau, H.-W. Schock, R. Schurr, A. Hölzing, S. Jost, R. Hock, *Thin Solid Films* 517 (2009) 2511-2514.
- [143] S.M. Pawar, B.S. Pawar, a V. Moholkar, D.S. Choi, J.H. Yun, J.H. Moon, S.S. Kolekar, J.H. Kim, *Electrochimica Acta* 55 (2010) 4057-4061.
- [144] N. Nakayama, *Applied Surface Science* 92 (1996) 171-175.
- [145] Y.B.K. Kumar, P.U. Bhaskar, G.S. Babu, V.S. Raja, *Physica Status Solidi A* 207 (2010) 149-156.
- [146] K. Tanaka, M. Oonuki, N. Moritake, H. Uchiki, *Solar Energy Materials and Solar Cells* 93 (2009) 583-587.
- [147] N. Moritake, Y. Fukui, M. Oonuki, K. Tanaka, H. Uchiki, *Physica Status Solidi C* 6 (2009) 1233-1236.



- [148] T. Todorov, M. Kita, J. Carda, P. Escibano, *Thin Solid Films* 517 (2009) 2541-2544.
- [149] N. Ryoki, *Ind. Eng. Chem. Res.* 28 (1989) 877-880.
- [150] R. Nomura, K. Miyawaki, T. Toyosaki, H. Matsuda, *Chemical Vapor Deposition* 2 (1996) 174-179.
- [151] R. Nomura, Y. Seki, H. Matsuda, *Journal of Materials Chemistry* 2 (1992) 765-766.
- [152] K. Ramasamy, M. a Malik, P. O'Brien, *Chemical Science* 2 (2011) 1170-1172.
- [153] H. Katagiri, K. Jimbo, W.S. Maw, K. Oishi, M. Yamazaki, H. Araki, A. Takeuchi, *Thin Solid Films* 517 (2009) 2455-2460.
- [154] C. Zou, L. Zhang, D. Lin, Y. Yang, Q. Li, X. Xu, X. Chen, S. Huang, *CrystEngComm* 13 (2011) 3310-3313.
- [155] G. Cliff, *Journal of Microscopy* 103 (1975) 203-207.
- [156] M. Altosaar, J. Raudoja, K. Timmo, M. Danilson, M. Grossberg, J. Krustok, E. Mellikov, *Physica Status Solidi A* 205 (2008) 167-170.
- [157] P. Fernandes, P.M.P. Salomé, A.F. da Cunha, *Journal of Alloys and Compounds* 509 (2011) 7600-7606.
- [158] B.S. Pawar, S.M. Pawar, S.W. Shin, D.S. Choi, C.J. Park, S.S. Kolekar, J.H. Kim, *Applied Surface Science* 257 (2010) 1786-1791.
- [159] A.V. Moholkar, S.S. Shinde, A.R. Babar, K.-U. Sim, Y.-bin Kwon, K.Y. Rajpure, P.S. Patil, C.H. Bhosale, J.H. Kim, *Solar Energy* 85 (2011) 1354-1363.
- [160] N. Khemiri, F. Chaffar Akkari, M. Kanzari, B. Rezig, *Physica Status Solidi A* 205 (2008) 1952-1956.
- [161] H. Katagiri, *Thin Solid Films* 480-481 (2005) 426-432.

## 7 List of figures

Figure 1: Energy share of global energy consumption[2] .....	1
Figure 2: Efficiency certification from National Renewable Energy Laboratory (left); device assembly [15] of the nanocomposite record device (right).....	5
Figure 3: Single layer device with Schottky contact[66] .....	9

Figure 4: Bilayer heterojunction device (left) working principle for charge separation of a bilayer photovoltaic solar cell (right)[66] .....	10
Figure 5: Bulk heterojunction device (left) working principle for charge separation of a bulk heterojunction photovoltaic solar cell (right)[66].....	11
Figure 6: Characteristic solar cell parameters.....	12
Figure 7: Dependency of the power conversion efficiency versus the band gap[72] .....	14
Figure 8: Adamantine compound family (left)[75] chalcopyrite crystal structure of CIS (right)[76] .....	16
Figure 9: Synthesis of PPV via the Wessling route[74] .....	19
Figure 10: Device assembly of a PPV/CIS nanocomposite solar cell.....	21
Figure 11: Special measurement chamber integrated into the GIWAXS measurement set up ....	22
Figure 12: GIWAXS patterns of a PPV/CIS active layer.....	22
Figure 13: Lorentz corrected integrated intensity from 25-32° 2θ versus temperature.....	23
Figure 14: Efficiencies of PPV/CIS solar cells.....	24
Figure 15: I-V curve of a PPV/CIS solar cell .....	25
Figure 16: Comparison of the IPCE spectra of a PPV/CIS solar cell and the UV-vis spectra of a PPV and a CIS thin film.....	26
Figure 17: Formation of CIS using metal dithiocarbonates.....	28
Figure 18: Precursor route to nanocomposite solar cells .....	28
Figure 19: ITO coated glass substrate .....	30
Figure 20: PEDOT:PSS hole transport layer.....	32
Figure 21: Comparison of I-V curves of solar cells with and without PEDOT:PSS interlayer .....	33
Figure 22: Influence of absorption of the laser light on the DLS measurements .....	34
Figure 23: DLS results of the respective precursor solutions.....	35
Figure 24: Chemical structures of conjugated polymers, which were tested in polymer/CIS nanocomposite solar cells.....	36
Figure 25: HOMO and LUMO levels of the active materials .....	38
Figure 26: Device assembly of a polymer/CIS nanocomposite solar cell.....	39
Figure 27: I-V curves of the respective polymers.....	41
Figure 28: Thermogravimetric analysis of PSiFDBT, showing the mass loss vs.temperature .....	42
Figure 29: GIWAXS patterns of a PSiFDBT/CIS device, showing the formation of CIS via the xanthate precursor route .....	43
Figure 30: Integrated intensity calculated from the GIWAXS patterns in the range between 24 and 32 ° 2θ.....	44
Figure 31: Determination of the primary crystallite size of the CIS nanoparticles using the Scherrer equation (Lorentz fit 24-32° 2θ) .....	45
Figure 32: Device assembly of a PSiFDBT/CIS nanocomposite solar cell (two-step coating procedure).....	46
Figure 33: Comparison of solar cell parameters of a one- and a two-step coating process .....	47

Figure 34: Variation of coating parameters .....	48
Figure 35: Comparison of characteristic cell parameters resulting from the variation of the coating speed .....	49
Figure 36: Comparison of characteristic cell parameters resulting from the variation of different substrate temperatures .....	51
Figure 37: Comparison of characteristic cell parameters resulting from the variation of the thickness of the wet layers.....	53
Figure 38: Device showing a power conversion efficiency of 2.8 % .....	53
Figure 39: I-V curve of a PSiFDBT solar cell showing a power conversion efficiency of 2.8 % .....	55
Figure 40: IPCE measurement of a PSiFDBT/CIS solar cell and UV-vis spectra of PSiFDBT, CIS and of a PSiFDBT/CIS blend .....	56
Figure 41: A, B bright field images of a cross section (FIB-lamella) of PSiFDBT/CIS nanocomposite solar cell: 1: glass; 2: ITO electrode; 3: PEDOT:PSS; 4: active layer; 5: aluminum electrode; 5a aluminum oxide 6: platinum (protective layer) (images taken by W. Haas, FELMI).....	57
Figure 42: Elemental maps gained from EDX spectrum imaging of the cross section 2: ITO anode; 3: PEDOT:PSS; 4: active layer; 5a: aluminum oxide; 5: aluminum (W.Haas) .....	58
Figure 43: Elemental maps gained from EELS spectrum imaging of the cross section of the PSiFDBT/CIS solar cell 2: ITO anode; 3: PEDOT:PSS; 4: active layer; 5a: aluminum oxide; 5: aluminum (W.Haas).....	59
Figure 44: TEM-EDX results: Final elemental composition of the active layers depending on various reduced pressures (A: absolute values; B: normalized values).....	60
Figure 45: TEM EDX results: Comparison of the final concentration of indium and copper of the converted active layer to the applied indium to copper ratio of the precursor materials. (A: absolute values; B: normalized values).....	61
Figure 46: XRD of equimolar and indium rich CIS phases .....	62
Figure 47: Characteristic solar cell parameters of PSiFDBT/CIS solar cells having varied indium to copper ratios .....	64
Figure 48: UV-vis spectra of PSiFDBT/CIS solar cells having varied copper to indium ratios (vertically shifted for better visibility).....	65
Figure 49: Characteristic solar cell parameters of PSiFDBT/CIS solar cells having varied acceptor-to donor material ratios .....	67
Figure 50: UV-vis spectra of PSiFDBT/CIS solar cells having varied acceptor to donor material ratios (shifted vertically for better visibility).....	68
Figure 51: Improvement of the power conversion efficiencies of polymer/CIS solar cells.....	69
Figure 52: Synthesis of the respective metal dialkyldithiocarbamates .....	71
Figure 53: Synthesized metal dialkyldithiocarbamates .....	72
Figure 54: XRD-pattern of CIS converted at 200 and 350 °C (vertically shifted for better visibility) .....	74

Figure 55: XRD-pattern of CIS having varied precursor ratios (vertically shifted for better visibility) .....	75
Figure 56: Comparison of XRD- patterns of various CIS phases resulting from different precursor materials. The peaks are in good agreement with the reference patterns of CIS (chalcopyrite phase ICSD600239 and the wurtzite phase ICSD163489) (vertically shifted for better visibility). 76	76
Figure 57: Structures of the prepared metal-dibenzylthiocarbamates .....	80
Figure 58: Scheme of the preparation of the nanostructured CZTS layers .....	80
Figure 59: TGA-analysis of copper- , zinc- and tin- dibenzylthiocarbamates.....	81
Figure 60: X-ray diffraction patterns of the CZTS layers prepared with different precursor ratios. The peaks are in good agreement with the reference pattern of CZTS (PDF 26-0575, sharp grey lines at the bottom). The corresponding indexation is given. As reference for the additionally arising peaks of the CuDTC rich samples a copper sulfide digenite phase PDF 24-0061 (sharp red lines at the bottom) fits well. (vertically shifted for better visibility) .....	83
Figure 61: SEM- images of the CZTS layer with different magnifications (A,B) and a TEM micrograph (C) indicating that the microspheres consist of smaller crystallites with diameters of 10-20 nm. (W.Haas).....	84
Figure 62: Summary of the EDX results and EDX spectrum of the CZTS sample (1.3/1/0.55) .....	84
Figure 63: Raman Spectrum of the sample ((CuDTC)/(ZnDTC)/(SnDTC) = 1.3/1/0.55). .....	85
Figure 64: XPS-Spectra of CZTS compared to ZnS.....	87
Figure 65: XPS-Spectra. (a) Cu 2p: binding energy at 932.4 eV and 952.4 eV with a peak splitting of 20.0 eV from Cu(I); (b) S 2p: binding energy at 161.7 eV and 162.9 eV with a peak splitting of 1.2 eV; (c) Sn 3d: binding energy at 487.0 eV and 495.4 eV with a splitting of 8.4 eV from Sn(IV); and (d) Zn 2p: binding energy at 1022.3 eV and 1045.4 eV with a peak splitting of 23.0 eV from Zn(II); .....	87
Figure 66: Absorption spectrum of sample CZTS 1.3/1/0.55. The $(\alpha h\nu)^2$ vs. $h\nu$ – plot for band gap determination is given in the insert. ....	89
Figure 67: Reaction scheme for the synthesis of sodium diallyldithiocarbamate.....	106
Figure 68: Reaction scheme for the synthesis of sodium dihexyldithiocarbamate.....	107
Figure 69: Reaction scheme for the synthesis of sodium dibenzylthiocarbamate.....	108
Figure 70: Reaction scheme for the synthesis of metal dialkyldithiocarbamates.....	109
Figure 71: Precursor route to nanocomposite solar cells .....	123
Figure 72: IV-plot (left) and TEM image of the cross-section of a PSiFDBT/CIS solar cell showing a power conversion efficiency of 2.8 % .....	124
Figure 73: production scheme for the preparation of CZTS layers using metal dialkyldithiocarbamates as precursor materials.....	125

## 8 List of tables

Table 1: Contact angle of differently pretreated ITO substrates .....	31
Table 2: Properties of conjugated polymers [113][110][114][111][115][74][116] .....	37
Table 3: Characteristic parameters for various polymer/CIS nanocomposite solar cells .....	40
Table 4: Thickness of converted layers using two coating speeds (two-step coating procedure) .....	49
Table 5: Thickness of converted layers using different substrate temperatures (two-step coating procedure) .....	50
Table 6: Thickness of converted layers using different wet layer thicknesses (two-step coating procedure) .....	52
Table 7: Layer thickness of solar cells having varied copper to indium ratios .....	65
Table 8: Layer thickness of solar cells having varied acceptor to donor material ratios .....	68
Table 9: Results of STA-analysis .....	73
Table 10: Chemicals and materials .....	90
Table 11: Weighed portion of polymer and xanthates for the preparation synchrotron samples .....	94
Table 12: Weighed portion of polymer and xanthates for the preparation of nanocomposite solar cells (1.active layer/PEDOT:PSS) .....	95
Table 13: Weighed portion of polymer and xanthates for the preparation of nanocomposite solar cells (2.active layer/PEDOT:PSS) .....	95
Table 14: Weighed portion of polymer and xanthates for the preparation of nanocomposite solar cells (F8T2) .....	96
Table 15: Weighed portion of polymer and xanthates for the preparation of nanocomposite solar cells (FPC) .....	97
Table 16: Weighed portion of polymer and xanthates for the preparation of nanocomposite solar cells (PFDMB) .....	97
Table 17: Weighed portion of polymer and xanthates for the preparation of nanocomposite solar cells (PSBTBT) .....	98
Table 18: Weighed portion of polymer and xanthates for the preparation of nanocomposite solar cells (PSiFDBT) .....	98
Table 19: Weighed portion of polymer and xanthates for the preparation of nanocomposite solar cells (1. active layer) .....	99
Table 20: Weighed portion of polymer and xanthates for the preparation of nanocomposite solar cells (2. active layer) .....	99
Table 21: Weighed portion of polymer and xanthates for the preparation of nanocomposite solar cells (1. active layer) .....	101
Table 22: Weighed portion of polymer and xanthates for the Preparation of nanocomposite solar cells (2. active layer) .....	101

Table 23: Weighed portion for the preparation of nanocomposite solar cells having varied Cu/In ratio .....	102
Table 24: Weighed portion for the preparation of nanocomposite solar cells having varied PSiFDBT/CIS ratio.....	103
Table 25: Weighed portions of the chemicals for the preparation of PSiFDBT/CIS nanocomposite thin films on NaCl-crystals.....	105
Table 26: Weighed portion of dibenzylidithiocarbamates for the synthesis of CIS layers .....	114
Table 27: Weighed portion of dihexylidithiocarbamates for the synthesis of CIS layers .....	114
Table 28: Weighed portion of diallyldithiocarbamates for the synthesis of CIS layers .....	115
Table 29: Weighed portion of diallyldithiocarbamates for the synthesis of CIS layers .....	115
Table 30: Weighed portion of dibenzylidithiocarbamates for the synthesis of CZTS (2/1/0.55) layers .....	116
Table 31: Weighed portion of dibenzylidithiocarbamates for the synthesis of CZTS (1.7/1/0.55) layers .....	116
Table 32: Weighed portion of dibenzylidithiocarbamates for the synthesis of CZTS (1.5/1/0.55) layers .....	116
Table 33: Weighed portion of dibenzylidithiocarbamates for the synthesis of CZTS (1.3/1/0.55) layers .....	116

## 9 List of publications

### Papers

#### 2010

Fischereder, A.; Rath, T.; Haas, W.; Amenitsch, H.; Albering, J.; Meischler, D.; Larissegger, S.; Edler, M.; Saf, R.; Hofer, F.; Trimmel, G.: Investigation of Cu<sub>2</sub>ZnSnS<sub>4</sub> Formation from Metal Salts and Thioacetamide. *Chemistry of Materials* 22 (2010) 3399 - 3409

### Posters

#### 2011

Trimmel, G.; Fischereder, A.; Edler, M.; Moscher, S.; Trattinig, R.; Mauthner, G.; List, E.; Haas, W.; Hofer, F.; Rath, T.: CuInS<sub>2</sub>-Polymer Nanocomposite Solar Cells Prepared via Metal Xanthate Precursors. *EMRS Spring Meeting* (2011). Nizza

#### 2010

Rath, T.; Maier, E.; Edler, M.; Haas, W.; Santis Alvarez, A.; Amenitsch, H.; Hofer, F.; Trimmel, G.: Application of Nanocomposite Layers consisting of Electroactive Polymers and Copper Indium Disulfide Nanoparticles in Hybrid Photovoltaics. *ISOS 3 (2010)* Dänemark

Edler, M.; Fischereder, A.; Maier, E.; Rath, T.; Haas, W.; Mauthner, G.; Albering, J.; Hofer, F.; List, E.; Trimmel, G.: Various Metal Sulfides as Acceptor Phase in Inorganic/Organic Hybrid Photovoltaics prepared by an In-Situ Formation Process. *ISOS 3 (2010)* Dänemark

Rath, T.; Fischereder, A.; Haas, W.; Amenitsch, H.; Maier, E.; Albering, J.; Meischler, D.; Edler, M.; Saf, R.; Hofer, F.; Trimmel, G.: Preparation of Copper Zinc Tin Sulfide Layers for Photovoltaic Applications. *25th European Solar Energy Conference and Exhibition* (2010) Spanien

#### 2009

Trimmel, G.; Maier, E.; Rath, T.; Larissegger, S.; Fischereder, A.; Edler, M.; Haas, W.; Fradler, C.; Moscher, S.; Santis Alvarez, A.; Saf, R.; Mauthner, G.; List, E.; Hofer, F.: Direct Formation of Sulfidic Nanoparticles in Semiconducting Organic Matrices for Hybrid Photovoltaics. *E-MRS* (2009) Frankreich

Edler, M.; Trimmel, G.; Stubenrauch, K.; Popovski, G.: pH-Sensitive and Dye Labeled Block Copolymer Micelles. *EPF* (2009) Österreich

Rath, T.; Maier, E.; Edler, M.; Fischereeder, A.; Larissegger, S.; Pein, A.; Haas, W.; Mauthner, G.; Hofer, F.; List, E.; Trimmel, G.: Organic-Inorganic Semiconductor Blends for Photovoltaic Applications. *Nano and Photonics* (2009) Österreich

Edler, M.; Fischereeder, A.; Maier, E.; Rath, T.; Haas, W.; Hofer, F.; Trimmel, G.: Comparison of Binary and Ternary Metal Sulfides as Acceptor Phase in Inorganic/Organic Hybrid Photovoltaics prepared by an In-situ Formation Process. *MRS* (2009) USA

Larissegger, S.; Rath, T.; Maier, E.; Edler, M.; Fischereeder, A.; Pein, A.; Haas, W.; Hofer, F.; List, E.; Trimmel, G.; Mauthner, G.: Organic-Inorganic Semiconductor Blends for Photovoltaic Applications. *24th European Photovoltaic Solar Energy Conference* (2009) Deutschland

Edler, M.; Stubenrauch, K.; Popovski, G.; Trimmel, G.: Dye Labelled Amphiphilic Block Copolymers prepared by Ring Opening Metathesis Polymerization. *ASPM* (2008) Österreich

## **Oral presentations**

### **2010**

Larissegger, S.; Maier, E.; Rath, T.; Fischereeder, A.; Edler, M.; Haas, W.; Moscher, S.; Mauthner, G.; List, E.; Hofer, F.; Meissner, D.; Trimmel, G.: New Nanocomposite Solar Cells prepared by an In-Situ Formation Process. *MRS* (2010) USA

Fischereeder, A.; Haas, W.; Rath, T.; Amenitsch, H.; Albering, J.; Meischler, D.; Larissegger, S.; Edler, M.; Saf, R.; Hofer, F.; Trimmel, G.: Investigation of Cu<sub>2</sub>ZnSnS<sub>4</sub> Formation from Metal Salts and Thioacetamide *MRS* (2010) USA

### **2009**

Rath, T.; Maier, E.; Larissegger, S.; Fischereeder, A.; Edler, M.; Haas, W.; Fradler, C.; Moscher, S.; Santis Alvarez, A.; Saf, R.; Mauthner, G.; List, E.; Hofer, F.; Trimmel, G.: Application of Nanocomposite Layers of Sulfidic Nanoparticles and Electroactive Polymers in Hybrid Photovoltaics. *EPF* (2009) Österreich

Maier, E.; Edler, M.; Fischereeder, A.; Fradler, C.; Haas, W.; Hofer, F.; Larissegger, S.; Mauthner, G.; Meischler, D.; Pein, A.; Rath, T.; Saf, R.; Santis Alvarez, A.; Trattinig, R.; Stelzer, F.; List, E.; Trimmel, G.: Hybrid Photovoltaic Cells via a Novel Direct Route. *NAWI* (2009) Österreich

Rath, T.; Maier, E.; Fischereeder, A.; Edler, M.; Haas, W.; Fradler, C.; Moscher, S.; Larissegger, S.; Santis Alvarez, A.; Meischler, D.; Saf, R.; Mauthner, G.; List, E.; Hofer, F.; Trimmel, G.: Application of Nanocomposite Layers consisting of Electroactive Polymers and Sulfidic Nanoparticles in Hybrid Photovoltaics. *SLONANO* (2009) Slowenien



## 10 Curriculum vitae

### Personal details

Name: Dipl.-Ing. Michael Edler  
Address: Berliner Ring 6, 8047 Graz  
E-mail: [edler@tugraz.at](mailto:edler@tugraz.at)  
Date of birth: 27. 12. 1983  
Citizenship: Austria

### Education

1990 - 1994 Elementary school (Volksschule Graz-Berliner Ring)  
1994 - 2002 Secondary school (BG und BRG Graz-Seebachergasse)  
Sep. 2002 – Mai 2003 Military service in Leibnitz and Graz  
2003 - 2008 Graz University of Technology – Industrial Chemistry  
Branch of study: Chemical Engineering  
2007 - 2008 Diploma thesis: pH-sensitive and dye labeled block copolymer micelles  
2008 - PhD-Thesis at Graz University of Technology (supervisor: Assoc.Prof. DI Dr. Gregor Trimmel)